UNIVERSIDADE FEDERAL DE SANTA CATARINA
CAMPUS REITOR JOÃO DAVID FERREIRA LIMA
PROGRAMA DE PÓS-GRADUAÇÃO EM ENGENHARIA MECÂNICA

Fernando Henrique Tanaka Santos

NUMERICAL ANALYSIS OF THE AIRFLOW DOWNSTREAM FROM A TRACHEOESOPHAGEAL VOICE PROSTHESIS

Florianópolis

2019

Fernando Henrique Tanaka Santos

NUMERICAL ANALYSIS OF THE AIRFLOW DOWNSTREAM FROM A TRACHEOESOPHAGEAL VOICE PROSTHESIS

Dissertação submetida ao Programa de Pós-Graduação em Engenharia Mecânica da Universidade Federal de Santa Catarina para a obtenção do título de Mestre em Engenharia Mecânica
Orientador: Prof. Andrey Ricardo da Silva, Ph.D.

Florianópolis
2019

Ficha de identificação da obra elaborada pelo autor,
através do Programa de Geração Automática da Biblioteca Universitária da UFSC.

Santos, Fernando Henrique Tanaka
Numerical analysis of the airflow downstream from a tracheoesophageal voice prosthesis / Fernando Henrique Tanaka Santos ; orientador, Andrey Ricardo da Silva, 2019.
130 p.

Dissertação (mestrado) - Universidade Federal de Santa Catarina, Centro Tecnológico, Programa de Pós-Graduação em Engenharia Mecânica, Florianópolis, 2019.

Inclui referências.

1. Engenharia Mecânica. 2. Voice prosthesis. 3. Tracheoesophageal speech. 4. Voice aerodynamics. I. da Silva, Andrey Ricardo. II. Universidade Federal de Santa Catarina. Programa de Pós-Graduação em Engenharia Mecânica. III. Título.

Fernando Henrique Tanaka Santos

NUMERICAL ANALYSIS OF THE AIRFLOW DOWNSTREAM FROM A TRACHEOESOPHAGEAL VOICE PROSTHESIS

O presente trabalho em nível de mestrado foi avaliado e aprovado por banca examinadora composta pelos seguintes membros:

Prof. Dr. Stephan Paul
Universidade Federal de Santa Catarina

Dr. Luiz Roberto Medina dos Santos
Centro de Pesquisas Oncológicas

Prof. Dr. Marcio Holsbach Costa
Universidade Federal de Santa Catarina

Certificamos que esta é a **versão original e final** do trabalho de conclusão que foi julgado adequado para obtenção do título de mestre em Engenharia Mecânica.

Assinado de forma digital por
Jonny Carlos da Silva:51451506449
Dados: 2019.11.26 09:08:41 -03'00'

Prof. Jonny Carlos da Silva, Dr.
Coordenador do Curso

Documento assinado digitalmente
Andrey Ricardo da Silva
Data: 26/11/2019 08:59:54-0300
CPF: 023.554.909-61

Prof. Andrey Ricardo da Silva, Ph.D.
Orientador

Florianópolis, 05 de Novembro de 2019

ACKNOWLEDGEMENTS

Firstly, I would like to thank Prof. Andrey R. da Silva for introducing me to this research, guiding me through this work, understanding my struggles, and encouraging me.

A great deal of this work was completed thanks to the contributions of the people involved in this research group; André, Andressa, Guilherme, Matheus Reiser, Nicolas, Bárbara, and Camila all contributed in their own way. And also to the people of the lab going through the same daily grind, supporting each other and making the lab a great place to be. Anderson and Kleber for our struggle of figuring the ins and outs of the simulation software, Ricardo, Priscila, Thayle, Aldren, Gil, Nivaldo, and many more. Special thanks to Zé Pedro for giving me several tips on how to simulate fluid flow, even if in the end they were not put to good use. And Marcos Takahama for being a good friend and supporting me.

This research would not have been possible without the support of the CEPON team. Dr. Elisa Gomes and Dr. Luiz Roberto Medina for their contributions on the understanding of the tracheoesophageal speech, and Dr. Fabiana Thomaz for assisting with the CT scans that allowed this work to progress to a better direction than initially planned. My gratitude also goes to the people of the GAL, the support group for mouth and throat cancer patients, for welcoming me and my colleagues; especially to the volunteers, whose contribution to this work go beyond being subject to a CT scan.

I am grateful to Prof. Byron D. Erath of Clarkson University for providing not only the experimental data that was essential in the development of the numerical model used in this work, but also for providing insights on the idiosyncrasies of his own experiment. And Prof. Scott L. Thomson from the Brigham Young University for the suggestions and shared knowledge during his brief stay in Florianópolis.

I would like to thank CAPES, CNPq, and FINEP for the financial support that enabled the development of this work.

And finally, I would like to thank Carol for standing by my side during this whole process and for not only understanding, but also living her own parallel challenges and showing me how to do it. And also my family for their unending love and support, even if from afar.

"The future is already here—it's just not very evenly distributed."

William Gibson

RESUMO

Próteses fonatórias traqueoesofágicas são a solução mais atrativa para a recuperação da fala de pacientes que foram submetidos a uma laringectomia total. A vibração induzida pelo escoamento através do segmento faringoesofágico, também conhecido como pseudoglote, pode ser influenciada pelo comportamento aerodinâmico dentro da prótese fonatória e pelas característica do escoamento a jusante da prótese. Trabalhos anteriores investigaram a queda de pressão através de diferentes próteses tanto em experimentos *in-vitro* quanto *in-vivo*. Ademais, os aspectos aerodinâmicos do escoamento na região esofágica somente foram investigados experimentalmente *in-vitro* para um modelo idealizado do sistema traqueoesofágico. Este trabalho propõe investigar a queda de pressão entre traqueia e esôfago, e também a distribuição de pressão ao longo do segmento faringoesofágico, como função do posicionamento e angulação da prótese. Os aspectos aerodinâmicos do escoamento a jusante da prótese também são avaliados. A investigação foi conduzida desenvolvendo um modelo numérico baseado em uma geometria idealizada encontrada na literatura. Após aferir as limitações do modelo idealizado, um experimento foi conduzido para se obter as relações entre pressão, vazão volumétrica de ar e abertura da prótese, relações fundamentais na criação de um modelo mais preciso do sistema traqueoesofágico. Após essas investigações preliminares, imagens de tomografia computadorizada foram utilizadas para construir um modelo mais realista. Este modelo foi utilizado para aferir a influência da posição da prótese na distribuição de pressão dentro do segmento faringoesofágico. Os resultados indicam que o posicionamento de prótese não tem influência significativa na queda de pressão utilizada para verificar a influência do posicionamento da prótese fonatória. Entretanto, a distribuição de pressão dentro do segmento faringoesofágico é influenciada pela posição da prótese, especialmente para altos valores de vazão de ar.

Palavras-chave: Prótese fonatória. Voz traqueoesofágica. Aerodinâmica da voz.

RESUMO EXPANDIDO

Introdução

O câncer de laringe aflige uma parcela significativa da população mundial, consistindo 25% dos casos de câncer na região da cabeça e pescoço. Dentre as formas de tratamento deste câncer, a laringectomia total se destaca devido à sua principal consequência, a perda da capacidade de produção da voz. Devido à alta taxa de sobrevivência e à grave consequência do tratamento, são grandes os esforços relacionados à reabilitação dos pacientes. As três principais formas de recuperação da fala são a eletrolaringe, a voz esofágica e a prótese traqueoesofágica. As próteses fonatórias traqueoesofágicas são a solução mais atrativa para recuperação da fala devido à intuitividade e boa qualidade da voz produzida. A prótese traqueoesofágica permite que o ar do pulmão seja redirecionado para o esôfago, passando através do segmento faringoesofágico e produzindo uma nova voz. Desde sua introdução na década de 80, a prótese vem sendo aprimorada por diversos fabricantes. Para que melhorias possam ser desenvolvidas para estas próteses, é necessário compreender os mecanismos de produção da voz traqueoesofágica. Diversos autores buscam compreender os mecanismos que atuam na prótese, mas poucos consideram o sistema traqueoesofágico como um todo.

Objetivos

Este trabalho tem como objetivos o desenvolvimento de um modelo numérico capaz de capturar os fenômenos fluidodinâmicos que ocorrem no sistema traqueoesofágico; a determinação da relação entre vazão volumétrica de ar, queda de pressão e ângulo de abertura da válvula da prótese através de um experimento; e estimar a influência do posicionamento da prótese nas forças que agem sobre o segmento faringoesofágico.

Metodologia

Desenvolveu-se um modelo computacional baseado no método de Volumes Finitos para que o escoamento de ar através do segmento faringoesofágico pudesse ser simulado. Este modelo consiste de um algoritmo de solução segregado, com modelagem de turbulência do tipo *realizable two-layer* k-ϵ. Inicialmente foi criado um modelo baseado em um experimento da literatura. Este modelo consiste em um sistema idealizado do segmento traqueoesofágico construído em uma escala maior e utilizando água como fluido de trabalho. Posteriormente, este modelo experimental foi utilizado como validação do modelo numérico. Devido às características da prótese, o modelo idealizado não representava elementos fundamentais do escoamento. Para contornar este problema, construiu-se uma bancada experimental para determinar a relação entre a vazão

volumétrica de ar, a queda de pressão e o ângulo de abertura do mecanismo de válvula da prótese. Determinados estes parâmetros e utilizando imagens de tomografia da região da cabeça e pescoço, o modelo numérico pode ser aplicado a uma geometria simplificada do sistema traqueoesofágico para estimar as forças atuantes sobre o segmento faringoesofágico. Com este modelo, variando-se a posição da prótese no sistema traqueoesofágico, pode-se quantificar a influência deste posicionamento nas forças que atuam no segmento faringoesofágico.

Resultados e Discussão

Para o modelo inicial, baseado no modelo experimental idealizado, foram obtidos os campos de velocidade e vorticidade nos planos designados na literatura. Através do experimento foram obtidas curvas para relacionar a diferença de pressão, a vazão volumétrica de ar e o ângulo de abertura do mecanismo da prótese. Com o modelo final, foram obtidas as quedas de pressão através da prótese e as distribuições de pressão nas paredes anterior e posterior do plano sagital médio do segmento faringoesofágico para três posições distintas da prótese e três condições de escoamento de ar. Os campos de velocidade no plano sagital médio do segmento faringoesofágico também foram obtidos.

Considerações Finais

A recuperação da fala através da prótese traqueoesofágica é sem dúvida a técnica mais avançada para a recuperação da fala disponível nos dias de hoje. Entretanto, ainda existem questionamentos em relação à produção da voz no segmento faringoesofágico. Os resultados sugerem que a influência do posicionamento na perda de carga é desprezível, e o grande limitador é o segmento faringoesofágico, e não a prótese. Por outro lado, a distribuição de pressão no segmento faringoesofágico é afetada pelo posicionamento da prótese, o que pode impactar diretamente na vibração do segmento faringoesofágico. Os resultados também sugerem que a geometria do esôfago é de suma importância no escoamento que entra no segmento faringoesofágico.

ABSTRACT

Tracheoesophageal voice prostheses are the most appealing solution for the voice recovering process of patients that have undergone a total laryngectomy. The flow-induced vibration of the pharyngoesophageal segment, also known as the pseudoglottis, might be influenced by the aerodynamic behavior inside the prosthesis itself and by the characteristics of the flow structures downstream from its outlet. Previous works have investigated the pressure drop across different prosthesis designs with both *in-vitro* and *in-vivo* experiments. Nevertheless, the aerodynamic aspects of the flow in the tracheoesophageal region have been only investigated *in-vitro* with an idealized geometry. In the present study, the pressure drop between the trachea and the esophagus, as well as the pressure distribution along the pharyngoesophageal segment, are investigated as a functions of the prosthesis position and angulation. Moreover, the aerodynamic aspects of the flow downstream from the prosthesis outlet are assessed. The investigation was conducted by developing a computational model based on the idealized geometry available in the literature. After assessing the limitations of the idealized model, an experiment was performed in order to obtain the relationship between pressure, volume flow, and prosthesis opening, which was used to create a more accurate representation of the airflow through the prosthesis. The obtained results along with computed tomography images from laryngectomized subjects were used to build a more realistic computer model. This model was finally used to assess the influence of the voice prosthesis position on the pressure distribution inside the pharyngoesophageal segment. The results suggest that the prosthesis positioning does not play a significant role on the pressure drop across the prosthesis. Nevertheless, the pressure distribution inside the pharyngoesophageal segment is influenced by the prosthesis position, particularly for high volume flows.

Keywords: Voice prosthesis. Tracheoesophageal speech. Voice aerodynamics.

LIST OF FIGURES

LIST OF TABLES

LIST OF ABBREVIATIONS

CAE	Computer-Aided Engineering
CFD	Computational Fluid Dynamics
CT	Computed tomography
FVM	Finite Volume Method
PE	Pharyngoesophageal
PIV	Particle Image Velocimetry
RANS	Reynolds-averaged Navier-Stokes
SPVP	Sound-Producing Voice Prosthesis
TE	Tracheoesophageal

LIST OF SYMBOLS

Latin alphabet

A	Area	m^2
A, B	Reference positions	m
c	Speed of sound	$m \cdot s^{-1}$
C_f	Skin friction coefficient	-
D	Diameter	m
f	Frequency	s^{-1}
k	Kinetic energy	J
L	Characteristic dimension	m
Ma	Mach number	-
P	Pressure	Pa
Q	Volume flow	$m^3 \cdot s^{-1}$
R	Resistance to flow	$Pa \cdot m^{-3} \cdot s^1$
r	Radius	m
Re	Reynolds number	-
St	Strouhal number	-
u	Velocity	$m \cdot s^{-1}$
$\bar{u}$	Mean velocity	$m \cdot s^{-1}$
u_τ	Friction velocity	$m \cdot s^{-1}$
u_∞	Free stream velocity	$m \cdot s^{-1}$
x, y, z	Orthogonal coordinates	-
y^+	Dimensionless wall distance	-

Greek alphabet

ΔP	Pressure difference	Pa
ϵ	rate of kinetic energy dissipation	$J{\cdot}kg^{-1}{\cdot}s^{-1}$
μ	Dynamic viscosity	Pa·s
ν	Kinematic viscosity	$m^2{\cdot}s^{-1}$
ρ	Density	$kg{\cdot}m^{-3}$
τ	Shear stress	Pa
$\vec{\omega}$	Vorticity	s^{-1}

Superscripts and subscripts

air	Air
E	Endoesophageal
ef	effective
p	Prosthesis
T	Endotracheal
wall	Wall
water	Water

CONTENTS

1 INTRODUCTION

This work proposes to investigate the fluid flow phenomena that occur through the trachea, esophagus and pharynx of laryngectomized patients—people who have had their larynges removed due to cancer or other diseases of the neck region.

The larynx is an organ that composes part of the respiratory system, located between the pharynx and the trachea. It houses the vocal folds and, as such, plays an important role in voice production. Being subjected to a laryngectomy, a patient loses the capability to speak.

The voice is one of the defining characteristics of individual identity and human expression. Technology has been following a path in which voice-activated and voice-controlled devices are more and more commonplace. From personal assistant applications to security systems, being unable to speak can be a hindrance. The social impact is even more significant and can lead to several lifestyle and psychosocial issues. Patients have reported reduced olfactory and taste response, respiratory issues, communication problems, and social stigma (HILGERS et al., 1990; BLOM; SINGER; HAMAKER, 1998; NALBADIAN et al., 2001).

1.1 BACKGROUND

Laryngeal cancer is one of the most common diseases to afflict the head and neck region, comprising around 25% of the malignant tumor occurrences in this area, with a larger incidence on males (STEWART; WILD, 2014; INSTITUTO NACIONAL DE CâNCER, 2018). The specific causes of this cancer are not well known and the risk factors include excessive use of alcohol and tobacco—especially when combined—and contact with asbestos (STEWART; WILD, 2014). More recently, correlations between laryngeal cancer and the human papillomavirus (HPV) have been reported, though no direct relation has been established (CHEN et al., 2017). Table 1 shows the number of cases per continent logged by the World Health Organization (2018).

This type of cancer has a high five-year survival rate[1] when compared to other forms of cancer, in countries with both high and low Human Development Indexes (SANKARANARAYANAN et al., 2011; CANCER RESEARCH UK, 2015; NATIONAL CANCER INSTITUTE, n.d.). Due to the high survivability and the severe consequences of this cancer, rehabilitation efforts are of great concern.

There are a few standard treatments for this type of cancer, including surgery, radiotherapy and chemotherapy. Surgical interventions include partial or total removal of the vocal folds

[1] The percentage of people in a study or treatment group who are alive five years after they were diagnosed with or started treatment for a disease.

Table 1 – Incidence of larynx cancer in 2018 (WORLD HEALTH ORGANIZATION, 2018).

Region	Registered cases	Per 100000
Africa	10058	0.78
Asia	93373	2.1
Europe	39875	5.4
Latin America and the Caribbean	17044	2.6
North America	16352	4.5
Oceania	720	1.7
Total	177422	

(cordectomy) and the partial or total removal of the larynx (laryngectomy). In most cases, it results in the loss of the voice production capability (AMERICAN CANCER SOCIETY, n.d.).

1.1.1 Total laryngectomy

Throughout this work the three anatomical planes commonly referred in medicine will be used: the sagittal plane divides the body in left and right parts; the coronal plane which divides the body in front and back parts (or anterior and posterior, respectively); and the transverse plane that separates the body in top and bottom parts. These can be visualized in Figure 1.

The total laryngectomy procedure consists of removing the larynx and, therefore, disconnecting the mouth and nasal cavities from the respiratory system. In order for the patient to breath again, a puncture—the tracheostoma— is created at the base of the neck. This puncture is connected to the top-end of the trachea. The procedure is described in-depth by Schwartz, Hollinshead and Devine (1963) and Tucker (1990).

The pharyngoesophageal (PE) segment is the segment that connects the upper portion of the esophagus to the lower portion the the pharynx. It is also known as the upper esophageal sphincter—usually when referring to its function. It precludes the passage of air from the pharynx to the esophagus, as well as the esophageal contents to the pahrynx (SINGH; HAMDY, 2005), and so, it stays closed. When a patient undergoes a total laryngectomy, the PE segment maintains its functions, but it also becomes the primary source of sound in post-laryngectomy voice production. This will be further discussed in Section 1.1.2.

In Figure 2 a sagittal cut of the anatomy of the head and neck before and after the procedure can be seen. In Figure 2a shows the trachea coming up into the larynx as well as the esophagus. Both of these enter the pharynx (the throat), which is part of both the respiratory and the digestive systems. Figure 2b shows the anatomy after laryngectomy, in which the larynx is absent and a tracheostoma was created to allow breathing.

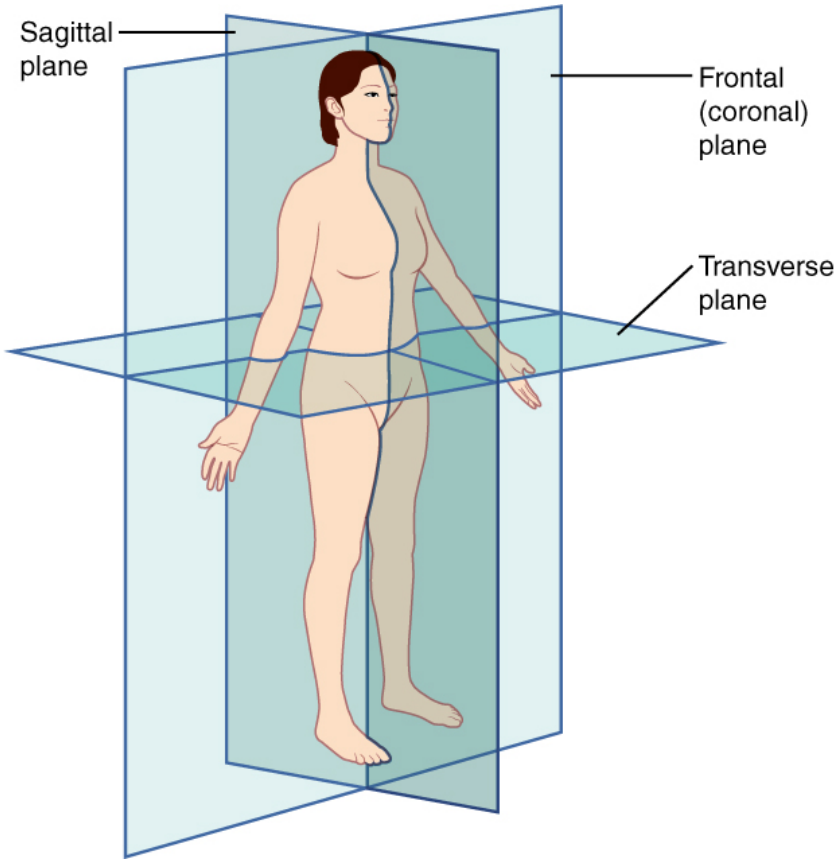

Figure 1 – The anatomical planes of the human body (BETTS et al., 2017).

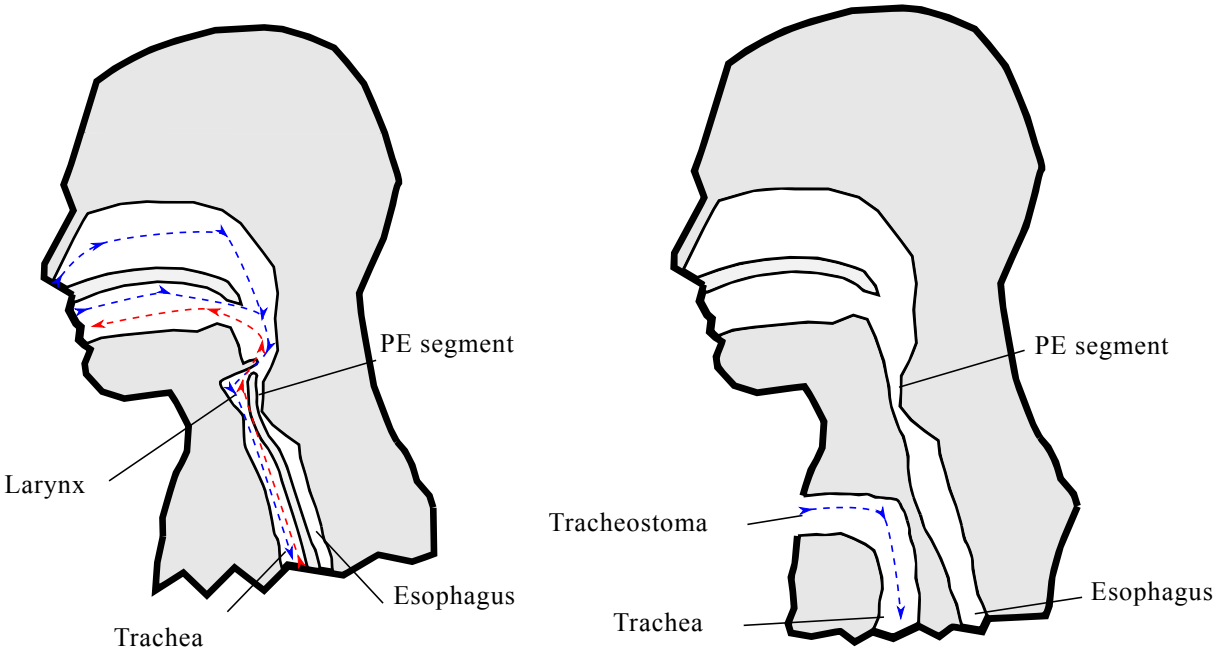

(a) Pre-surgery (b) Post-surgery

Figure 2 – Sagittal cut showcasing the difference in anatomy before and after a laryngectomy procedure. The lines indicate the path of the air during breathing (blue) and voice production (red).

1.1.2 Voice recovery after total laryngectomy

The most common methods currently available for voice recovery of laryngectomized patients are the electrolarynx, esophageal voice production and the TE voice prosthesis.

The electrolarynx, depicted in Figure 3, is a hand-held device, which has a vibrating diaphragm. It produces mechanical vibrations that induce vibration of the neck tissues, allowing the user to speak with a monotonic robot-like voice when held against the jaw. The main drawback of the electrolarynx is the lack of modulation of frequency and vibrational amplitude. Some manufacturers attempted to increase the emotion output of of the voice produced by these devices by allowing manual modulation of the fundamental frequency to help lessen the stigma.

The esophageal voice production is a technique that involves injecting air into the esophageal tube and releasing it in a controlled manner in order to induce the vibration of the PE segment, thereby producing voice. It is a learned skill and requires training and practice (VAN AS, 2001). It is characterized by Gates et al. (1982) as harsh and with low pitch and intensity. It is limited by the amount of air that can be trapped inside the esophagus. The esophagus has an approximate volume of 40–80 cm^3 (BLOM, 2000), while the lung inspiratory capacity—that is, the maximum amount of air that can be inhaled past a normal expiration—is approximately 3500 cm^3 (BETTS et al., 2017), which leads to very short and truncated sentences. Despite its limitations it allows the user to speak in a hands-free or device-free manner. It is also important as a form of alaryngeal communication, especially when cost and maintenance of tracheoesophageal prostheses or electrolarynges are prohibitive (ZENGA et al., 2018).

The tracheoesophageal (TE) voice production is a method developed by Singer and Blom (1980) based on a one-way valve. The valve mechanism opens when the tracheostoma is occluded and the endotracheal pressure, P_{T}, is greater than the endoesophageal pressure, P_{E},

(a) SolaTone Plus (ATOS MEDICAL, n.d.).

(b) Blom-Singer EL-1000 (INHEALTH TECHNOLOGIES, n.d.).

Figure 3 – Electrolarynges

allowing the air to pass from the trachea to the esophagus. In order to implement this voice prosthesis, the physician must puncture the posterior wall of the trachea to create a hole that leads into the esophagus. The voice prosthesis is inserted in this hole and acts as a gate that allows air to pass from the trachea to the esophagus when the tracheostoma is occluded and precludes the passage esophageal content into the lungs. The air diverted into the esophagus passes through the PE segment and induces the vibration of the PE segment, similarly to the esophageal speech. Figure 4 depicts a sagittal cut showing the prosthesis position in a laryngectomized patient. Although it is reportedly more intuitive than the esophageal voice production and considered the best voice rehabilitation method (ZENGA et al., 2018), it has several limitations when compared to laryngeal voice production. The prosthesis prone to failure due to *Candida* growth, which also leads to short lifespans, and the voice production success rate is high, but it varies significantly from patient to patient. Low pitch and low intensity are common limitations. Some problems can arise due to either the hypertonicity (high stiffness) or hypotonicity (insufficient stiffness) of the PE segment (VAN AS, 2001), which leads to patients incapable of producing voice.

TE voice prostheses are built with medical grade materials like silicone rubber, fluoroplastics, and titanium. Shaft diameters fall within the range of 12–22.5 Fr (approx. 4 mm–8 mm), while the length varies from 4 to 22 mm. Figure 5 depicts a typical voice prosthesis, with its components indicated. This prosthesis uses the most common valve mechanism found in

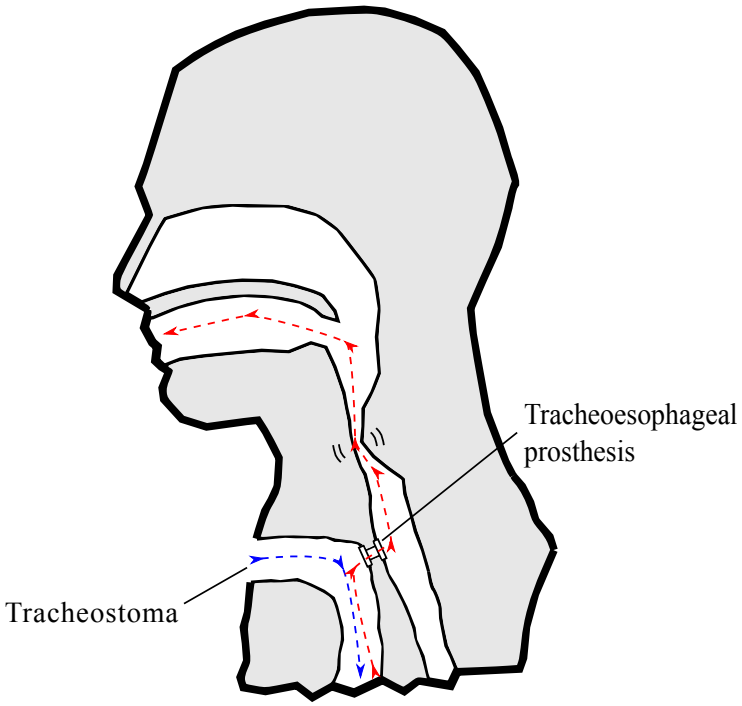

Figure 4 – Sagittal cut depicting an installed TE prosthesis. The blue line indicates the path of the air during breathing and the red line during phonation.

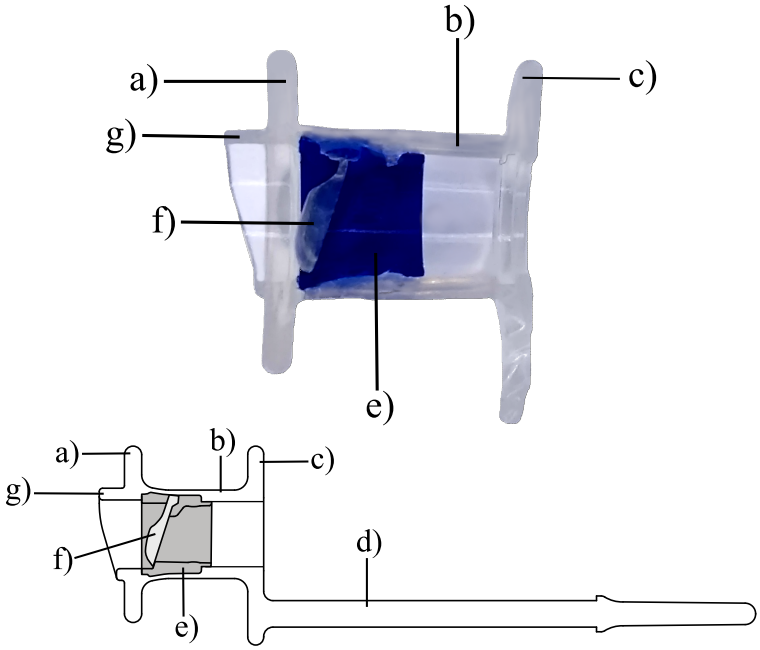

Figure 5 – A typical voice prosthesis and its components a) Esophageal flange b) Prosthesis shaft c) Tracheal flange d) Safety strap e) Radio-opaque fluoroplastic valve seat f) Valve flap g) Prosthesis hood.

theses prostheses, a hinged gate.

It is recommended that the prosthesis be replaced every few months, depending on the clinician's evaluation. However the elevated cost and usually short life-span are limiting factors for patients who cannot afford to replace prostheses regularly. A prosthesis cost is estimated at R$ 2500.00, which makes it cost-prohibitive for most. Life-span of the prosthesis is reported to be as low as 61 days median (LEWIN et al., 2017). It is difficult to predict how long a prosthesis will last due to differences in individual biological circumstances.

1.2 OBJECTIVES

In order to pursue a better quality of life for patients, it is necessary to understand the mechanisms that govern the fluid flow in the system. With this in mind, the primary objective of this work can be defined: the development of a computer model capable of reproducing the flow field within the tracheoesophageal system and its dependency on features, such as prosthesis position and prosthesis characteristics. To accomplish this, a few steps must be undertaken:

1. Develop a numerical approach that is capable of reproducing physical phenomena similar to the fluid flow found in the tracheoesophageal system;

2. Determine the relation between volume flow, pressure drop and valve opening angle by means of an experiment;

3. Estimate the influence of the prosthesis positioning on the forces acting on the PE segment by means of a computer model.

1.3 OUTLINE

This work is organized the following way:

Chapter 2 presents a literature review on the development of the TE voice and voice prostheses, as well as some investigations. The aim of these studies is twofold: first, to understand the mechanisms of the valve and, secondly, to understand the aerodynamics of tracheoesophageal voice production. Taking into account both *in-vitro* and *in-vivo* investigations, these works answer some fundamental questions necessary to the development of this work. Moreover, this section highlights some novel approaches to solve the voice production problem.

Chapter 3 provides a description of the computational procedures used to develop and build all the numerical models in this work. We discuss an idealized experimental model by Erath and Hemsing (2016), which serves as the reference for the developed model. We compare the experimental results of Erath and Hemsing (2016) with those obtained by the simulation in order to evaluate the quality of the results produced by the numerical models that were chosen.

Due to the nature of the experiment by Erath and Hemsing (2016), some simplifications had to be made, which limited the understanding of the flow in the TE system. In order to circumvent these limitations, Chapter 4 presents an experimental set-up devised to determine the relation between volume flow, pressure and the valve flap opening. By adjusting the numerical model presented in Chapter 3 to fit the observed experiment, we bring it closer to a realistic geometry.

Based on the data obtained in Chapters 3 and 4, Chapter 5 presents a more realistic model of the TE system of a laryngectomized patient. With this model, it is possible to approximate the fluid flow phenomena that occur in the TE system with more accuracy. With the results obtained by the latter model, we discuss the implications of valve positioning in the production of voice.

Chapter 6 provides a general discussion of what was observed in this work as well as the limitations, conclusions, and suggestions for future works.

2 LITERATURE REVIEW

2.1 VOICE RECOVERY AFTER LARYNGECTOMY

The first recorded laryngectomy for cancer treatment was performed by the Austrian surgeon Theodor Billroth on December 31, 1873. However, the first documented attempt of voice recovery was performed by his assistant, Carl Gussenbauer. Gussenbauer developed an internal voice prosthesis, which consisted of a tracheal cannula, a pharyngeal cannula. and a phonation cannula with a vibrating reed that was inserted in the tracheostoma. When the tracheostoma was occluded, the device would divert the air from the trachea to the pharynx, while passing though the the metal reed, which produced sound. A lid was placed on top of the pharyngeal cannula to prevent aspiration. The device, shown in Figure 6, was placed 21 days after the surgery and the patient was able to speak with a very poor quality of voice (WEIR, 1973).

Throughout the years, several other techniques have been proposed. David Foulis in 1877, Victor von Bruns in 1878, and Paul von Bruns in 1881 modified Gussenbauer's design according to their personal observations. Paul von Bruns' design was further improved by Julius Wolff in 1892. In 1894, Eugen Kraus tried to combat one of the main problems with the existent solutions, the accumulation of secretion. All of these developments occurred in a period when laryngectomy did not result in a complete separation of the respiratory and digestive systems. Gluck and Sörensen would later introduce a surgical method that completely separated

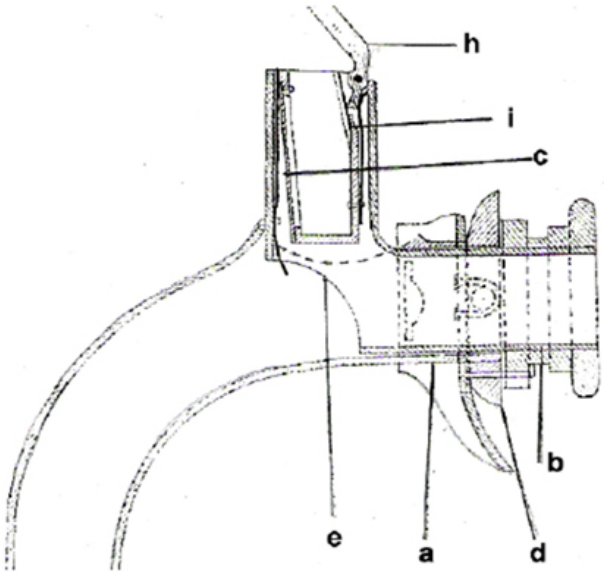

Figure 6 – Gussenbauer's voice recovery device. (a) Tracheal cannula, (b) pharyngeal cannula, (c) phonation cannula, (d) turnable sealing, (e) window to trachea, (h) artificial epiglottis, and (i) spring (LORENZ, 2017).

the respiratory and digestive systems in 1881. This new approach reduced mortality to less than 10%, but it also precluded the rehabilitation of voice using the current methods (KRAMP; DOMMERICH, 2009; LORENZ, 2017).

Several authors have reviewed the history of voice recovery of laringectomized patients using various techniques like the aforementioned esophageal voice production and the electrolarynx. Further reading on the subject can be found in Kramp and Dommerich (2009), Tang and Sinclair (2015), Lorenz (2017), Zenga et al. (2018), and Bohnenkamp (2019).

In 1980 a new solution emerged. Inspired by a patient described by Guttmann in 1932, who self-inflicted a tracheohypopharyngeal shunt with an ice-pick and managed to produce loud fluent tracheopharyngeal voice and the work by Taub and Spiro (1972), Mark I. Singer and Eric D. Blom developed what is now known as the TE voice prosthesis (BLOM; SINGER; HAMAKER, 1998). Nowadays, TE voice production is the most common voice recovery method (ZENGA et al., 2018).

2.2 TRACHEOESOPHAGEAL VOICE PROSTHESES

Singer and Blom (1980) developed the first commercially available tracheoesophageal prosthesis, the Blom-Singer Duckbill prosthesis. They created a device that was capable of diverting the air from the trachea into the esophagus while impeding the flow in the opposite direction. Their first attempt at a prosthesis was built in 1978 using a rubber catheter. The valve mechanism was made using a ball trapped in a cage at the esophageal tip. This design, however, would easily malfunction due to clogging.

The next design replaced the ball system with a simple slit cut on the closed end of the catheter. This model was nicknamed "duckbill" for its resemblance. This valve would open when air was forced through it and close due to its own elasticity when no airflow was applied. This design was successful in clinical trials and the prosthesis started to be produced and commercialized. Both designs' prototypes are shown in Figure 7.

This device was later classified as "non-indwelling", a design that could be inserted or removed by the patients themselves, contrary to the "indwelling" designs that would be introduced in the future, which required the intervention of a physician.

Not long after, flanges were added on the esophageal end of the prosthesis to avoid dislodgement. One problem of this design was that the "duckbill" valve tip length was causing problems. Being 8 mm long, it could touch the posterior wall of the esophagus and impede the valve mechanism of working. If it was longer than 8 mm, the tip would not close properly. If it was shorter, the airflow resistance was significantly higher.

To circumvent these issues, the valve mechanism had to be internalized. In 1983, the

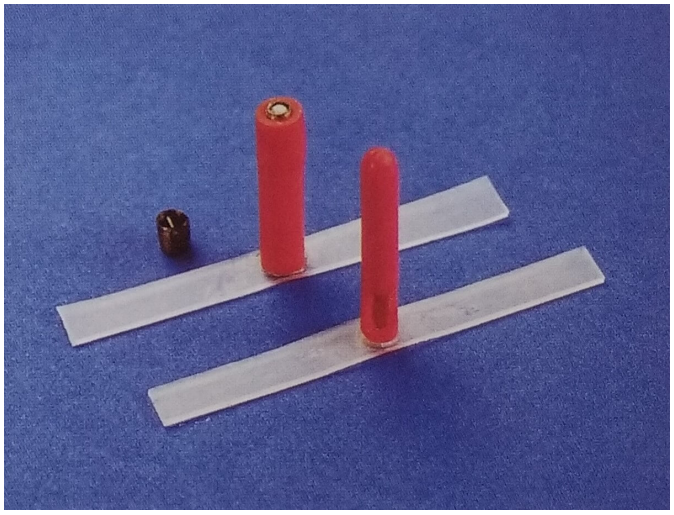

Figure 7 – Hand-fabricated prototypes, ball valve on the left and slit valve on the right (BLOM; SINGER; HAMAKER, 1998).

duckbill portion of the prosthesis was removed and the valve design was replaced by a hinged flap and was called "low-pressure" voice prosthesis (BLOM; SINGER; HAMAKER, 1998). This design went on to become very popular for voice prostheses.

Knapp and Panje (1982) developed a bi-flanged prosthesis called the Panje Voice prosthesis or voice button. It is based on the same principle as the one designed by Singer and Blom (1980). It had a slit valve similar to the duckbill, but with an extra slit perpendicular to the first one. The main advantage over the Blom-Singer prosthesis was that the device was held in place by the tracheostoma. It can be seen in a comparison of different prostheses in Figure 16.

Nijdam et al. (1982) further changed the design. Instead of a slit or hinged valve, the mechanism of the prosthesis was based on the hat on the esophageal side. Its sides pressed against the esophageal wall, closing the passage. When the air is forced through the valve, the hat's "brim" rises, as indicated by the arrows in Figure 8. They also reported that average device life was longer than those reported by the Blom-Singer and the Panje prostheses.

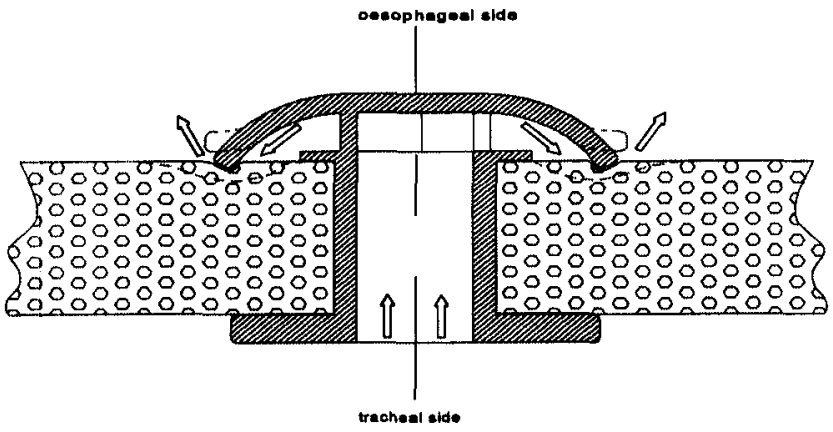

Figure 8 – Nijdam voice prosthesis (VERKERKE et al., 1997).

Karschay et al. (1986) attempted to address the limitations of the existing Blom-Singer duckbill and Panje prostheses. Their Herrmann voice prosthesis had a slit valve mechanism tilted upwards, nicknamed "tracheal chimney" for its appearance. This was done after investigations showed that the prosthesis contact with surrounding tissue had a significant impact in flow resistance. This prosthesis can be seen in Figure 16.

Hilgers and Schouwenburg (1990) presented the Atos Provox voice prosthesis developed between 1988 and 1990. It was a hinged valve, much like the Blom-Singer low-pressure design. Its geometry and dimensions can be seen in Figure 9. It became a very popular design along with the Blom-Singer classic. Moreover, it had a protective hood to avoid clogging of the valve mechanism by deviating the esophageal content from the prosthesis. It had an internal plastic ring to provide support to the soft shaft. The valve flap was also created with a pre-tension to increase the resistance to low pressure airflows and avoid leakage.

In 1996, the first indwelling Blom-Singer voice prosthesis was introduced (BLOM; SINGER; HAMAKER, 1998). It was an evolution of the non-indwelling hinged valve that was prototyped along with the "duckbill" prosthesis, but no significant differences in the mechanism were made, as depicted in Figure 10.

One year after, Hilgers and collaborators devised the Atos Provox 2 (HILGERS et al., 1997), as depicted in Figure 11. It was very similar to the original Provox from the mechanical view-

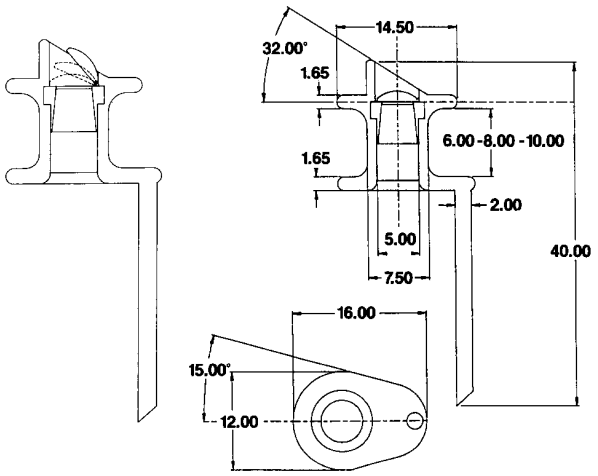

Figure 9 – Provox voice prosthesis schematics with dimensions in mm and degrees (HILGERS; CORNELISSEN; BALM, 1993).

Figure 10 – Blom-Singer classic indwelling voice prosthesis (INHEALTH TECHNOLOGIES, n.d.).

Figure 11 – Provox 2 voice prosthesis (ATOS MEDICAL, n.d.).

point. Its development was driven by the need of improving the patient's comfort during the replacement procedure.

Schouwenburg, Eerenstein and Grolman (1998) developed a new design called Voice-Master prosthesis. This prosthesis had a ball attached by springs at the esophageal end instead of the usual flange. The springs keep the ball flush against the valve tip and with airflow, the ball would be pushed out to allow air to pass through. They claimed that the valve performance was superior to other designs when tested *in-vitro* due to the shape of the valve mechanism. Instead of a hinged door that occludes most of the air path, the ball provided superior aerodynamic characteristics by only needing a very small opening. The material of the prosthesis was mostly Teflon, which prevented *Candida* growth. Some reported problems were the accumulation of debris, leakage, snapping of the suspension springs at their hinges, and incidental sticking of the ball. The main advantage of the model was its capability of being an indwelling prosthesis that was easily removed and put back on. However, this advantage also lead to one reported case of the prosthesis being swallowed by a patient (PHILIP, 2006). This prosthesis has since been discontinued.

Belforte et al. (1998) showed a newly developed Staffieri voice prosthesis. The valve principle was based on a hood that covered the esophageal tip of the prosthesis. This hood had a slit opening in the lower part of the prothesis end that allowed the air to pass through. Its mechanism can be seen in Figure 12

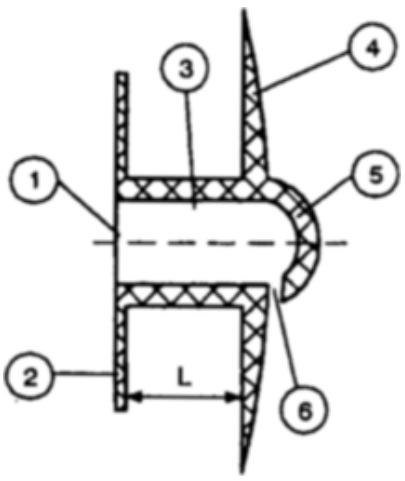

Figure 12 – Staffieri voice prosthesis (BELFORTE et al., 1998).

The Provox ActiValve was introduced by Hilgers et al. (2003) for people with reported early valve failure. This version had the same hinged valve mechanics, but it contained a magnet at the tip of the flap to increase the threshold of pressure for the opening of the flap. Unlike the Provox 2, this valve was not pre-loaded, relying only on the magnet force to keep the flap closed. After opening, the valve behaved similarly to the traditional prostheses.

The Blom-Singer Advantage (Figure 13) was created as an attempt to increase prosthesis life. The Blom-Singer classical design was working well for voice production, however, the device lifetime was shorter than desirable. This prosthesis was designed with silver oxide mixture embedded in the silicone, in order to reduce biofilm formation, which is the main cause of premature prosthesis failure (LEDER et al., 2005).

InHealth Technologies, the Blom-Singer prostheses manufacturer, developed the Blom-Singer Dual-Valve prosthesis Figure 14. The dual valve mechanism was created to prevent aspiration of liquids in case the esophageal valve failed. It uses the same simple hinge principle found in previous prostheses. This prosthesis was used for patients whose valves would fail regularly due to clogging. It required higher pressures to function, due to the double flap system. For patients who had a recurrent prosthesis failure, the device helped to alleviate the situation, at a significant price increase (BROWNLEE et al., 2018).

Hilgers et al. (2010a, 2010b) proposed the Provox Vega (Figure 15), the successor to the Provox 2. This model showcases several improvements in its design. The valve flap was inclined a few degrees to ease its opening and was brought back inside the prosthesis shaft to keep it away from esophageal content. The wall thickness of the shaft was also reduced to increase the cross sectional area further.

Figure 13 – Blom-Singer Advantage voice prosthesis (INHEALTH TECHNOLOGIES, n.d.).

(a) Blom-Singer Dual-Valve photo (INHEALTH TECHNOLOGIES, n.d.).

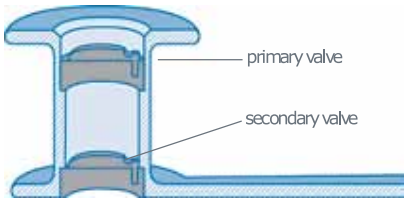

(b) Blom-Singer Dual-Valve schematics (INHEALTH TECHNOLOGIES, 2010).

Figure 14 – Blom-Singer Dual-Valve voice prosthesis

Figure 15 – Provox Vega voice prosthesis (ATOS MEDICAL, n.d.).

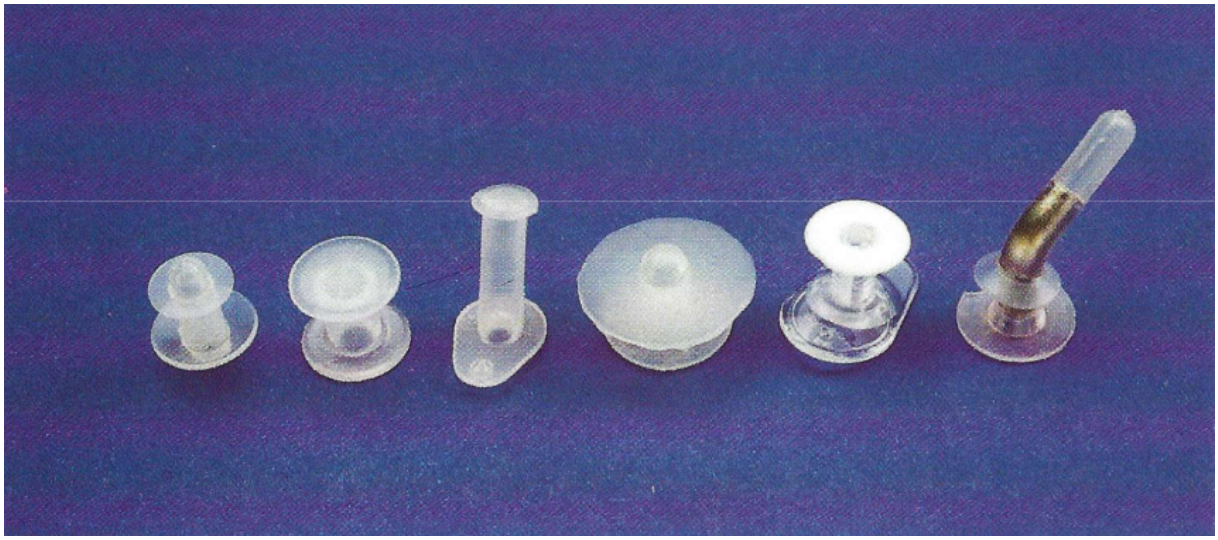

Figure 16 – Several models of voice prostheses. Left to right: Panje, Groningen, Algaba, Staffieri, Traissac, and Herrmann voice prostheses (BLOM; SINGER; HAMAKER, 1998).

In 2016, the oncologist Vishal Rao and Shashank Mahesh created the AUM voice prosthesis—nicknamed "dollar prosthesis"—, motivated by the high cost of imported European prostheses in India. It is a simple design, apparently very similar to the Blom-Singer classic indwelling prosthesis. As of 2019, it is not available for purchase and no further information has been released (INNAUMATION, n.d.).

2.3 NEWER TECHNIQUES

Despite the TE prosthesis still being considered the best approach to voice rehabilitation, other avenues are being investigated. Some have had success in recovering speech but still require further research to overtake the TE prosthesis as the *de facto* voice rehabilitation technique. These techniques include larynx transplantation, a sound-producing voice prosthesis and an artificial larynx.

In 1998 the first successful total laryngeal transplant was performed by Marshall Strome in Cleveland, Ohio, on a 40-year-old male patient who had had his larynx and pharynx crushed 20 years earlier. Three days after the surgery the patient uttered his first word in 20 years. 36 months after the surgery his voice was reported to be of good quality and natural sounding

(STROME et al., 2001). The second documented transplant was performed by Gregory Farwell in 2010 in Sacramento, California. The patient, a 52-year-old woman, underwent a laryngeal, thyroid gland, and tracheal transplantation. After the surgery the patient underwent rehabilitation for 2 months, relearning to speak and swallow. On the 13th day after the procedure, she spoke her first words in 11 years. Both patients used electrolarynges to communicate prior to the procedures (SAKALLIOGLU, 2015).

Several attempts have been made to develop a sound-producing voice prosthesis (SPVP), in order to offer patients increased voice intensity, modulation and frequency control. Early concepts relied on using a beam-like structure inside the prosthesis that would vibrate due to the airflow passing through (VAN DER TORN et al., 2001; DE VRIES et al., 2003). More recent SPVP designs tried to take advantage of the already established voice prosthesis. An insert comprised of a membrane attached to a set of masses inside a tube was developed. This would form a channel through which the airflow would excite the inner structure to an auto-oscillation that produces sound (TACK et al., 2006; VAN DER PLAATS et al., 2006; VAN DER TORN et al., 2006; TACK et al., 2007; THOMSON; TACK; VERKERKE, 2007; TACK et al., 2008). This design (Figure 17) has proven to be very successful at preliminary clinical trials, although the frequencies achieved were still high—particularly for male speakers—and the long term durability is still uncertain. A comprehensive review of the past and current state of SPVPs is given by Verkerke and Thomson (2014).

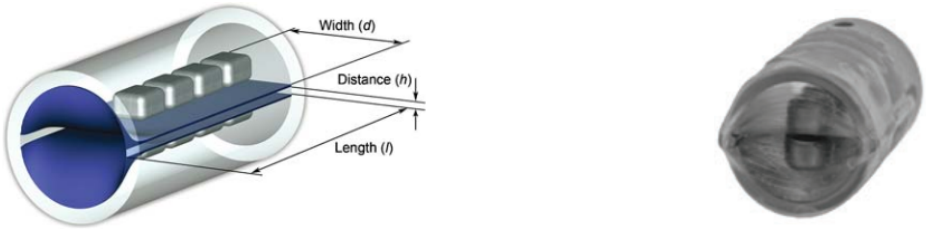

(a) (b)

Figure 17 – Membrane-element SPVP (a) schematic view (TACK et al., 2006) and (b) prototype used in clinical trials (VERKERKE; THOMSON, 2014).

Another approach was proposed by Debry et al. (2014), who developed an artificial larynx that reconnects the trachea to the pharynx. This artificial larynx is comprised of a tube made from silicone rubber and titanium, as well as a titanium cap which precludes the passage of food and liquids into the prosthesis. This cap works like the valve mechanism of the TE voice prosthesis. When the patient exhales, the cap opens allowing the air to flow through the PE segment, inducing its vibration and producing voice. The main difference occurs during inhalation. The patient does not need to undergo a tracheostomy to breath. While the curved top of the cap deflects food and liquids, its bottom is open, allowing the air to flow from the

pharynx into the artificial larynx. A design improvement has been reported in a a follow-up study (DEBRY; VRANA; DUPRET-BORIES, 2017), but the overall working mechanism remains the same. Figure 18 shows the newest iteration of this prosthesis and its components. Some remain skeptical due to medical concerns regarding accumulation of fungi and food remnants combined with feasibility of periodic removal of the prosthesis (D'ASCANIO; PIAZZA, 2017).

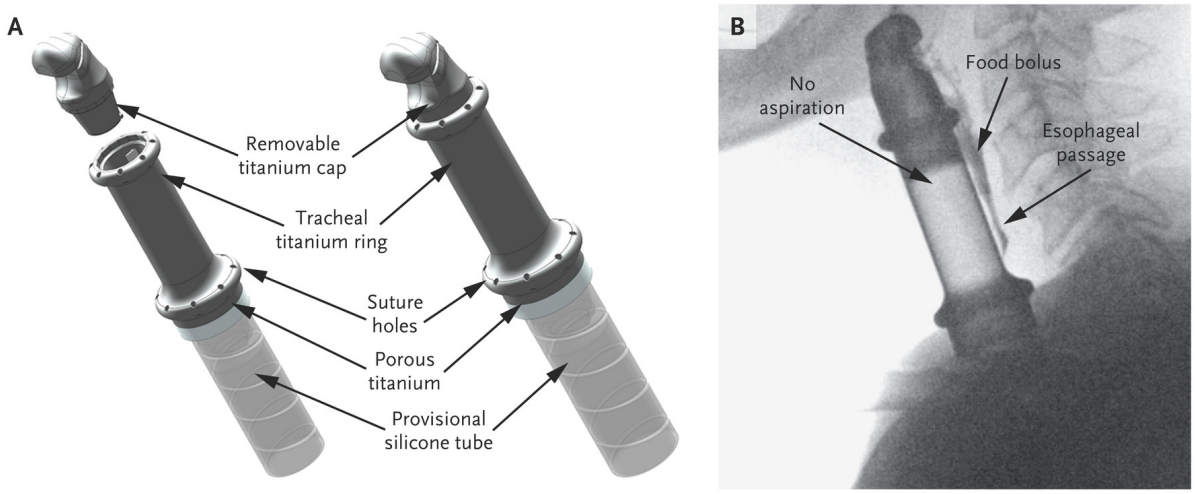

Figure 18 – Second iteration of the artificial larynx by Debry, Vrana and Dupret-Bories (2017).

2.4 EXPERIMENTAL STUDIES OF VOICE PROTHESES

To better understand what makes a good prosthesis, from the mechanical viewpoint, several studies have been performed through the years. These studies aim to characterize some particular properties or features of different prosthesis, and compare them to determine which are the most effective and why.

2.4.1 *In-vitro* studies

The most common form of experimental evaluation of a prosthesis is the relation between pressure drop between inlet and outlet and volume flow. The results are also expressed in terms of resistance to flow, defined as

$$R = \frac{\Delta P}{Q}, \tag{2.1}$$

in which ΔP is the pressure drop and Q is the volume flow of air. These experiments are usually performed with similar experimental set-ups, consisting of an airflow regulator and pressure transducers positioned up- and downstream and the prosthesis oriented along the main axis of the flow.

Hilgers, Cornelissen and Balm (1993) performed a test in order to evaluate their newly developed prosthesis against four other available prostheses. The five tested prostheses were the Provox, the Groningen low-resistance, the Groningen standard, the Blom-Singer low-resistance and the Blom-Singer duckbill. A schematic of the experimental apparatus is displayed in Figure 19, and the results are shown in Figure 20.

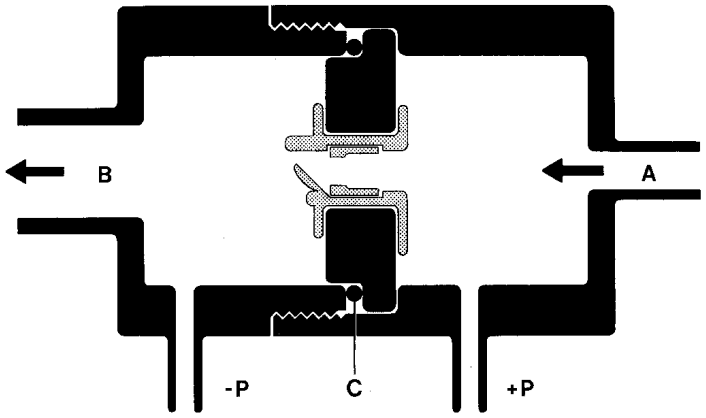

Figure 19 – Experimental set-up used by Hilgers, Cornelissen and Balm (1993).

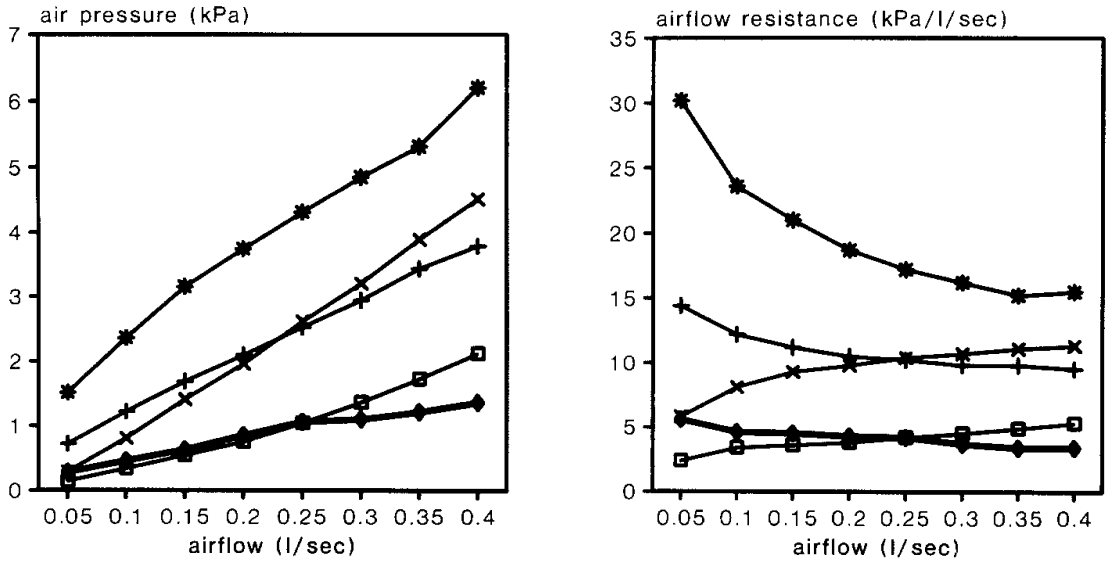

(a) (b)

Figure 20 – *In-vitro* experimental results of Hilgers, Cornelissen and Balm (1993). (a) Pressure drop by volume flow and (b) flow resistance by volume flow . ♦, Provox low-resistance prosthesis; +, Groningen low-resistance button; ∗, Groningen standard button; □, Blom-Singer low-resistance prosthesis; ×, Blom-Singer duckbill prosthesis.

Belforte et al. (1998) performed similar measurements, and were able to obtain the relations between pressure and volume flow for the Staffieri prosthesis (Figure 21). Again, the experiment was designed so that the main flow was oriented in the same direction as the main

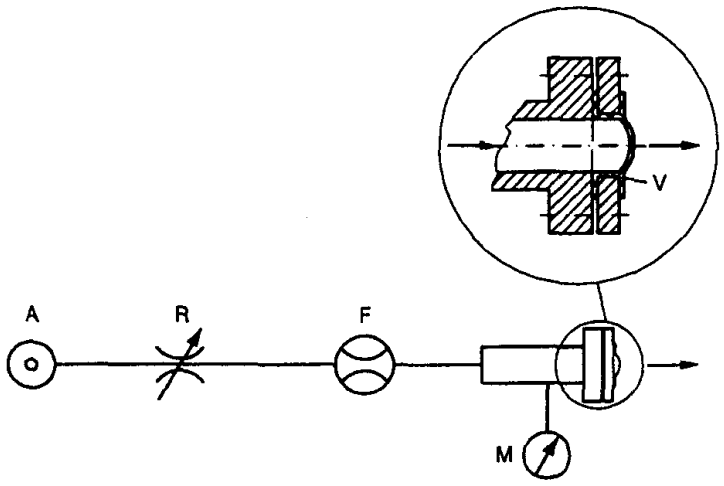

Figure 21 – Experimental set-up used by Belforte et al. (1998). A represents the airflow entrance, R is a variable resistance to the flow, F is a flow gauge and M is a manometer.

axis of the valve. Their results show the same linear trends as found by Hilgers, Cornelissen and Balm (1993), though for a different prosthesis model.

Hilgers et al. (2010b) do not provide details on the experimental set-up but they provide pressure drop by volume flow curves for the newly introduced Provox Vega models and a curve for the older Provox 2 for comparison. These are shown in Figure 22. The results show that the Provox Vega has a better performance, but there is no significant difference between the newer models and the old Provox 2. This can be explained by the fact that most of the advancements found in the newer prostheses are related to patient comfort and durability, with few improvements regarding performance.

Kress and Schäfer (2010) tested several prostheses commercially available using a simple experimental set-up to determine the relation between pressure drop and volume flow. The experimental apparatus is shown in Figure 23. Once again the prosthesis principal axis is aligned with the main flow orientation. The results are shown in Figure 24. All results, except for the Blom-Singer Dual Valve show a linear trend. The double-valve mechanism seems to impart a quadratic trend on the pressure drop. There is no significant difference between most prostheses.

Both Hilgers et al. (2010b) and Kress and Schäfer (2010) experimented on the Provox Vega 17 Fr and the Provox Vega 22.5 Fr. Figure 25 compares the results of these prostheses found in Figures 22 and 23. The results show similar trends, however, the pressure drop for high volume flows found by Kress and Schäfer (2010) is significantly higher than those found by Hilgers et al. (2010b). This could be attributed to differences in experimental setups, but, there is no information on the Hilgers et al. (2010b) equipment.

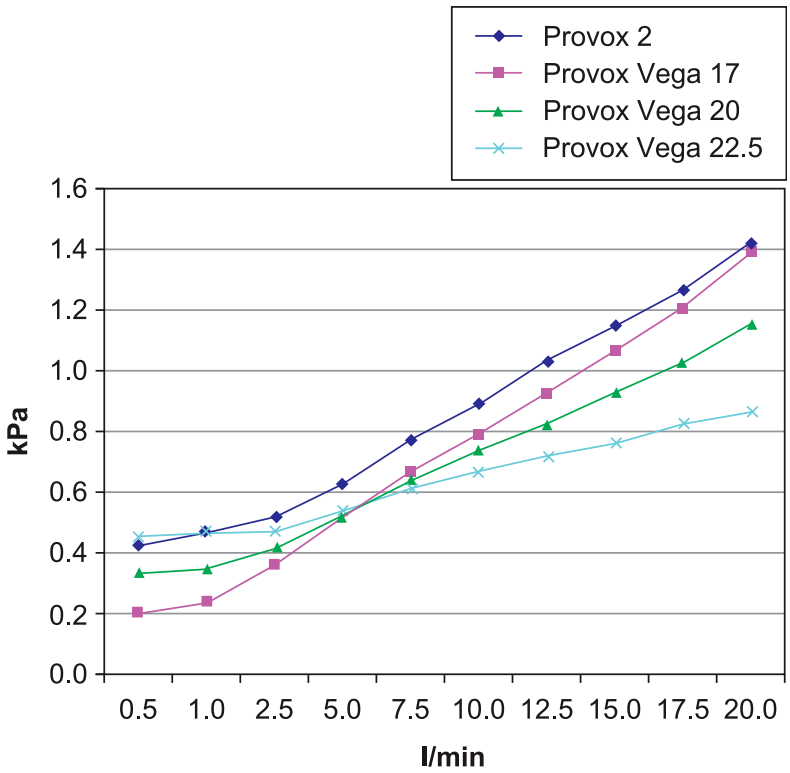

Figure 22 – Pressure drop by volume flow of the Provox 2 and the Provox Vega models (HILGERS et al., 2010b).

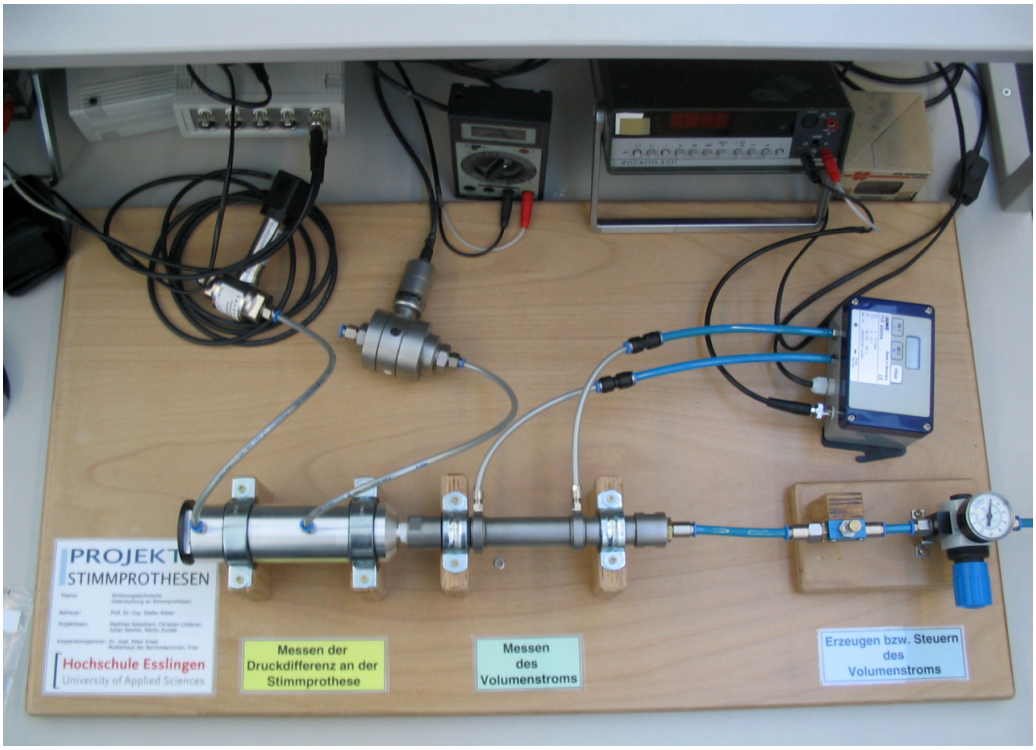

Figure 23 – Experimental set-up of Kress and Schäfer (2010).

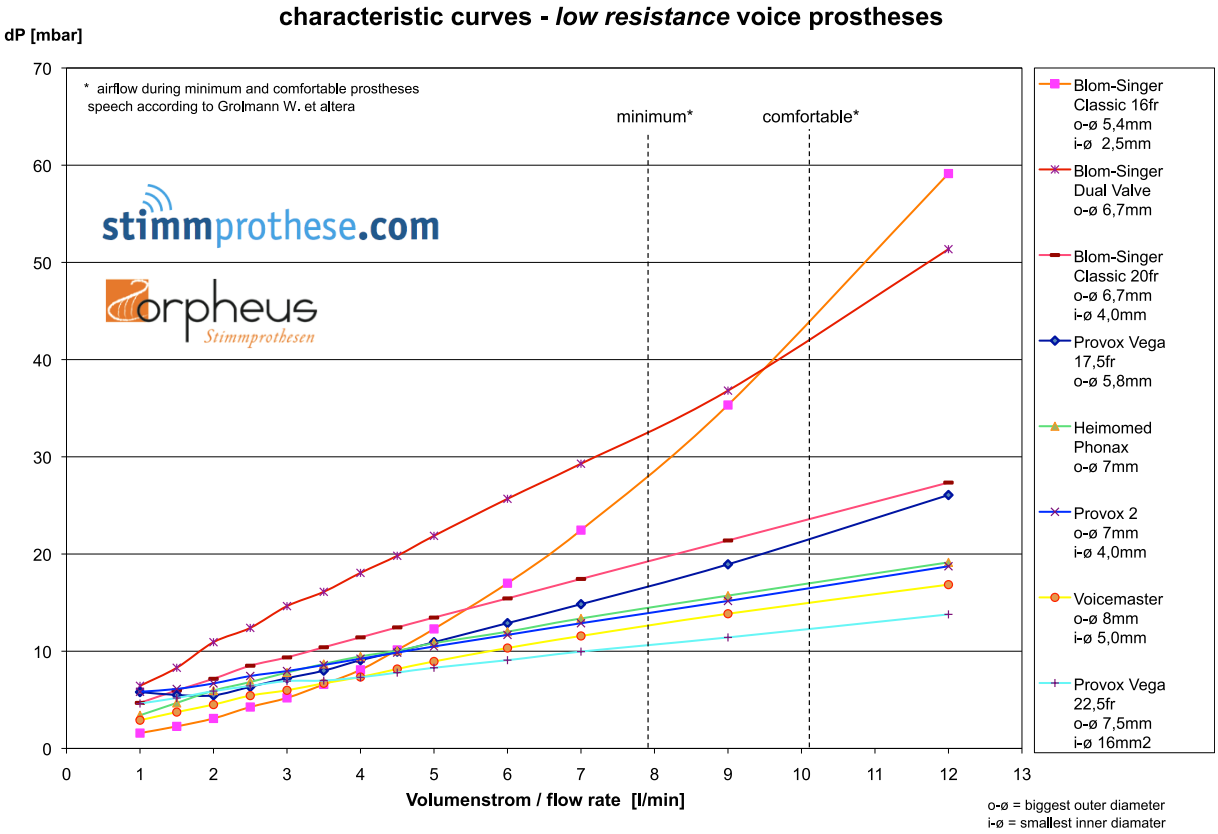

Figure 24 – Pressure drop by volume flow for low-resistance prostheses (KRESS; SCHäFER, 2010).

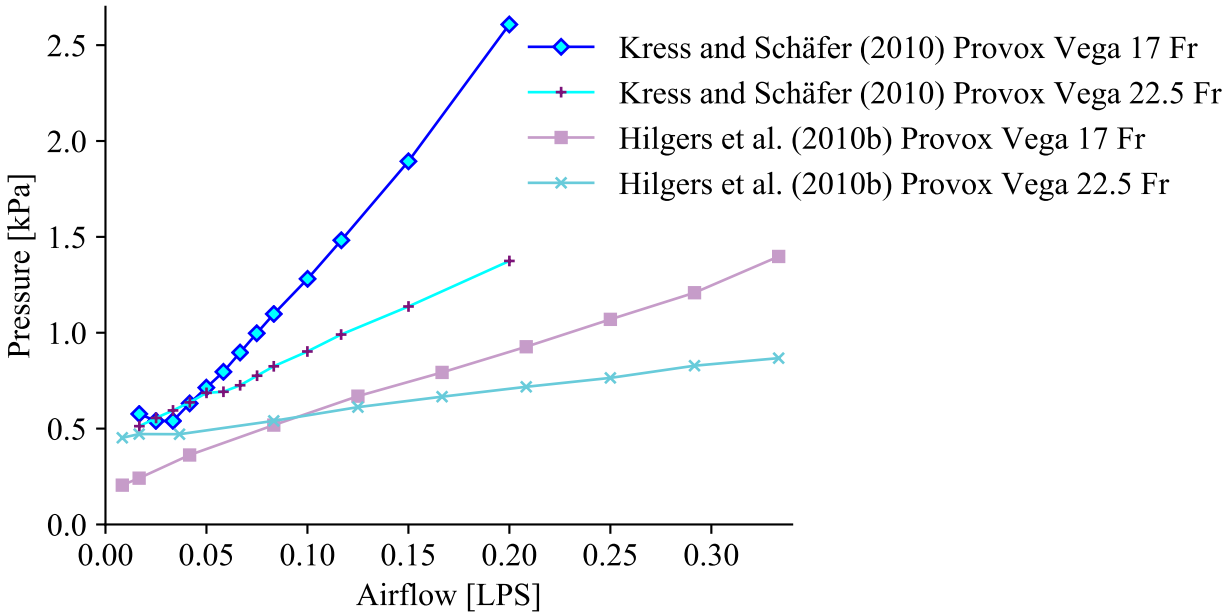

Figure 25 – Comparison of pressure drop by volume flow for Provox Vega 17 Fr and the Provox Vega 22.5 Fr by Hilgers et al. (2010b) and Kress and Schäfer (2010).

2.4.2 *In-vivo* studies

In-vivo studies attempt to understand the fundamental differences between the prosthesis in a controlled environment and during actual use, focusing on the tests that assessed trans-device pressure drop. Two such works have been found.

Van Den Hoogen et al. (1997) tested a Nijdam prosthesis with nine patients. The prosthesis valve mechanism depends on the pressure of the esophageal end on the wall between the trachea and the esophagus. That pressure could be controlled by varying prosthesis length. In order to understand the issues that could arise from wrong sized prostheses, they used added silicone rings between the tracheal flange and the tissue wall to emulate shorter prostheses with the same experimental setup. The setup is shown in Figure 26. The pressures were measured in the trachea, and in the esophagus next to the prosthesis.

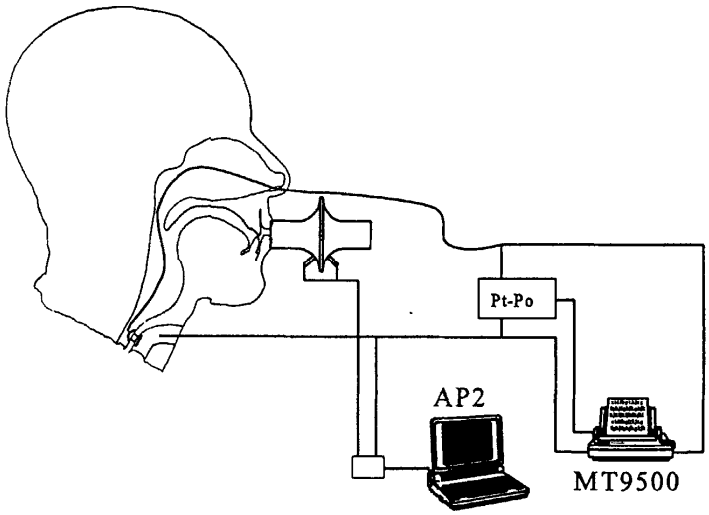

Figure 26 – Experimental set-up used by Van Den Hoogen et al. (1997).

Their results are shown in Figure 27. The plot shows the relation between pressure drop across the prosthesis and the air volume flow. Each line represents an average for all patients with a different prosthesis length.

Grolman et al. (2006) performed a study with eight patients, six men and two women. Half of them used the Provox 2 prosthesis while the other half used VoiceMaster prostheses. Their experimental setup is shown in Figure 28. The pressure was assessed inside the trachea near the tracheostoma and in the esophagus near the prosthesis esophageal end. The air volume flow was measured with a mask worn by the patients. They attempted to measure volume flow as a function of pressure for different speech efforts, varying between the minimal and maximum patient's effort to produce voice.

Their data was plotted against unpublished *in-vitro* results of five different prosthesis. We assume these results were averaged. Both data sets were fit to linear curves and are shown in

Figure 29.

The results suggest that there is a significant difference between the *in-vitro* and the *in-vivo* pressure drop. These differences could be attributed to the more complex physiological circumstances found in the *in-vivo* tests, as well as prosthesis age.

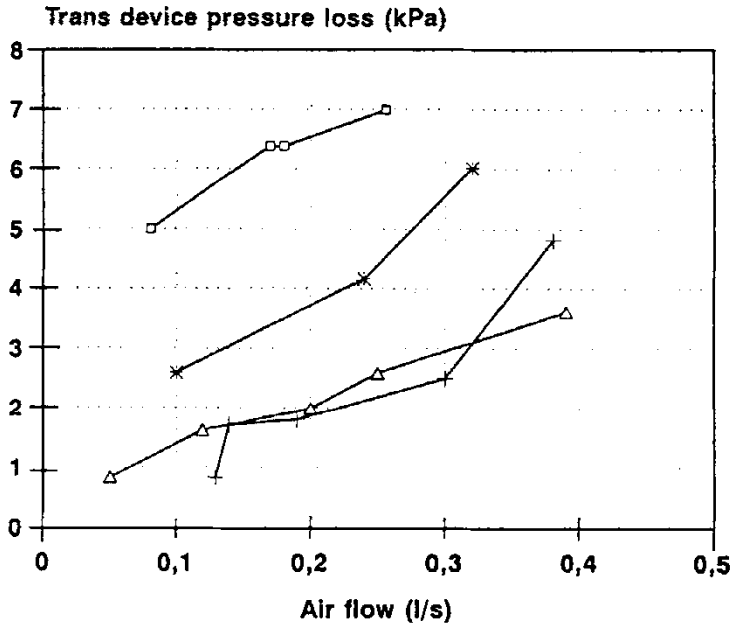

Figure 27 – Experimental results of pressure drop vs volume flow by Van Den Hoogen et al. (1997), *in-vivo*. Each line represents a different prosthesis length.

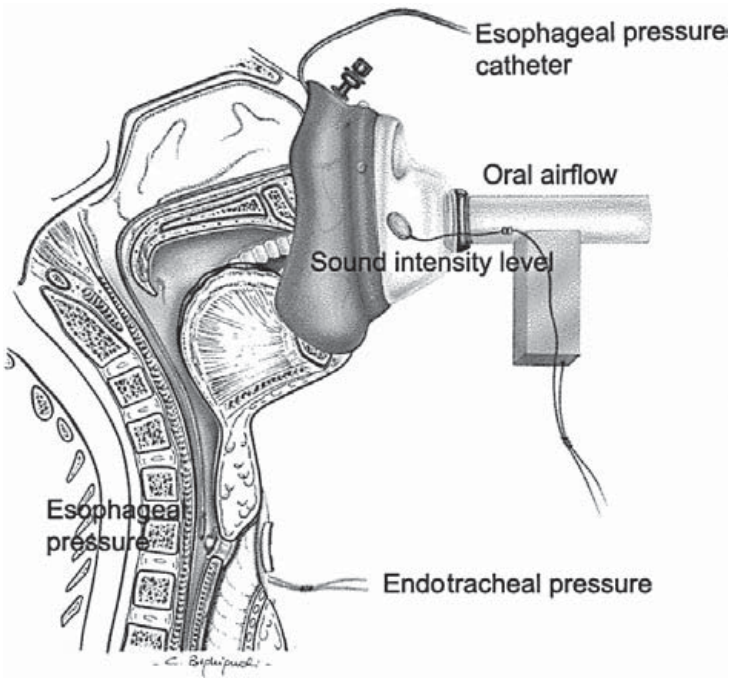

Figure 28 – Experimental set-up used by Grolman et al. (2006).

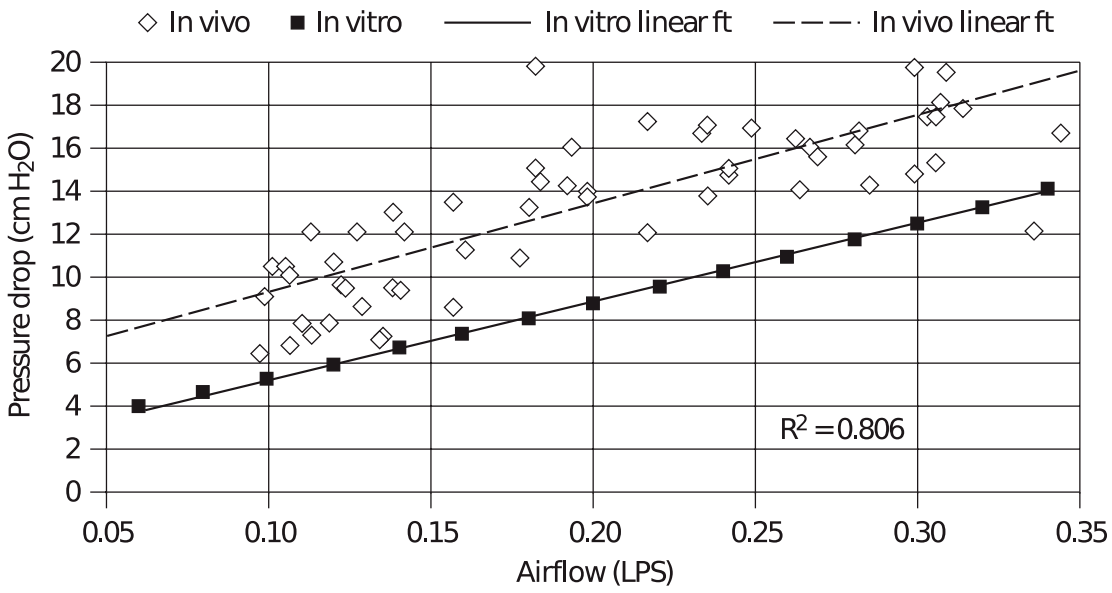

Figure 29 – Experimental results of pressure drop vs volume flow by Grolman et al. (2006), *in-vivo* and *in-vitro*.

2.4.3 Idealized tracheoesophageal system

Erath and Hemsing (2016) realized that the conventional prosthesis testing set-up could lack accuracy, mainly due to the orientation of the valve's main axis with the flow. Previous works used set-ups in which the prosthesis was positioned in-line with the airflow piping, with the prosthesis acting solely as a constriction in the flow. They hypothesized that the position of the prosthesis in relation to the flow could have a significant impact on the pressure drop. In order to understand the mechanisms behind the airflow through the TE system, they created an experimental model comprised of cylindrical tubes representing idealizations of the trachea, the prosthesis, and the esophagus, as shown in Figure 30.

The authors concluded that previous studies with the voice prosthesis aligned with the airflow did not capture the complex dynamics of TE flow, as observed in the real TE system. In the latter, a different flow phenomena is expected, such as flow detachment and vorticity, which would highly influence the pressure drop.

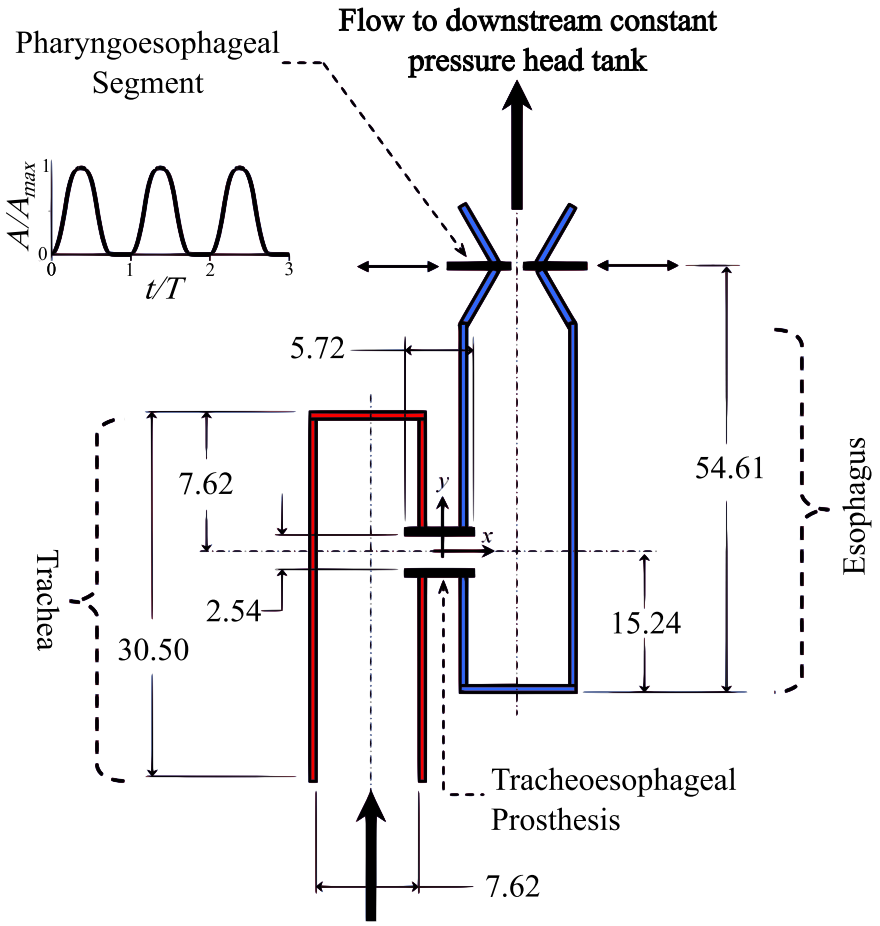

Figure 30 – Idealized tracheoesophageal model by Erath and Hemsing (2016). A is the transversal area of the idealized PE segment and t/T is the normalized time. All dimensions in cm.

2.5 VOICE PRODUCTION PARAMETERS OF TRACHEOESOPHAGEAL SPEAKERS

Several authors have compiled information on voice production parameters. These parameters, presented in Table 2, dictate under which circumstances speech can be produced, and will serve as a guideline through this work. The table presents ranges for the Reynolds number, the Strouhal number, the Mach number, the pressure drop through the TE system and the air volume flow. Many authors have obtained pressure readings for TE speakers, however, most authors focus on the endoesophageal (subglottal) pressure, P_{E}. The pressure drop given in Table 2 by Schutte (1980) and Ruty et al. (2007) are related to laryngeal speech, that is, the pressure drop across the vocal folds. Grolman et al. (2006) and Erath and Hemsing (2016) give values found for TE speakers. Searl (2019) provides a review of the literature concerning alaryngeal speech aerodynamics.

The Reynolds number, Re, a dimensionless quantity that relates the inertial forces and the viscous forces in a flow, is defined as

$$\text{Re} = \frac{\rho u L}{\mu}, \tag{2.2}$$

in which $\rho \left[\frac{\text{kg}}{\text{m}^3}\right]$ is the fluid density, $u \left[\frac{\text{m}}{\text{s}}\right]$ is the velocity, $L\,[m]$ is a linear characteristic dimension and $\mu\,[\text{Pa} \cdot \text{s}]$ is the dynamic viscosity of the fluid. It is used to determine the ratio between inertial and viscous forces, which ultimately indicates whether the flow regime is either laminar or turbulent. For internal flows, the transition point from laminar to turbulent begins at $\text{Re} = 2000$, and the flow is considered completely turbulent when $\text{Re} > 2300$ (VERSTEEG; MALALASEKERA, 2007). This means that the flows found in TE voice production range from laminar to turbulent.

The Strouhal number, St, gives the dimensionless frequency of vortex shedding,

$$\text{St} = \frac{f L}{u}, \tag{2.3}$$

in which $f \left[\frac{1}{\text{s}}\right]$ is the vortex shedding frequency. The Mach number, Ma, is

$$\text{Ma} = \frac{u}{c}, \tag{2.4}$$

in which c is the speed of sound. The Mach number represents the ratio between flow velocity and the speed of sound in the mean, and allows to determine whether the compressibility effects of a flow can be disregarded. For low Mach numbers—below $\text{Ma} = 0.3$—fluid flow models can be assumed incompressible (FOX et al., 2016).

With the exception of those provided by Ruty et al. (2007) and Erath and Hemsing (2016), the Reynolds and Mach numbers of Table 2 were obtained using Equations 2.2 and 2.4. Given the volume flow $Q = \bar{u}A$, the mean velocity $\bar{u}$ can be found by

$$\bar{u} = \frac{Q}{A},$$

in which A is the cross-sectional area of the prosthesis. The necessary air properties at $30°\text{C}$ are, air density, $\rho_{air} = 1.169$ kg/m^3, dynamic viscosity, and $\mu_{air} = 1.869 \cdot 10^{-5}$ Pa·s, and speed of sound, $c = 349$ m/s (BELL et al., 2014).

Table 2 – Usual voice parameters as compiled by several authors.

	Re	St	Ma	ΔP [kPa]	Q [LPS]
Schutte (1980)[a]	700–5500[b]		0.007–0.050[c]	0.20–3.00	0.045–0.350
Moon and Weinberg (1987)	550–9200[b]		0.005–0.088[c]		0.035–0.577
Motta, Galli and Di Rienzo (2001)	310-955[b]		0.012–0.036[c]		0.078–0.240
Grolman et al. (2006)	1600–5500[b]		0.015–0.050[c]	0.70–2.00	0.100–0.350
Ruty et al. (2007)[a]	700–1300	0.01–0.02	0.060–0.120	0.30–1.00	
Erath and Hemsing (2016)	O(10^3)–O(10^4)	O(10^{-2})–O(10^0)		0.98–3.92	

[a] Reported for laryngeal speakers

[b] Approximated from the volume flow considering a prosthesis diameter of 5 mm, $\rho_{air} = 1.169$ kg/m^3, and $\mu_{air} = 1.869 \cdot 10^{-5}$ Pa·s.

[c] Approximated from the volume flow considering a prosthesis diameter of 5 mm and the speed of sound on air $c = 349$ m/s

2.6 DISCUSSION

While several TE voice prostheses have been developed through the years, the mechanism of the classical indwelling voice prosthesis created by Singer and Blom remains the most popular in voice prostheses. Despite the differences, some prostheses are so similarly designed to the point of being interchangeable (VAN DEN HOOGEN et al., 1996).

Blom (1988) addresses the particular shortcomings of the duckbill prosthesis, but several of these observations still remain relevant for modern prostheses, such as the need for the prosthesis to be kept in place and how the overall size of the prosthesis and puncture position will impact insertion and removal. They also raise concerns on materials used, arguing that despite the qualities of silicone rubber, it is has limited durability and high adherence to certain *Candida* growths. However, more durable materials such as stainless steel and titanium were too heavy and could not be supported long-term by the TE fistula. Blom (2003) also comment on the ever increasing size of prosthesis diameter and its consequences, such as increase leakage due to enlargement of the TE fistula and using larger prostheses to combat this issue. Initial prostheses were made using a 16 Fr (approx. 5 mm) catheter, while current prostheses sit between 20–23 Fr (6.7–7.7 mm). The optimal diameter for the prosthesis is still the subject of scientific discussion.

Brown et al. (2003) show that there is no significant difference between non-indwelling and indwelling voice prostheses in matters of voice quality and voice production. As for prosthesis maintenance, there is an overall patient preference for the indwelling prosthesis type.

Several prostheses models are seemingly discontinued or didn't make it even past the first studies phase. About prostheses like the Traissac/Newvoxx (in Figure 16), the Adeva Bigflow, and the Heimomed Phonax little to no information is readily available.

There is a significant amount of *in-vitro* research for these prostheses. Most are very similar and produce similar results, showing that for hinged flap prostheses, the relation between volume flow and pressure drop is fairly linear. However, it is important to note that no attempts to perform *in-vitro* tests on prostheses while using a testing apparatus that approximate the human TE system have been found. On the other hand, the amount of *in-vivo* results for trans-device pressure is limited. To the author's knowledge, no works have attempted to numerically simulate the fluid flow inside the TE segment.

From the parameters presented in Section 2.5, we can reasonably assume that, for the displayed Reynolds number range, a model of TE voice flow will require turbulence modeling. On the other hand, the Mach number range shows that an incompressible model is a reasonable approximation. The pressure drops are less straightforward, because several authors only relay the pressure measured inside the trachea, or the subglottal pressure inside the esophagus.

3 COMPUTATIONAL PROCEDURES

To further explore physics in voice productions with voice prostheses, numerical tools were developed, which allowed to better understand the phenomena that occurs in the tracheoesophageal system. This approach allows for a better understanding of the flow that occurs inside the system. With *in-vivo* and *in-vitro* models, it is not possible to observe certain aspects of the flow, for instance, inside the prosthesis or inside the PE segment. By using computational methods, geometry variations and different boundary conditions are explored with ease, not restrained by experimental procedure limitations. The method most traditionally associated with Computational Fluid Dynamics (CFD) is the Finite Volume Method (FVM). The FVM is a widely used method for many applications. It has been developed for decades, and has been thoroughly researched and validated (VERSTEEG; MALALASEKERA, 2007).

3.1 COMPUTATIONAL METHOD

As the model parameters are expected to fall within the range of values given in Section 2.5, it is reasonable to assume from the Mach number that there is no need to consider compressibility issues. On the other hand, the Reynolds number range means that the model will require turbulence modeling. To model the problem, an incompressible segregated flow solver was used, for both steady and unsteady situations. The turbulence modeling was achieved by using a Reynolds-Averaged Navier-Stokes (RANS) two-layer realizable k-ϵ model.

3.1.1 Computational models

The FVM is a method for solving partial differential equations and consists in dividing the domain in a finite number of control volumes, in which the conservation laws must be satisfied. Each volume corresponds to a cell in a computational grid. This results in a set of linear equations, the same amount as the number of cells. When dealing with time dependent problems, the time can also be subdivided into time-steps. A full description of the method can be found in Versteeg and Malalasekera (2007) and SIEMENS (2016). It was selected for this work for its availability and ease of use.

Recalling Equation 2.2, the Reynolds number is defined as

$$\mathrm{Re} = \frac{\rho u L}{\mu}.$$

As discussed in Section 2.5, a Reynolds number greater than 2300 means that a viscous flow inside pipes with low Mach numbers is usually turbulent. Since the Reynolds number of the experiment falls within the turbulent range, turbulence modeling is required.

The experimental velocity fields were phase-averaged in time in order to obtain a mean velocity field. In a computational domain the Reynolds-Averaged Navier-Stokes (RANS) can be considered the analogous model when applied to a time dependent simulation. In the RANS model, all flow quantities are decomposed into a mean value and its fluctuation. This approach has been a mainstay of CFD for over the last three decades. (VERSTEEG; MALALASEKERA, 2007)

In order to properly solve the fluctuation part of the RANS equations, a turbulence model is needed. The k-ϵ turbulence model is a two-equation model that solves the equations for the turbulent kinetic energy and the turbulent dissipation rate. There are several approaches for the k-ϵ model.

Since the interest lies in the phenomena that occur near the wall, it is necessary to use a method that allows for the flow to be properly solved near the wall in the boundary layer region. The two-layer approach, first suggested by Rodi (1991) fulfills this criteria. In this approach, the region next to the wall has the turbulent dissipation rate and the turbulent viscosity formulated as functions of the wall distance and are blended smoothly with the layer far from the wall. The equation for the turbulent kinetic energy is solved across the entire flow domain. The realizable model adds an equation for the turbulent dissipation rate (SIEMENS, 2016).

In order to make use of the capabilities of the model and solve the flow near the wall, we must make sure that the mesh being used is adequate. To do so, a dimensionless quantity known as the dimensionless wall distance, y^+, is used. It gives a parameter to which one can evaluate the mesh near the wall. The y^+ is defined as

$$y^+ = \frac{y u_\tau}{\nu}, \tag{3.1}$$

where u_τ is the friction velocity, y is the absolute distance from the wall, and ν is the kinematic viscosity, defined as $\nu = \mu/\rho$.

Versteeg and Malalasekera (2007) give the friction velocity

$$u_\tau = \sqrt{\frac{\tau_{\text{wall}}}{\rho}}, \tag{3.2}$$

and the wall shear stress, τ_{wall}, as

$$\tau_{\text{wall}} = \frac{C_{\text{f}} \rho u_\infty^2}{2}, \tag{3.3}$$

with C_{f} being the skin friction coefficient. This coefficient is usually obtained using empirical

correlations found in the literature. Schlichting (1979) gives

$$C_{\mathrm{f}} = \left[2\log_{10}\left(\mathrm{Re}_x\right) - 0.65\right]^{-2.3}, \tag{3.4}$$

for Re $< 10^9$.

In order to properly model the boundary layer one needs to obtain a value of $y^+ \approx 1$.

3.1.2 Star-CCM+

STAR-CCM+ is a Computer-Aided Engineering (CAE) software for solving multidisciplinary problems in both fluid and solid continuum mechanics, within a single integrated user interface (SIEMENS, 2016).

It allows the user to import geometries, generate surface and volume meshes, solve the governing equations, and post-process the results.

3.2 IDEALIZED TRACHEOESOPHAGEAL MODEL

Erath and Hemsing (2016) developed an experimental procedure to analyze the flow through an idealized model of the TE system. They used a Particle Image Velocimetry (PIV) method to obtain the velocities of the fluid flowing through the idealized system. In order to be able to visualize the flow structures inside the system, the components—the trachea, the esophagus, and the prosthesis—were represented by straight cylinders and water was used as the fluid medium. Figure 30 shows the idealized model and its dimensions. The set-up was designed on a scale of 3.5:1. The flow was controlled by two constant pressure head tanks, keeping a pressure difference of 1000 Pa in the system. The idealized PE segment had a gate system to mimic the fluctuation of pressure caused by its vibration by gradually opening and closing the constriction during each cycle. The plot at the top-left of Figure 30 shows the area ratio of the PE segment at given times during the opening and closing cycle.

To simulate this set-up, a computational mesh based on the dimensions displayed in Figure 30 and the information provided by Erath and Hemsing (2016) was created. The solid model is shown in Figure 31.

The boundary condition was set as a pressure difference between the inlet and the outlet of the system. Markόw et al. (2017) show that the area of the glottic opening correlates inversely to the pressure drop across the vocal folds. In order to simulate the area ratio change, a constant pressure in the inlet and a variable pressure in the outlet was used. Figure 32a shows a reproduction of the inset plot of Figure 30, giving the area ratio versus time that was imposed on the idealized PE segment. Figure 32b shows the pressure versus time that was applied to the

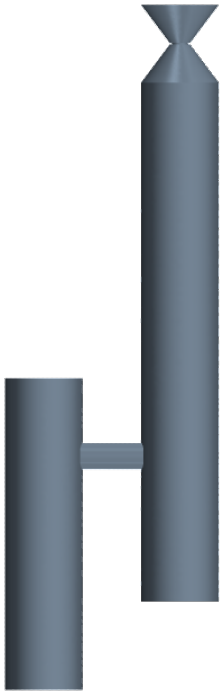

Figure 31 – CAD model of the idealized TE system.

outlet boundary condition. As mentioned, the area ratio and the pressure are inversely related. To obtain the pressure curve, the area ratio curve was flipped upside down and squared; this square relationship was established through preliminary simulations. This yielded a normalized pressure curve, which was then multiplied by 1000 Pa to obtain the actual boundary condition.

In the experiments carried out by Erath and Hemsing (2016) three visualization planes were defined, which are depicted in Figure 33. These planes were analogous to the conventional anatomical planes found in Figure 1. However, they were defined only in the trachea region next to the prosthesis. To compare the results obtained in the simulation with the literature's experimental results, the numerical data was extracted at the same locations. Due to the limitations of the PIV used in the experiment, the velocities are only obtained in the in-plane configuration. Out-of-plane components could not be captured.

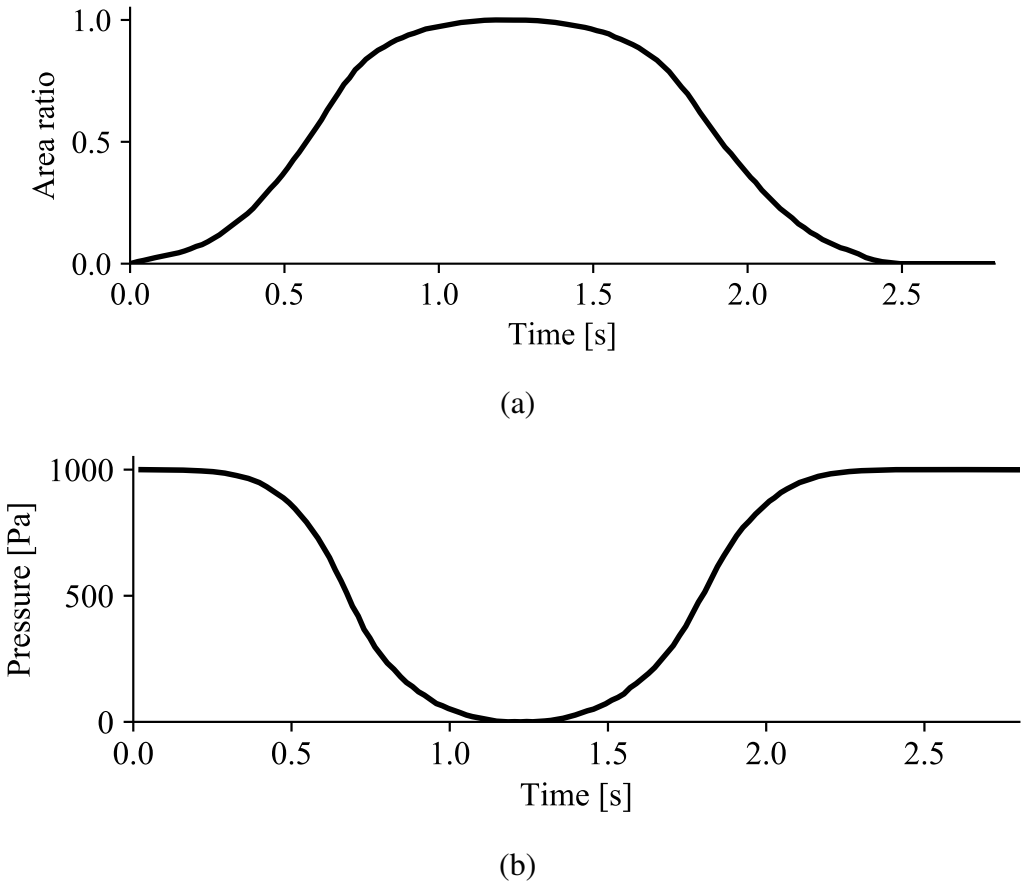

Figure 32 – Variation of (a) area ratio $\left(\frac{A}{A_{max}}\right)$ and (b) pressure at the outlet vs time.

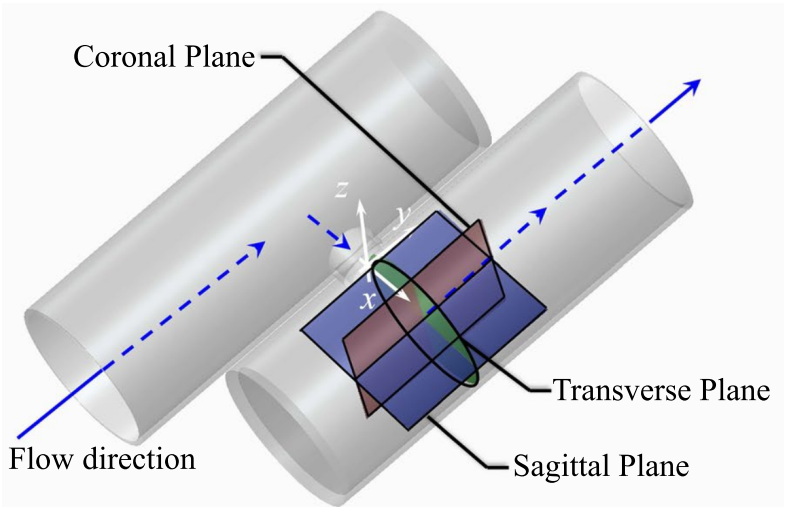

Figure 33 – Experimental visualization planes of Erath and Hemsing (2016).

In order to assure mesh independence, a convergence analysis was carried out. To perform the analysis, several meshes with decreasing volume sizes—and consequently, higher cell counts—were created. For each mesh size, a control variable was computed to be compared for different mesh refinements. In this case, the velocity was chosen. After the first simulation, each subsequent computed velocity was compared to the velocity obtained with the preceding mesh, until a the solution became mesh independent and satisfactory mesh was achieved.

In the test, a steady-state model that would yield the highest velocities was used. That is, the boundary conditions were set to the maximum pressure difference in our range, 1000 Pa.

3.3.1 Mesh convergence

Two types of mesh were tested, tetrahedral and polyhedral. Both types perform well with arbitrary geometries. By using a set of reference dimensions, the meshing tool of the software generated a mesh for each. Table 3 shows the information for each tested mesh, including type, reference dimension and the total cell count for the domain.

Table 3 – Mesh details for convergence analysis.

Type	Reference dimension	Cell count	Vertices
Tetrahedral	20mm	166990	65343
	15mm	200316	77410
	10mm	241459	92396
	7.5mm	298235	111622
	5.0mm	718514	236048
	4.0mm	1150026	365133
Polyhedral	7.5mm	115573	321317
	5.0mm	239026	748124
	4.0mm	330189	1055391

For each mesh, the x-velocity profiles on the y- and z-axes at the prosthesis exit were computed. Then, the velocity at the center point of each profile was extracted and plotted against the cell count in Figure 34. Both types of mesh achieve convergence within the range displayed in Table 3; however, the polyhedral mesh reaches convergence levels with a significantly lower cell count, which leads to a better overall performance. For the simulations, the Polyhedral mesh with the 0.50 cm reference dimension was selected. This choice is based on the performance

and results of all the meshes. The velocity profiles of u_x in the y- and z-axes are displayed in Figure 35. The two meshes produce very similar velocity profiles, with the tetrahedral mesh giving a slightly higher velocity.

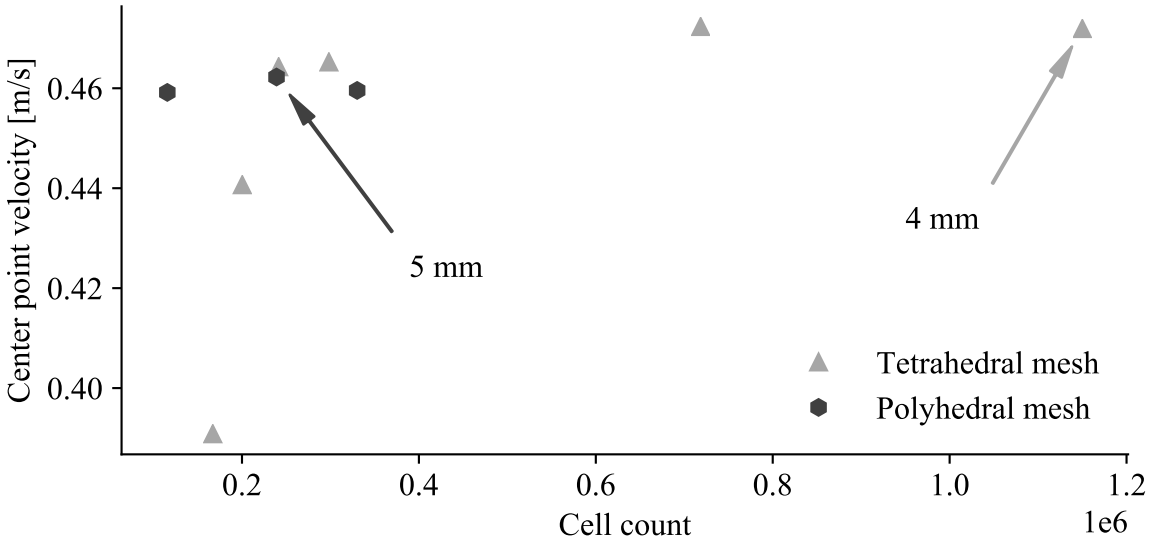

Figure 34 – Comparison of velocity at the center point of the prosthesis for each mesh.

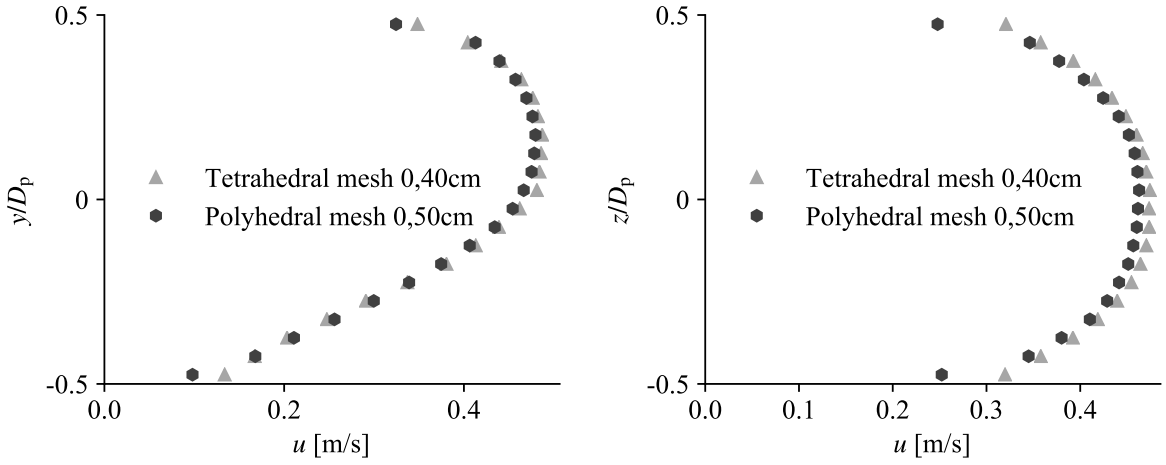

Figure 35 – Velocity u_x (a) in the sagittal (x-y) plane and (b) in the transverse (x-z) plane.

With the mesh size established, it is necessary to determine a time-step length that would allow the correct modeling of the flow while maintaining reasonable processing times. The chosen time-step was $\Delta t = 0.001$ s with 10 iterations per time-step, small enough to properly model the flow and with enough inner iterations to allow the convergence of each time-step.

The relations described in Equation (3.1) were used to determine the prism layer mesh that would allow us to capture the boundary-layer. For water at room temperature, the density

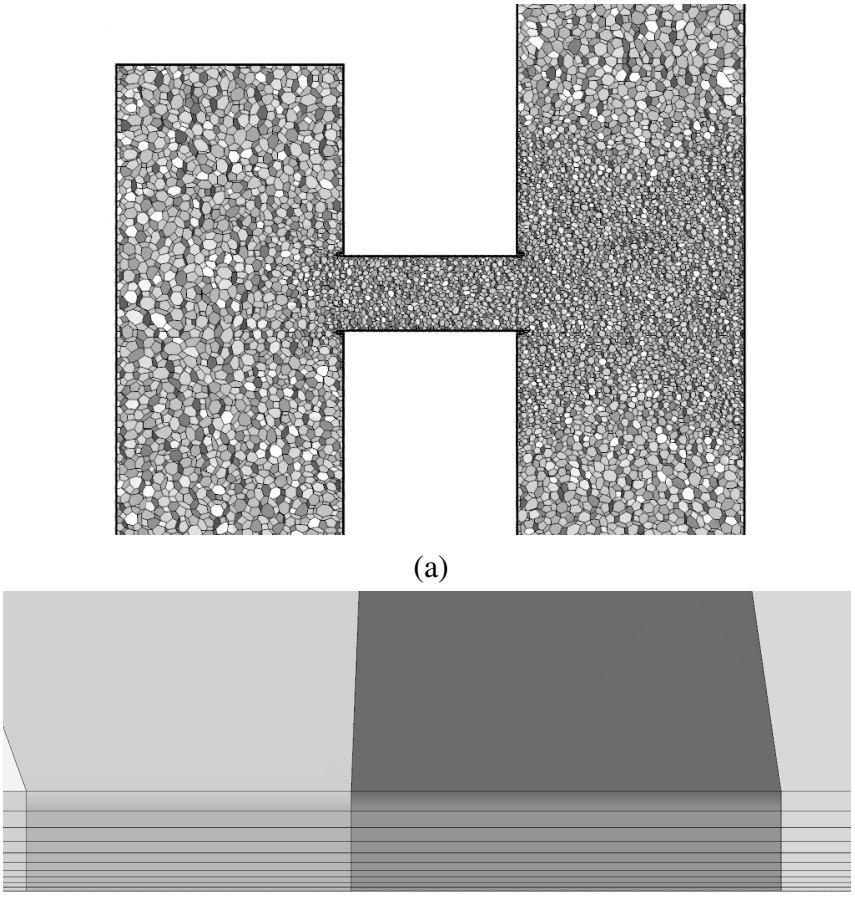

(a)

(b)

Figure 36 – Sagittal view of the (a) final polyhedral mesh and (b) mesh prism layer detail.

is $\rho_{\text{water}} = 998.3$ kg/m^3, and the dynamic viscosity is $\mu_{\text{water}} = 1.0139 \cdot 10^{-3}$ Pa·s (BELL et al., 2014). The characteristic dimension was considered to be the prosthesis diameter, $D_{\text{p}} = 25.4 \cdot 10^{-3}$ m. Erath and Hemsing (2016) mention a peak velocity of 0.6 m/s, to avoid underestimation of the freestream velocity and obtain a value of y^+ greater than 1, the expected freestream velocity was set to 0.5 m/s. This yielded a Reynolds number of 12657.

With these values, the required wall distance for the first mesh layer is $2.93 \cdot 10^{-5}$ m. With 10 layers, a stretch factor of 1.2 and a total prism layer thickness of $5 \cdot 10^{-4}$ m, the obtained first layer had a thickness of of $1.92 \cdot 10^{-5}$ m.

The initial conditions for the steady state simulations were set to $P = 0$ Pa and $u = 0$ m/s. For the transient analysis, the steady state solutions were used as initial conditions.

3.4 COMPARISON WITH LITERATURE RESULTS

Flow velocities were extracted from the numerical model and processed to be plotted on a vector field. The vorticity was calculated and then plotted on a contour map on top of the veloc-

ity vectors. In a two-dimensional field, the vorticity is computed parallel to the orthogonal axis. Following the orientation in Figure 33, in the transverse plane (x-z) the vorticity coordinate is on the y-axis. The vorticity in a two-dimensional field is given by

$$\vec{\omega} = \left(\frac{\partial u_z}{\partial x} - \frac{\partial u_x}{\partial z} \right) \vec{y}, \tag{3.5}$$

in which u_x and u_z are the flow velocities obtained in the x-z-plane (transverse plane). The results were then compared to the experimental results obtained by Erath and Hemsing (2016).

3.4.1 Transverse plane

The transverse plane was positioned at the center of the prosthesis diameter, as indicated in Figure 33. Figure 37 shows transverse plane velocities for eight time-steps. The distances are given in relation to the prosthesis diameter, D_p. The flow forms a jet that leaves the prosthesis and hits the far-side of the esophagus, creating some recirculation zones on both sides of the jet that dissipate quickly as the boundary conditions approaches the end of the cycle. The flow structure in this plane is very symmetrical, as expected, for a cylindrical tube with the flow entering with no asymmetry.

The numerical approach captures the phenomena very well, there is a very good agreement on the formation of the jet structures and the velocity field. The numerical model yielded lower velocities and vorticities when compared to the literature experimental results. To compare them side-by-side, the numerical values were normalized dividing by 3, and the experimental values were normalized dividing by 4. The different normalization value could be associated with approximation of the boundary condition to a fluctuating pressure instead of the variation of area constrictions, as well as the exact geometry of the idealized PE segment.

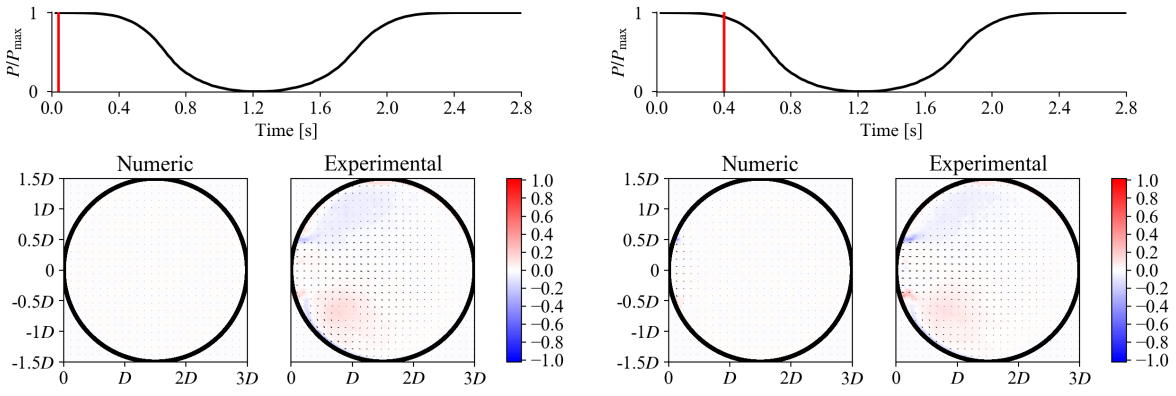

(a) 0.04 s

(b) 0.40 s

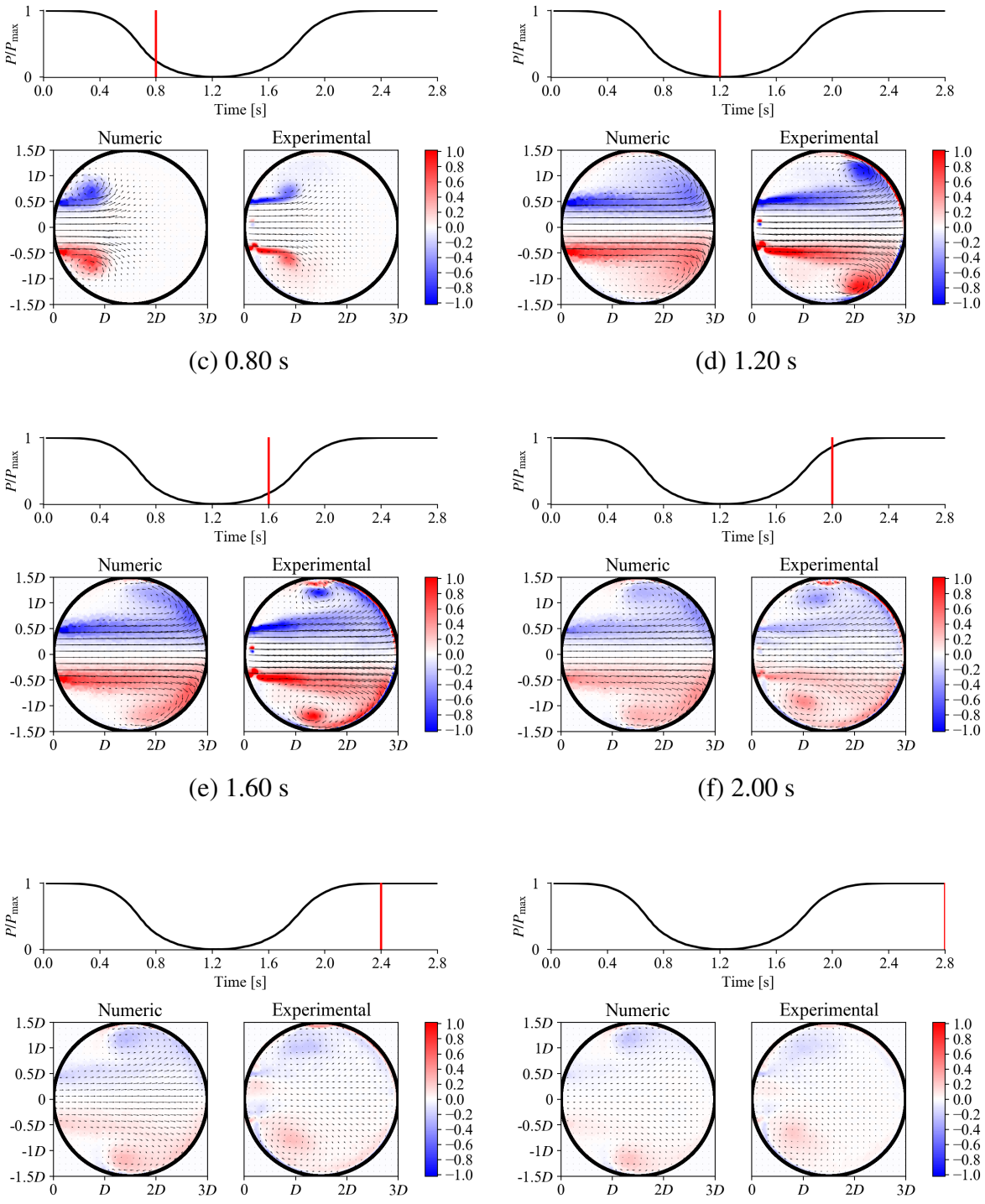

(c) 0.80 s (d) 1.20 s

(e) 1.60 s (f) 2.00 s

(g) 2.40 s (h) 2.80 s

Figure 37 – Transverse plane velocities, u_x and u_z , and vorticities, $\vec{\omega_y}$.

3.4.2 Sagittal plane

Figure 38 shows the results of u_x, u_y, and $\vec{\omega_z}$ obtained in the sagittal plane at the same eight instants showcased for the transverse plane (Figure 37). The same representations are applied. The jet formation is very similar, with the jet coming straight out of the prosthesis and

hitting the posterior esophageal wall. When the vortex structures of the jet hit the wall, they travel up and down, stretching the vortexes and causing recirculation of flow both above and below the jet. The positive vortex (red in Figure 38) travels upwards towards the PE segment far above. The negative vortex (blue in Figure 38) travels toward the bottom end of the esophagus where the path is much shorter, causing a recirculation to occur and interact with the jet. This causes the jet to tilt slightly up in the direction of the PE segment. This can be noticed in the sequence of Figures 38d, 38e, and 38f, in which the velocity vectors above the jet have little to no velocity in the negative y direction, while the velocity vectors below the jet form a recirculation zone. Again there is a good agreement between the numeric and the literature's experimental results.

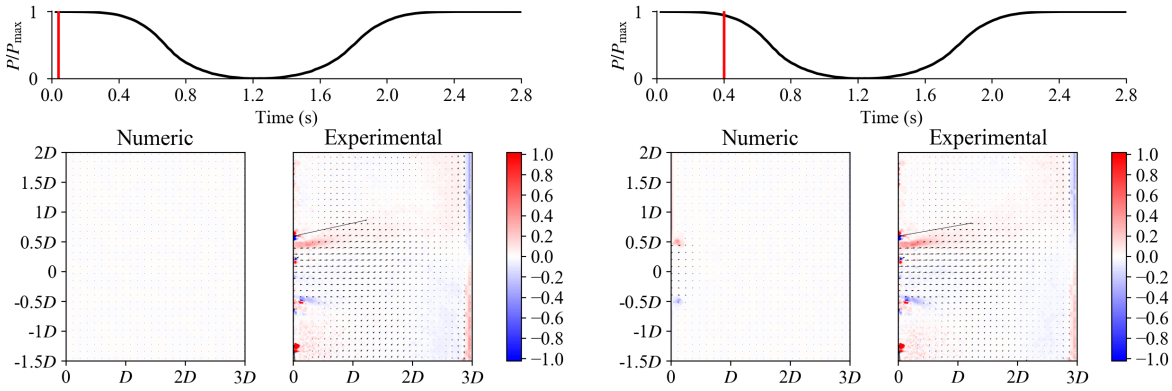

(a) 0.04 s

(b) 0.40 s

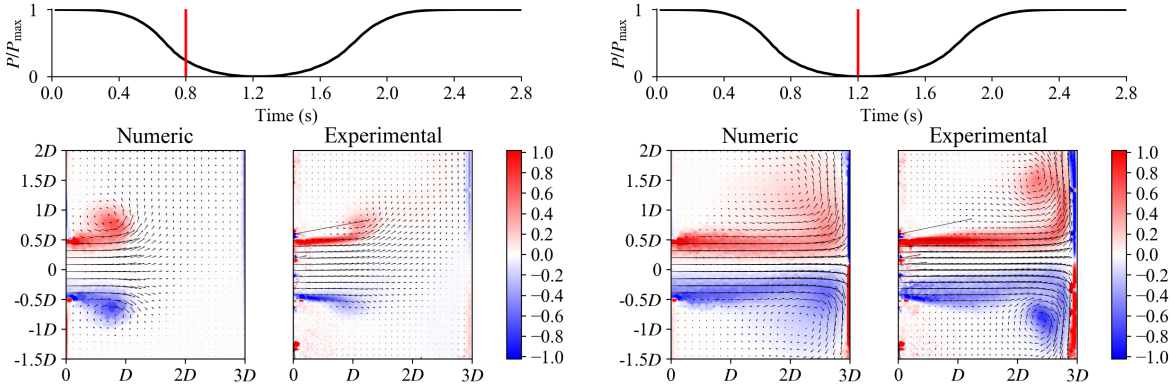

(c) 0.80 s

(d) 1.20 s

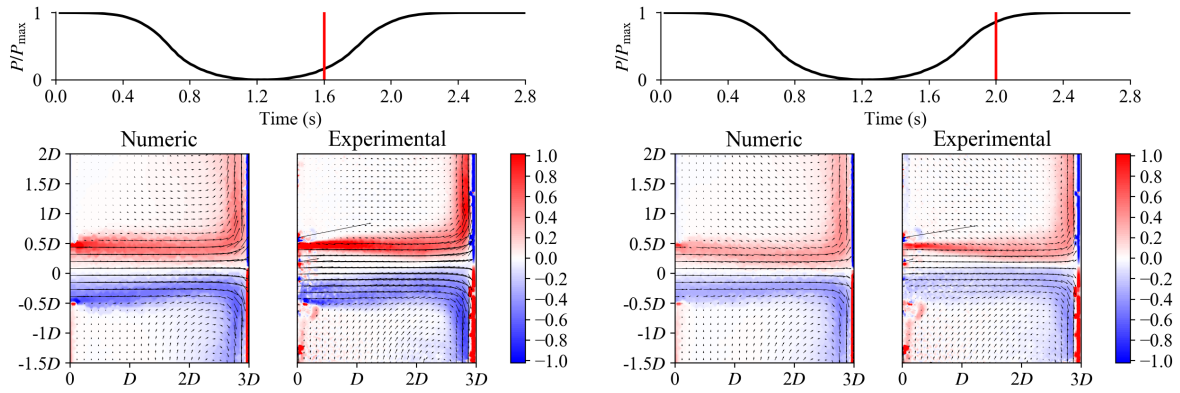

(e) 1.60 s (f) 2.00 s

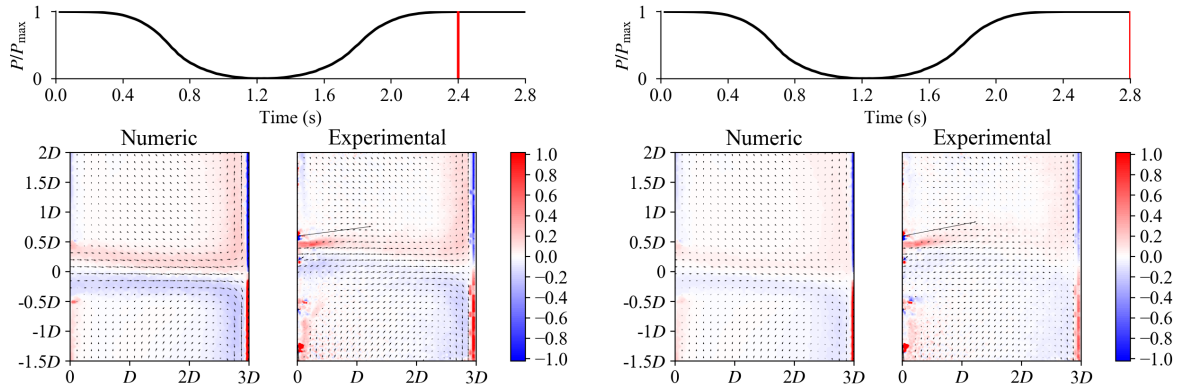

(g) 2.40 s (h) 2.80 s

Figure 38 – Sagittal plane velocities, u_x and u_y , and vorticities, $\vec{\omega_z}$.

3.4.3 Coronal plane

Figure 39 shows the results of u_y and u_z, $\vec{\omega_x}$ for the eight time-steps for the coronal plane. Once again the velocity vectors are plotted on top of the vorticity contour map. There is a significant amount of noise in the experimental results, especially close to the esophageal walls. This happens due to the bulk of the velocity being normal to the coronal plane. While the overall structure of the flow appears to be similar, with the vorticity contour showing positive and negative values at roughly the same positions, the flows appear to be out-of-phase. This happens due to the imprecisions related to the manual positioning of the measuring plane in the experimental model, while in the computer model the data can be extracted at exact positions.

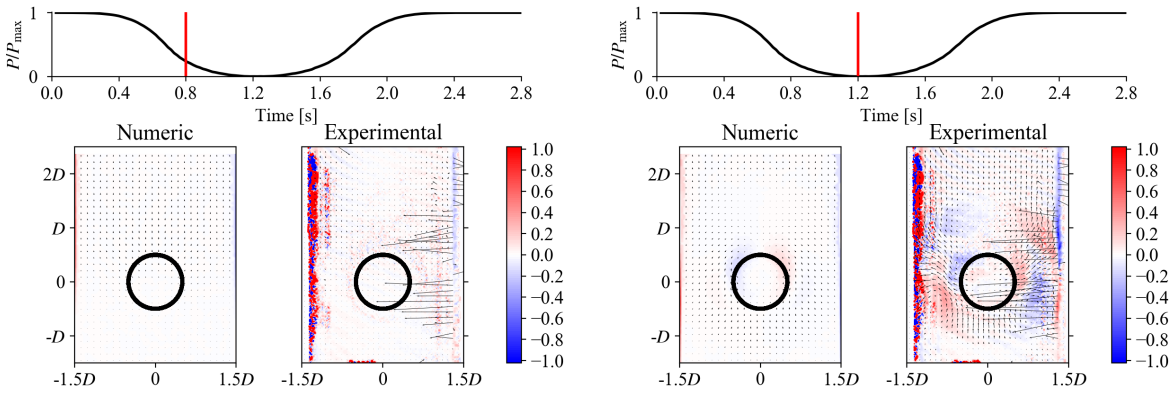

(c) 0.80 s

(d) 1.20 s

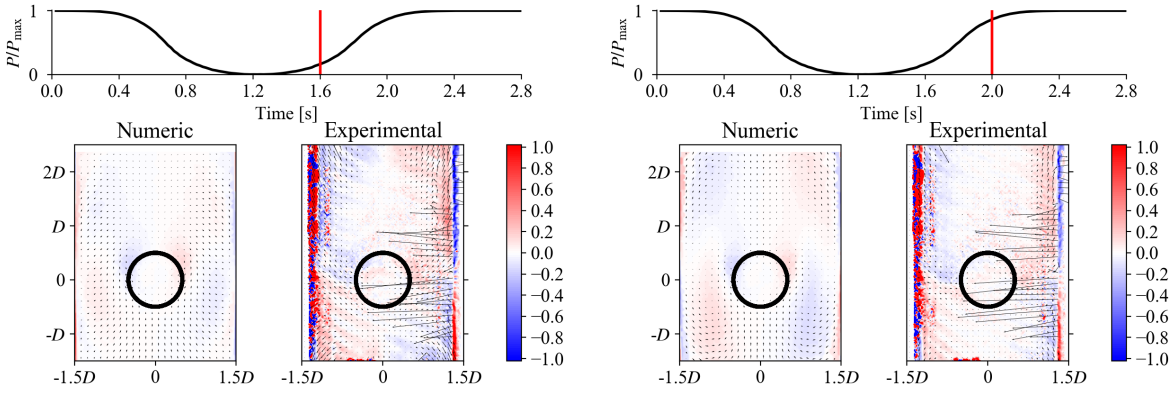

(e) 1.60 s

(f) 2.00 s

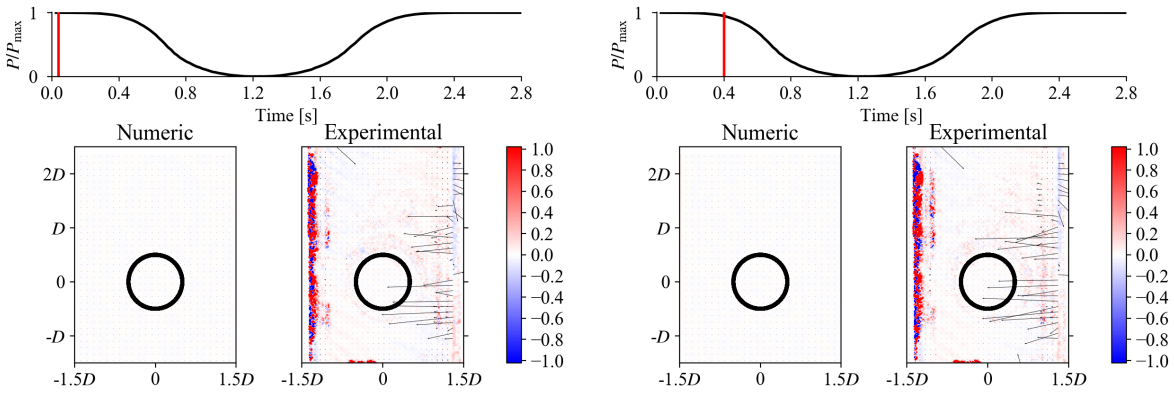

(a) 0.04 s

(b) 0.40 s

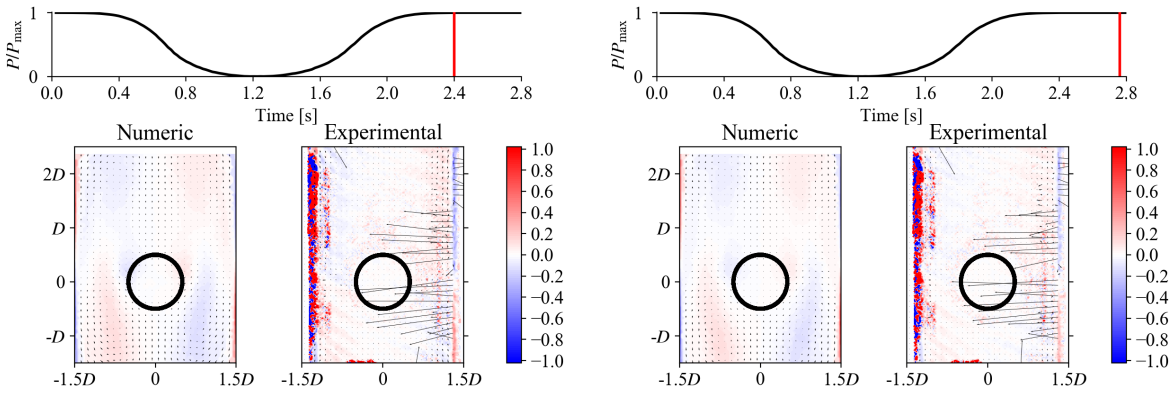

(g) 2.40 s (h) 2.80 s

Figure 39 – Coronal plane velocities, u_y and u_z , and vorticities, $\vec{\omega_x}$.

3.5 DISCUSSION

The idealized experiment is well represented by the numerical model. The FVM was able to reproduce the flow inside an idealized TE system by means of an incompressible segregated solver combined with a k-ϵ turbulence model. It was also possible to establish a good methodology to estimate the necessary values of the dimensionless wall distance, y^+, to allow the turbulence model to properly solve the flow near the wall. The velocities and vorticities in the numeric transverse and sagittal planes are in excellent agreement with what was observed experimentally by Erath and Hemsing (2016). In the coronal plane, on the other hand, the experimental data has too much noise to draw conclusions.

This analysis is still limited by the simplifications that were necessary to conduct the experiment. The valve flap mechanism plays an important role in the flow downstream of the prosthesis and cannot be neglected in further analysis to understand the mechanisms that drive TE voice production.

4 QUASI-STEADY BEHAVIOR OF A REAL PROSTHESIS

After developing a computer model capable of reproducing the experiment performed by Erath and Hemsing (2016), the natural next step was to bring the computer model closer to a real geometry. The idealized model of Erath and Hemsing (2016) was built 3.5 times life size. However, when the model was scaled down to match the actual size of the TE system, the results did not agree with the expectations. Hilgers, Cornelissen and Balm (1993), found that the volume flow magnitude *in-vivo* was significantly lower than that found experimentally in an idealized setup. The problem is likely to be in the assumption that the valve flap opens completely during the beginning of the phonatory cycle.

By observing a real prosthesis, it is possible to notice that the opening is heavily dependent on the volume flow. The opening changes the behavior of the airflow by limiting the sectional area through which the air will exit the prosthesis. This leads to a significant pressure drop and change in flow direction downstream of the prosthesis.

4.1 DETERMINING THE OPENING ANGLE OF A FLAP IN A VOICE PROSTHESIS

In order to further develop the computational model, we must first understand the relation between boundary conditions and the valve's flap opening. To achieve that, an experimental apparatus was devised to measure air volume flow, pressure drop and prosthesis' flap opening angle.

Figure 40 depicts a schematic representation of the experimental setup used to evaluate the valve flap opening. The setup is comprised of a prosthesis with its tracheal flange attached to a plenum chamber, a rotameter, a portable pressure sensor, a camera with magnifying lenses, and a laptop computer. The prosthesis considered for the study was a Provox 2 voice prosthesis (depicted in Figure 11), due to availability in the lab and possibility of visualizing the movement of the flap through the prosthesis' shaft. The rotameter is an Omega FL-2043, designed for volume flows in the range of 4 to 50 LPM. The portable pressure sensor is a KIMO MP-105, used to measure pressure difference between its two probes. The camera is a microscope-mounted AmScope MA1000 which connects to a computer using a proprietary software, ISCapture.

A compressed air line feeds the rotameter, which serves as an volume flow regulator. The compressed air is then fed into the lower part of the plenum and exits to the atmosphere through the prosthesis. The difference between internal pressure in the plenum end external pressure is assessed with two probes. One is inserted in the plenum and the other measures outside pressure. The camera connected to a computer is placed perpendicular to the valve's main axis,

as depicted in Figure 40.

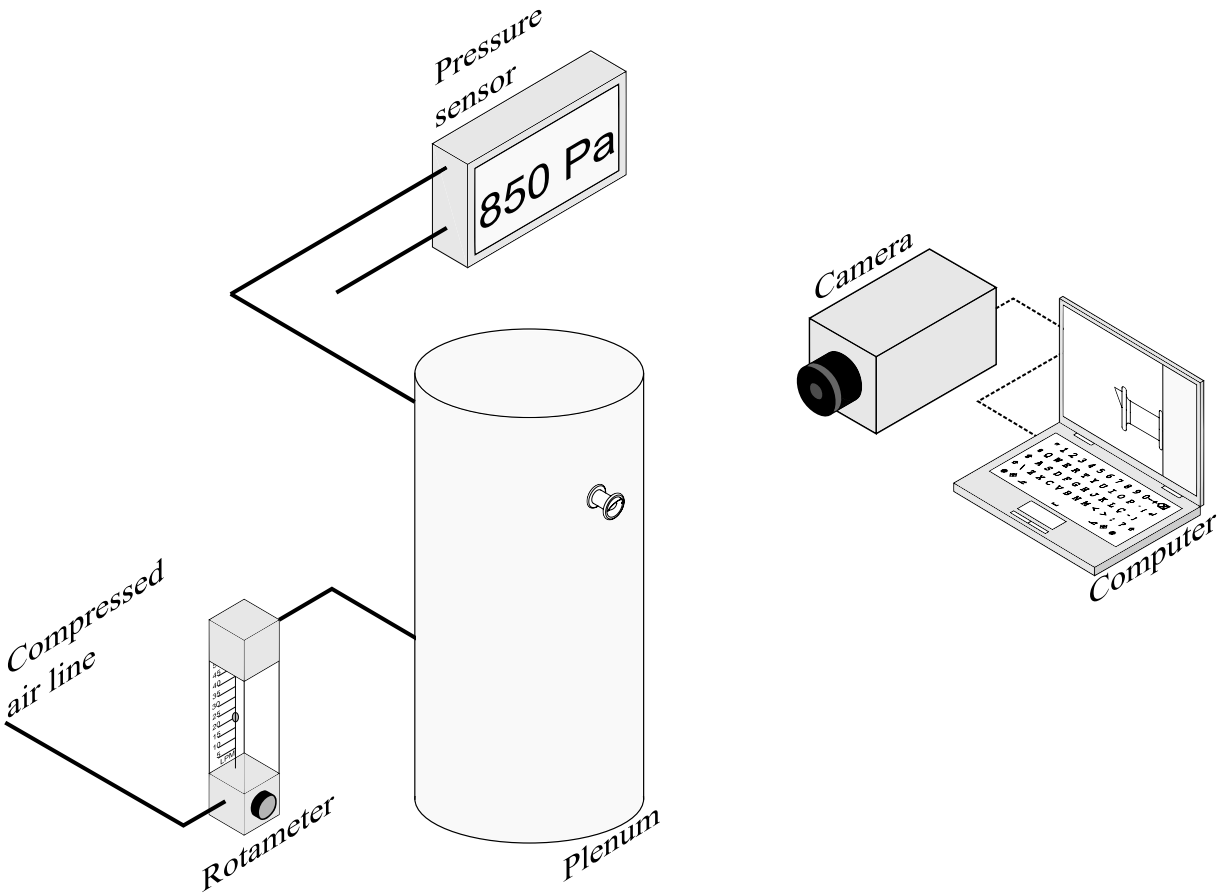

Figure 40 – Graphical representation of the experimental set-up.

The experimental procedure consisted of setting the rotameter to a known volume flow value, wait a few seconds for the flow to stabilize and assess both the pressure difference and the position of the flap through the camera. This was repeated for different volume flow values from 5 to 45 LPM, at 5 LPM intervals. For low values of the volume flow the assessment was straightforward. However, at high volume flows the measurements were compromised by significant oscillations on the pressure readings caused by the high flow velocity. Despite this limitation, an attempt was made to obtain at least two readings of pressure and their respective valve openings at high volume flow regimes. It is expected that this readings carry some uncertainties due to the pressure oscillations. Nevertheless, this flow rate is much higher than that found in normal phonation (GROLMAN et al., 2006).

Examples of the photos obtained with this method are showcased in Figure 41. The photos were then processed using the open source package ImageJ (SCHNEIDER; RASBAND; ELICEIRI, 2012), in order to evaluate the angle of the valve flap for each volume flow/pressure difference. The angle was evaluated by manually tracing a line parallel to the valve flap and another line parallel to the blue valve seat.

Table 4 presents the values obtained for air volume flow, Q, in LPM; pressure difference,

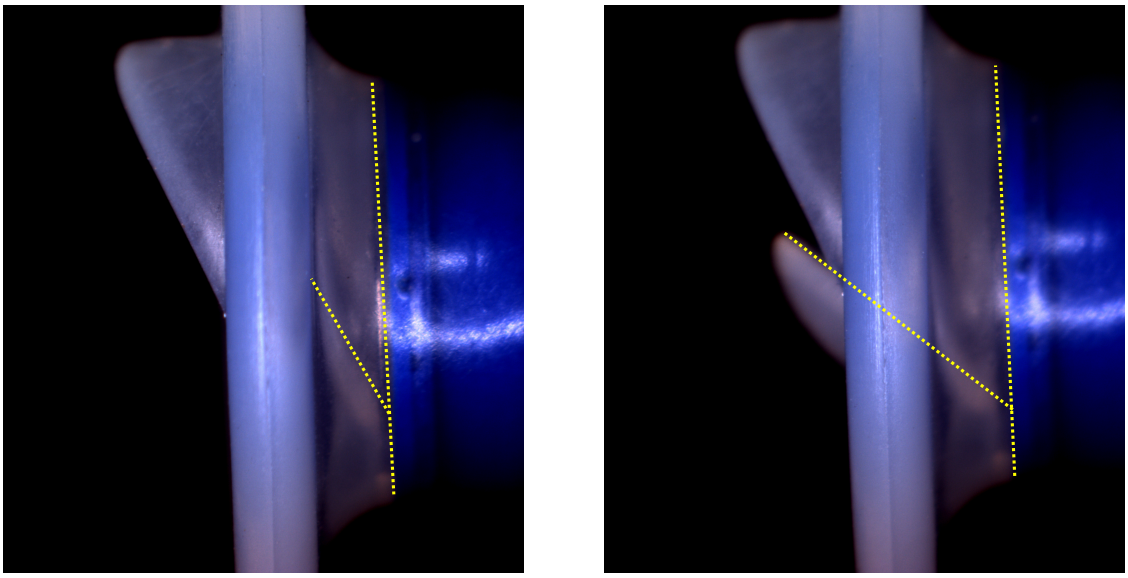

(a) $Q = 20$ LPM and $\Delta P = 1100$ Pa. (b) $Q = 40$ LPM and $\Delta P = 3040$ Pa.

Figure 41 – Examples of photos taken with the experimental set-up.

ΔP, in kPa; and the valve flap angle, Θ—each line represents one data set. For the low volume flow values, the pressure readings inside the plenum were steady and allowed two pictures of the same volume flow–pressure couple to be obtained. For values of the volume flow above 30 LPM, the oscillations of the pressure readings started to be significant.

Table 4 – Volume flow, Q, pressure drop, ΔP, and valve flap angle, Θ obtained from the experimental setup.

Q [LPM]	ΔP [Pa]	Θ [°]
5	360	9.1
5	360	8.9
10	610	18.7
10	610	19.9
15	850	24.3
15	850	22.9
20	1100	27.2
20	1100	26.9
25	1420	39.2
25	1420	35.8
30	1840	39.6
30	1900	41.8
35	2500	—[a]
40	3040	48.4
40	3040	50.4
40	3110	52.4
45	4300	59.3
45	4400	58.3

[a] Opening angle could not be determined.

4.2 RELATION BETWEEN VOLUME FLOW, FLAP OPENING AND PRESSURE DIFFERENCE

After extracting the necessary data from the experiment, the results were plotted for better visualization. Figure 42 presents a scatter plot of the relation between pressure drop and volume flow. The relationship appears to be quadratic, however, as discussed in Section 2.5, the usual range of speech volume flow lays within 0 and 0.4 LPS, or 24 LPM. Within this range, the relationship between volume flow and pressure is fairly linear.

Two similar studies have been found in the literature. Both studies show data sets from experiments conducted with the voice prostheses *in-vitro*, in which the pressure drop and volume flow through the prosthesis are related.

Grolman et al. (2006) performed an *in-vivo* study with eight patients to compare with data of an unpublished study. Half of the patients used the Provox 2 prostheses, while the other half used the VoiceMaster prostheses. The unpublished study tested five different voice prostheses

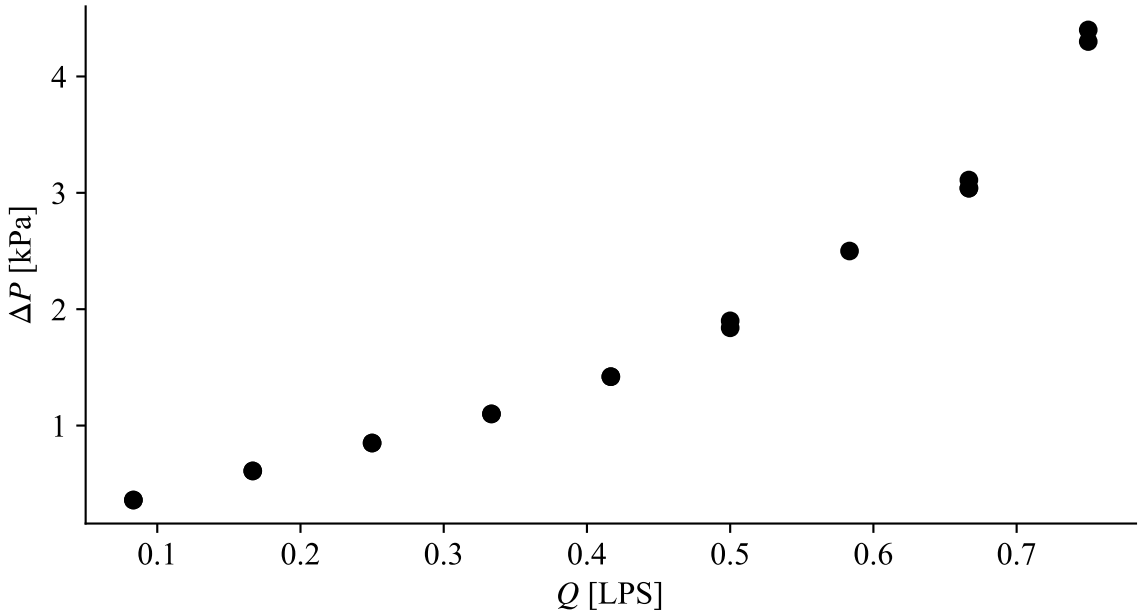

Figure 42 – Pressure drop vs volume flow.

in order to obtain their aerodynamic characteristics. The *in-vivo* study data were then plotted along with the average of the *in-vitro* study data (Figure 29). Only the *in-vitro* data is used for comparison in Figure 43.

Hilgers et al. (2010b) tested four different prostheses to obtain the relation between pressure drop and volume flow; the Provox 2, and three Provox Vega models (Figure 22). The Provox 2 data is used for comparison in Figure 43.

Using the obtained data up to 0.42 LPS (25 LPM), and considering a linear relation between pressure and volume flow for this range, a linear curve for the data was adjusted using the least squares method (JONES et al., 2001). Best linear fits were also obtained for both literature data sets using the same method. The three curves are displayed in Figure 43.

The pressure drop ranges for all three studies are very similar, ranging from around 0.3 kPa to 1.4 kPa. After curve-fitting the three data sets, the following line equations were obtained: for this work,

$$\Delta P = 0.085 + 3.132Q;$$

for Grolman et al. (2006),

$$\Delta P = 0.167 + 3.524Q;$$

and for Hilgers et al. (2010b),

$$\Delta P = 0.396 + 3.016Q.$$

The slopes of the three curves are very similar. However, there is a slight offset between the curves. These differences can be explained by the different experimental techniques employed, similarly to what happens in Figure 25. While the prostheses used by Grolman et al. (2006) are not known, the prosthesis used by Hilgers et al. (2010b) is the same used in this experiment.

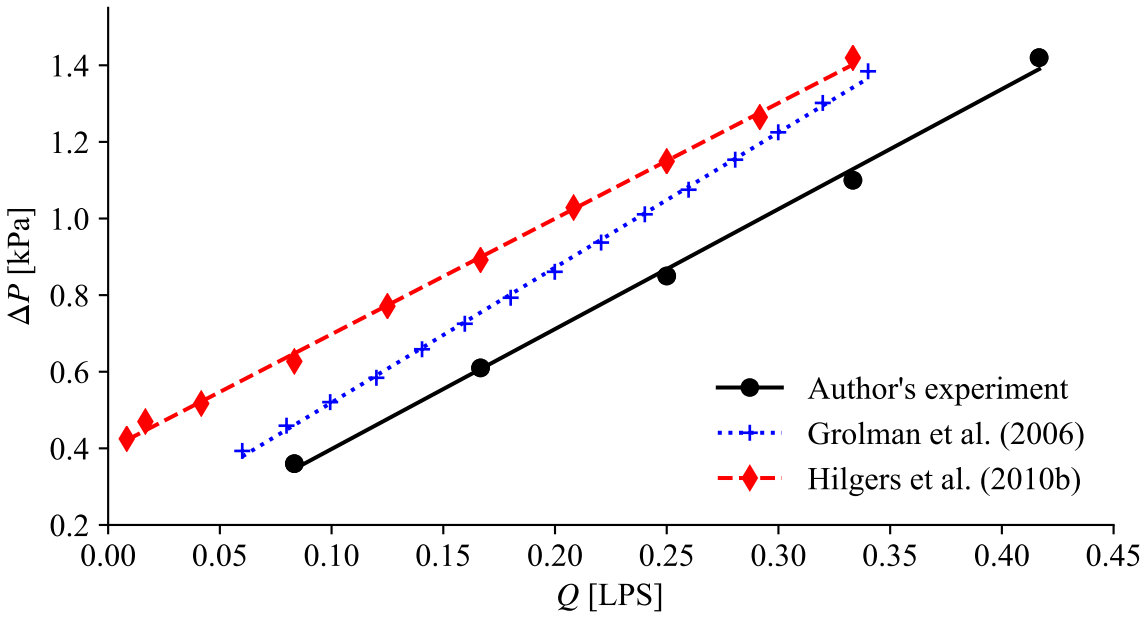

Figure 43 – Pressure drop vs volume flow compared to results from the literature.

Figure 44 shows the relation between pressure drop and valve flap angle. Much like the relation between pressure drop and volume flow, it appears to be quadratic but roughly linear up to 1.4 kPa as well. A curve was fitted according to

$$\Delta P = 0.6190 - 0.0325\Theta + 0.0016\Theta^2.$$

Figure 45 shows the relation between volume flow and valve flap angle. This relation is fairly linear through the whole range of pressure and yielded the linear curve, described by

$$Q = -0.0711 + 0.0141\Theta.$$

Within the range of TE voice production, all three variables appear to be linearly related to each other. These curves can be used to interpolate new sets of boundary conditions for simulations that were not determined by the experiments.

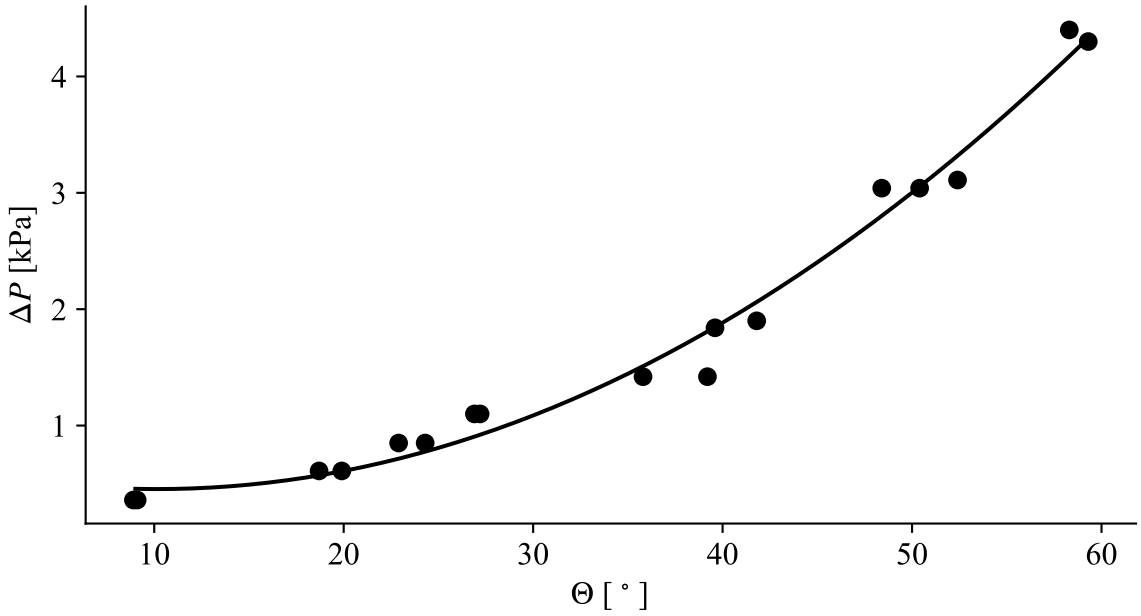

Figure 44 – Pressure drop vs valve flap angle.

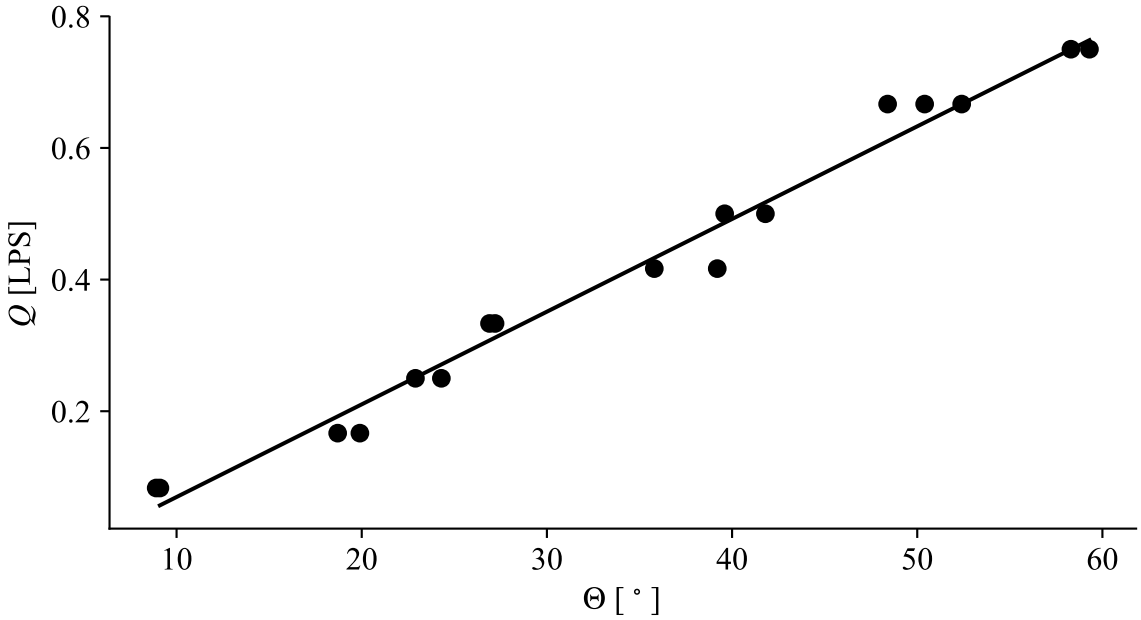

Figure 45 – Volume flow vs valve flap angle.

4.3 COMPUTER MODEL

In Chapter 3, a computer model based on an unsteady incompressible RANS-based solver using a two-layer realizable k–ϵ turbulence model was developed and validated. The model, however, is based on an experiment performed with a simpler geometry, considering water as the fluid medium. Although the experiment was designed in order to maintain dynamic similarity

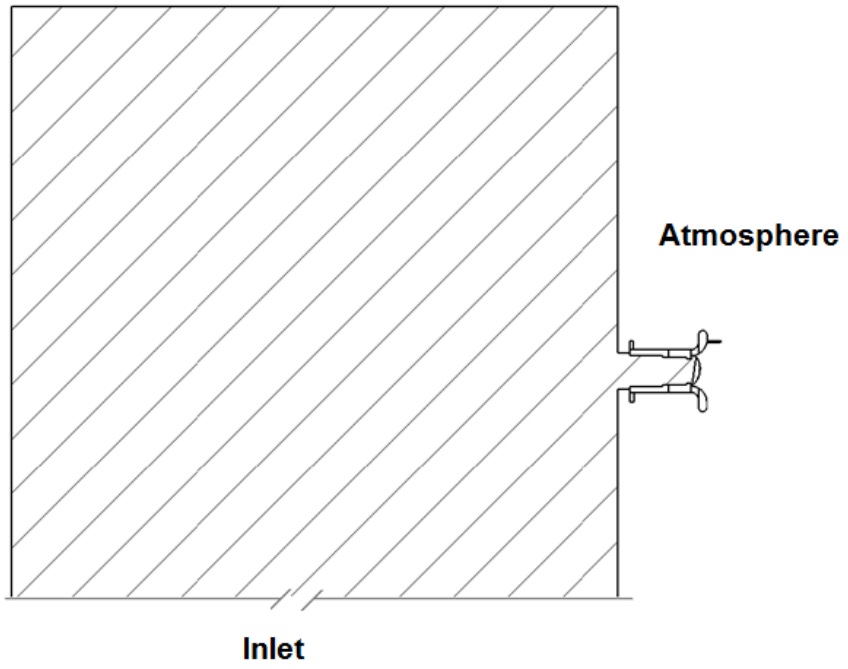

Figure 46 – Mid-sectional view of the upper portion of the plenum chamber and the valve used in the simulation.

by Reynolds, Strouhal, and Euler numbers, we must redefine some of the model characteristics in order to simulate an air flow through a more complex valve geometry.

The upper portion of the plenum chamber with the valve attached was modeled via CAD software to be used in the Star-CCM+ simulation tool. The bottom of the chamber was used as the inlet and the atmosphere was modeled as a large box around the prosthesis. A mid-sectional view of this model is displayed in Figure 46. The dimensions of the Provox 2 prosthesis used are given in Figure 47.

The experimental results previously discussed were representative of a steady state situation. In order to reproduce the experiment, the numerical model was resolved with a steady state incompressible solver. Following the guidelines of turbulence modeling present in the software manual, the same RANS two-layer realizable k–ϵ turbulence model was maintained.

The experimental results for the flap angle were rounded for a more convenient CAD modeling. Table 5 presents the results of Section 4.1 with the volume flow displayed in LPS and the angles rounded.

A geometry was created for each valve flap angle. The chosen boundary condition was a pressure difference between the inlet and the atmosphere (outlet). The inlet was set to the values of pressure found in Table 5 and the outlet boundary was set to 0 kPa to maintain the pressure drops measured by the pressure sensor. The volume flow was then assessed inside the prosthesis. Given that the flow is considered incompressible, the volume flow is constant throughout the flow path due to mass conservation.

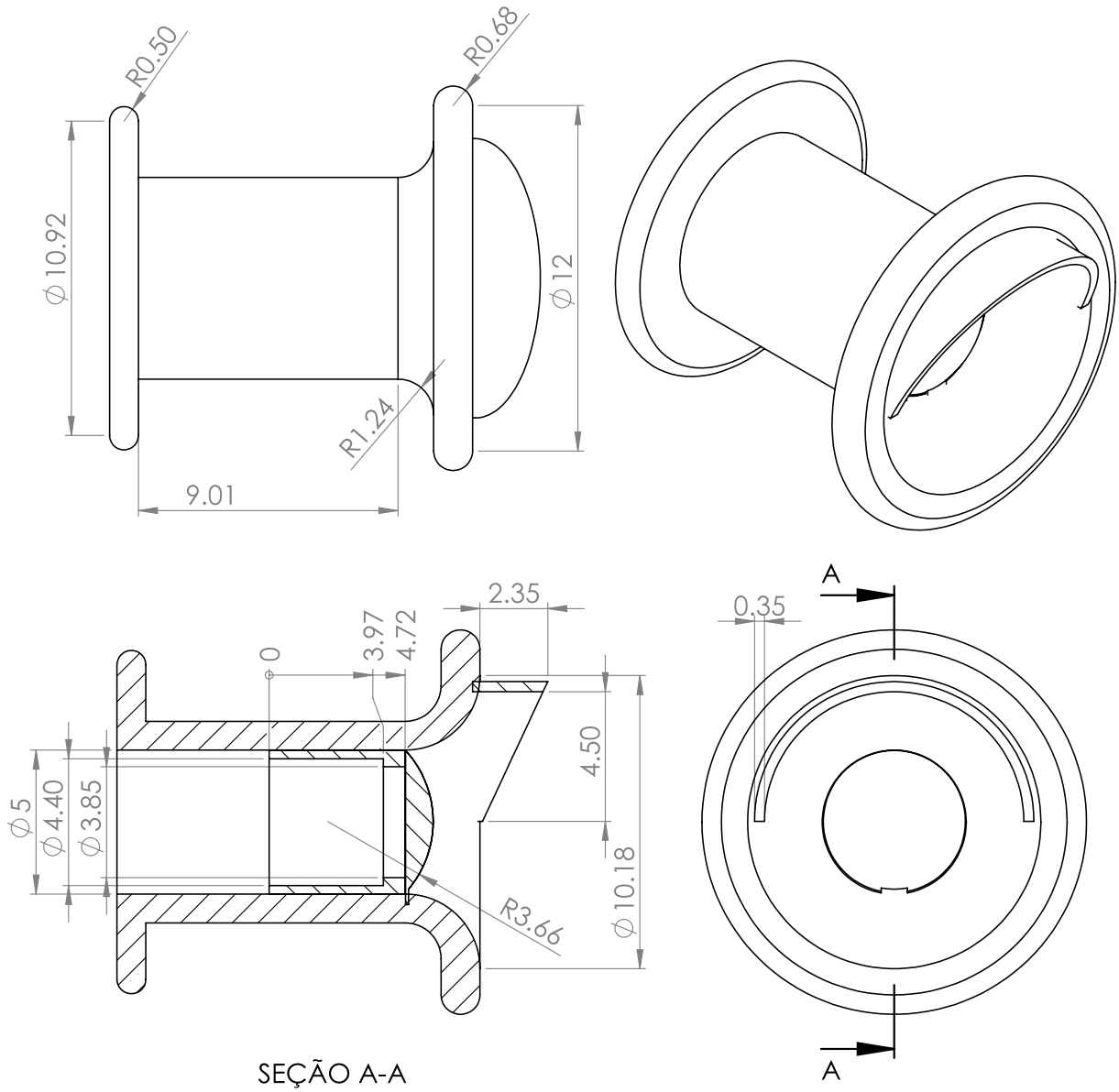

Figure 47 – Dimensions for the Provox 2. All values in mm.

Table 5 – Volume flow, Q, pressure drop, ΔP, and valve flap angle, Θ, obtained to be used with the computational model.

Q [LPS]	ΔP [Pa]	Θ [º]
0.083	360	9
0.166	610	19
0.250	850	23
0.333	1100	27
0.416	1420	36

In order to assure numerical accuracy, a new convergence test and a new boundary layer analysis were performed to determine, respectively, the mesh size and the boundary layer discretization.

4.3.1 Mesh convergence

With a new dimensional scale and a significant constriction, a new mesh size to perform the simulation was necessary. In order to achieve a mesh-independent solution, the two edge cases were selected (9 degrees and 36 degrees flap angle) to perform a mesh refining process. Once again, the polyhedral mesh was selected due to the complex geometry of the valve. The control variable was the volume flow inside the valve. Figure 48 showcases this process by plotting the volume flow against the number of volume cells per valve diameter.

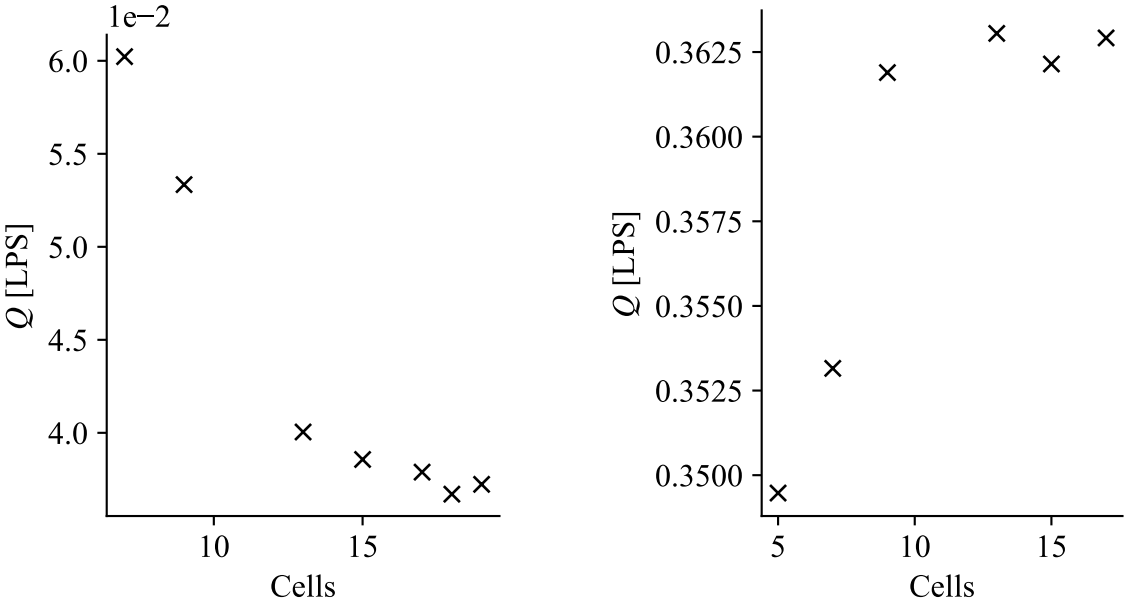

Figure 48 – Volume flow values for different cell counts across the transversal mid-section of the prosthesis for a (a) 9 degrees opening angle and (b) 36 degrees opening angle.

Figure 48a depicts a fast descent for the first refinement steps, starting at 13 volumes across the diameter, the volume flow stabilizes. In Figure 48b, the stabilization of the volume flow occurs for a coarser mesh, due to the airflow passageway for a 36 degree opening being larger than the one for a 9 degree opening. The variation for both meshes after stabilization is lower than 5%. In order to maintain uniformity with all simulations, the mesh with 15 volumes across the prosthesis diameter was chosen for a balance of accuracy and performance.

In order to assure numerical accuracy, the dimensionless wall distance, y^+, can be calcu-

lated using Equation (3.1). This value was used with all the meshes tested. In order to attain a $y^+ \approx 1$, the freestream velocity was set to $u_\infty = 35$ m/s and the characteristic dimension to $L = 5 \cdot 10^{-4}$ m (approximating the constriction characteristic dimension to $1/10$th of the prosthesis diameter). These, alongside with $\rho_{\text{air}} = 1.169$ kg/m^3 and $\mu_{\text{air}} = 1.869 \cdot 10^{-5}$ Pa·s (BELL et al., 2014), yield a Reynolds number of Re $= 1094$.

The wall distance necessary to obtain a value of $y^+ \approx 1$ was $4.56 \cdot 10^{-6}$ m. A wall distance of $2.78 \cdot 10^{-6}$ m was achieved with total prism layer thickness of $1 \cdot 10^{-4}$ m, 16 layers and a stretch factor of 1.1. This kept the overall y^+ value below 1 for most of the domain.

The initial conditions throughout the domain were set to $P = 0$ Pa and $u = 5$ m/s on the prosthesis axial direction. The turbulence initial conditions were set to an intensity of 0.1224, a length scale of $2.45 \cdot 10^{-4}$ m, and turbulent velocity scale of 3.5 m/s.

4.3.2 Comparison with literature results

After the simulation, the volume flows for each case were extracted and plotted against the pressure differences used as boundary conditions. These can be seen in Figure 49. The results are also compared with those previously displayed in Figure 43. Once again, best fit linear curves were found. The slope of the curve found for the numerical results is very similar to those found experimentally, 3.298 kPa/LPS.

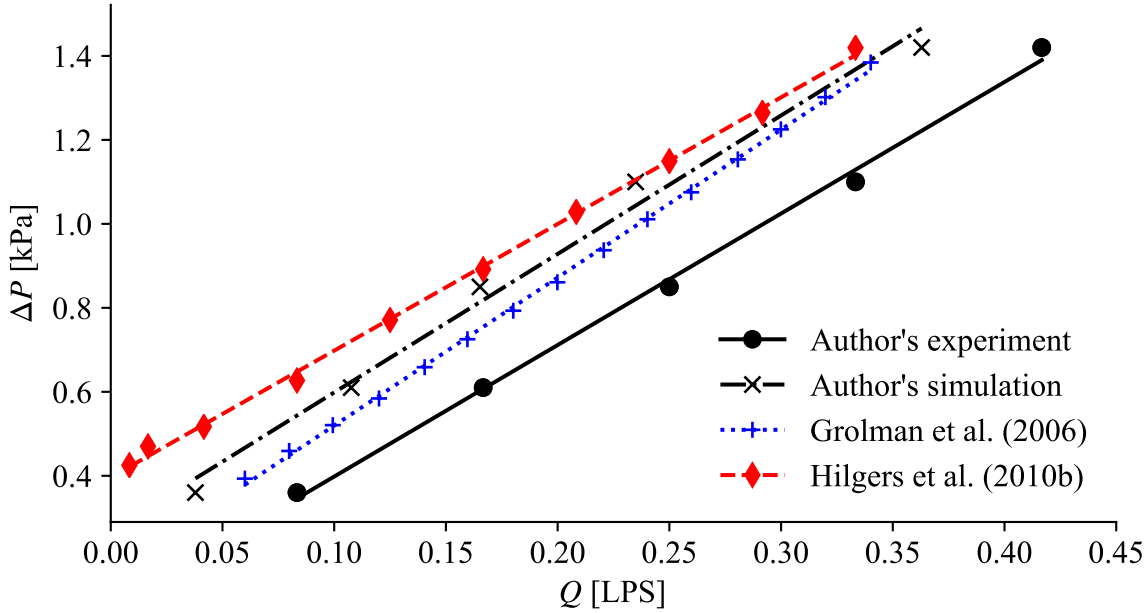

Figure 49 – Pressure drop vs volume flow for numerical, experimental and literature results.

The results show that the numeric model underestimates the volume flow obtained in the experiment for the given pressures. This can be attributed to the measurement of the volume

flow. In the experiment, the volume flow was measured using the rotameter in the inlet of the plenum. However, the volume flow exiting the prosthesis might not be the same being read on the inlet due to possible leakages around the inlet, the pressure sensor probe or around the prosthesis. Also not considered, is the force that the fluid exerts on the flap. In the numerical model, the geometry is fixed and the flow does not need to push against the prosthesis' elastic reaction force.

4.4 DISCUSSION

The experiment described in this chapter has shed some light on the behavior of the prosthesis' flap. It has been concluded that the two possible flap stages (closed and open) is an over simplified assumption to describe the valve dynamics. This issue had to be addressed before moving on to a more complex geometry for the TE system. Moreover, it was possible to understand the relation between the boundary conditions—volume flow and pressure difference—and the prosthesis' flap opening angle.

Even though the relation between pressure drop and the other parameters appear to be quadratic for the values of volume flow considered in the experiments. This is not the case for volume flow values within the range of human speech. For those, all the relationships were observed to be linear. This information can be useful if further analyses on the material properties of the prosthesis are performed.

The computer model was able to capture the behavior of the flow through the prosthesis reasonably well. There is a very good agreement with the experimental results and those found in the literature from previous *in-vitro* experiments with similar prosthesis.

It is important to remark that only one prosthesis was evaluated in this work. It is possible that a larger sample could improve the accuracy of the experimental results. The experiment reported in this chapter was a necessary stepping stone to allow for further analyses of the TE system, as will be discussed in the next Chapter.

5 FLUID DYNAMIC BEHAVIOR FOR A SIMPLIFIED TE GEOMETRY

In the previous chapters a numerical model for an idealized TE system and an experiment with a prosthesis were performed. In this chapter, a more realistic take on the TE system will be given. A new model was created based on the real geometry of the TE system. Assuming that the flow behavior can be approximated to a quasi-steady state, simulations were performed using the numerical models established previously in order to assess the flow behavior inside the PE segment in the presence of a TE voice prosthesis.

5.1 COMPUTED TOMOGRAPHY

To create a more realistic geometry, computed tomography[1] (CT) scan images of two male TE speakers were obtained. Both patients were users of the Provox Vega voice prosthesis for a while at the time. Both spoke with clear intelligible voice and could sustain speech for a considerable amount of time. The scan was accomplished on a Canon Aquilion Prime SP Star, with the capability of perform 160 slices per rotation. Figures 50 and 51 show sagittal cuts for patients 1 and 2, respectively. The grayscale in the image represents the different densities, with white components showcasing the bones and black the "empty" spaces filled with air. The planes depicted do not represent the same visualization plane for each patient, they were chosen to enable the best visualization of the PE segment. The PE segment is indicated by green arrows and the TE voice prosthesis location is indicated by the red arrows. Figures 50a and 51a show patients during apnea (holding breath), while Figures 50b and 51b show the patients during phonation of the vowel /a/. The hands of the patients can be seen occluding the tracheostoma in the images that display the phonation.

In Figure 50a the esophagus of patient 1 appears closed from the prosthesis up to the PE segment, while the esophagus of patient 2, in Figure 51a, is only closed at the PE segment. During apnea, the PE segment remains closed, as it is expected from the upper esophageal sphincter function.

In Figures 50b and 51b, the esophagi of both patients is expanded, and the PE segment is open to allow the passage of air. Interestingly, during phonation, the esophagus of both patients

[1]Tomography is a technique of imaging by sections. A computed tomography is an imaging technique that uses a computer to perform several cross-sectional X-rays to obtain a complete spatial image of the structures inside the body. The technique—developed in the 1970s—is based on the principle that X-rays are reflected at different levels by different body structures. The procedure is performed with a patient lying on a platform while a computed tomography scanner rotates around the patient taking X-ray scans. These scans are then processed by a computer and combined to form images of "slices" of the human body. The computed tomography has become a routine analysis tool in medicine as it is minutely precise (BETTS et al., 2017).

is closed right below the prosthesis. We believe that the pressure exerted by the patient's hand on the tracheostoma pushes the trachea against the esophagus. While the trachea maintains its form, the esophagus is soft and offers little resistance, causing it to close.

Figures 52 and 53 show a more detailed view of the sagittal plane of both patients, focusing on the prostheses. The planes showcased are not the exact same ones from Figures 50 and 51. These were obtained roughly where the plane cuts at the center of the prosthesis diameter. In Figure 52a, the esophagus is not visible, but the voice prosthesis appears to be or-

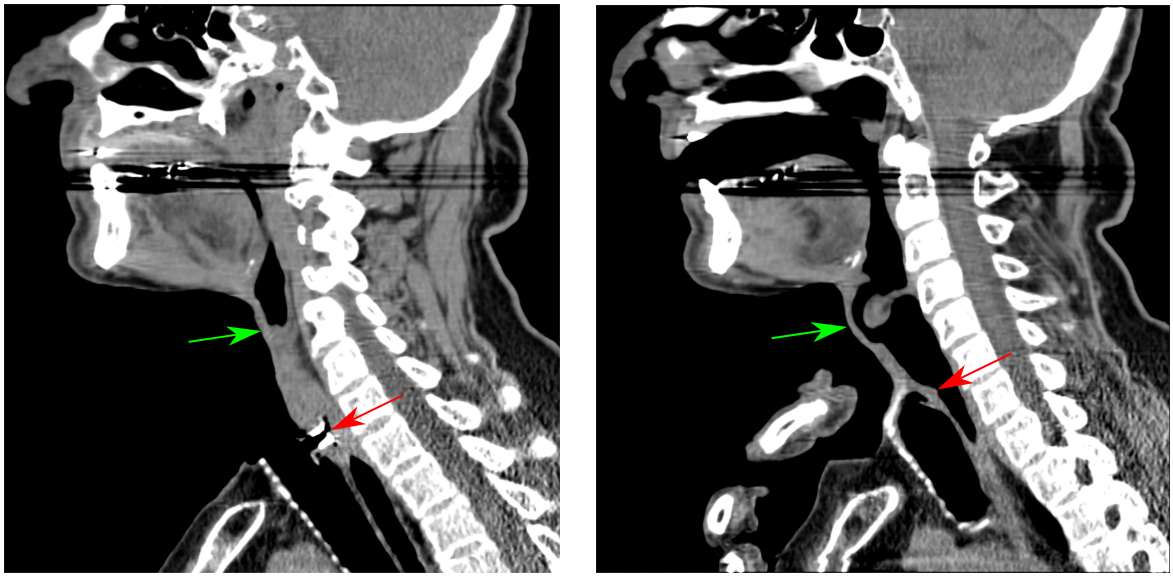

(a) (b)

Figure 50 – CT scan of patient 1 during (a) apnea and (b) phonation. Green arrow indicates the PE segment, red arrow indicates TE voice prosthesis.

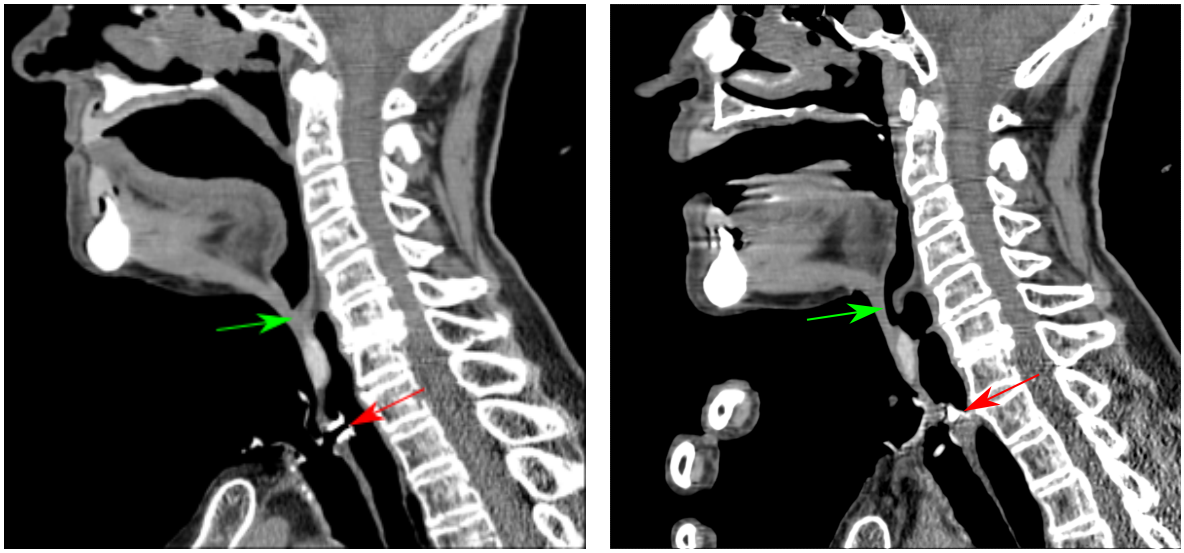

(a) (b)

Figure 51 – CT scan of patient 2 during (a) apnea and (b) phonation. Green arrow indicates the PE segment, red arrow indicates TE voice prosthesis.

thogonal to the trachea. In Figure 53a both the trachea and the esophagus are visibly orthogonal to the prosthesis. These images alone are in accordance to the assumptions made in the model of Chapter 3 about the prosthesis position.

Figures 52b and 53b show a close-up on the prostheses during phonation. Both prostheses appear to have been tilted up. This is related to the trachea being pushed back, as aforementioned. This is an interesting observation, as in prior assumptions the prosthesis was thought to remain static. The images, however, show that the position of the prosthesis in relation to the flow is not orthogonal as expected.

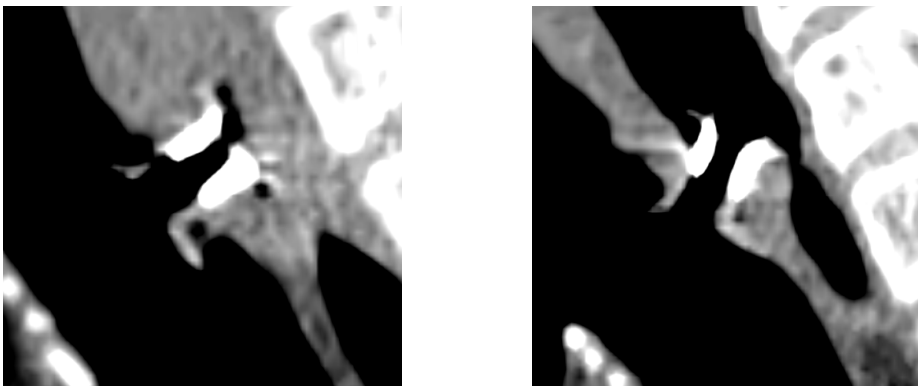

(a) (b)

Figure 52 – Detail of the prosthesis in CT scan of patient 1 during (a) apnea and (b) phonation.

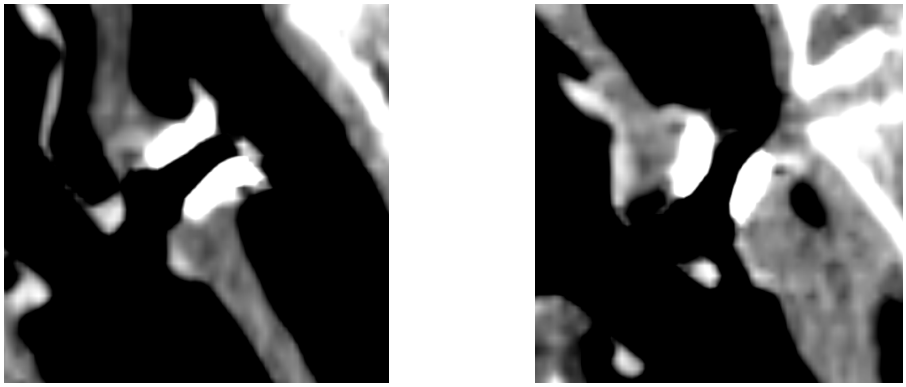

(a) (b)

Figure 53 – Detail of the prosthesis in CT scan of patient 2 during (a) apnea and (b) phonation.

The 3D Slicer software (KIKINIS; PIEPER; VOSBURGH, 2014) allows the manipulation and post-processing of the geometries obtained with the CT scans. Using this tool, the internal geometries of the TE airways were extracted. Figure 54 shows the 3D recreation of the TE airway of patient 1, and Figure 55 shows the recreation for patient 2. The prosthesis appears as just a very thin line in Figure 54 and cannot be visualized for patient 2 in Figure 55. This happens due to the method used to extract the geometries.

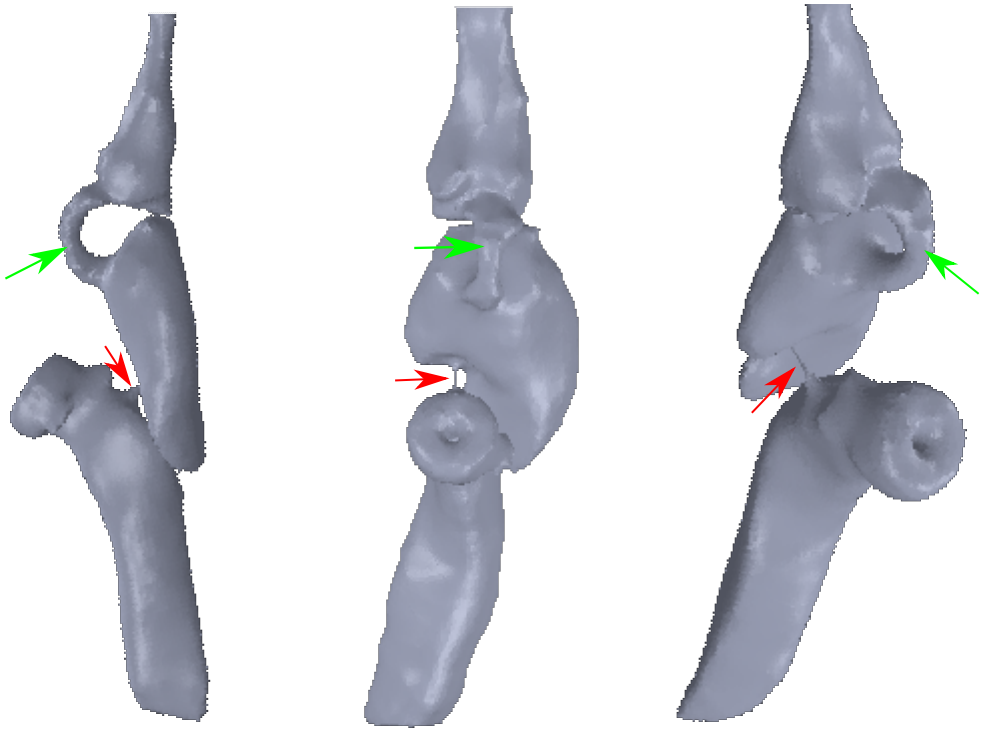

Figure 54 – 3D recreation of the tracheoesophageal airway of patient 1. Green arrows indicate the PE segment, red arrows indicate TE voice prosthesis.

The extracted geometries illustrate better what was observed in Figures 50 and 51, the portion of the esophagus below the prosthesis is mostly closed. The esophagus itself is inflated and the PE segment appears to be completely open. In Figure 54 it is possible to notice a slight buckling of the trachea, when compared to the almost straight trachea in Figure 50a. The curvature of the trachea seems to coincide with the bottom shape of the esophagus, further supporting the assumption that the trachea pressing against the esophagus causes it to close below the prosthesis. The images for patient 2 neither corroborate nor disprove that assumption.

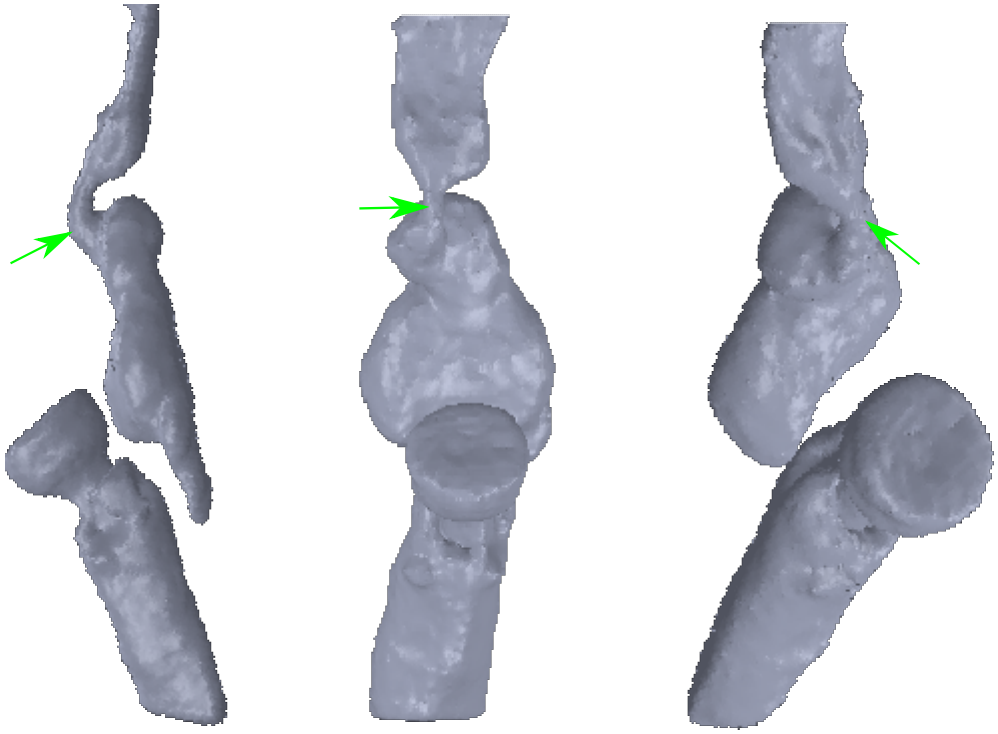

Figure 55 – 3D recreation of the tracheoesophageal airway of patient 2. Green arrows indicate the PE segment, the TE voice prosthesis cannot be visualized in this image.

5.2 COMPUTER MODEL

An approximate computational mesh was created based on the 3D recreations of Figures 54 and 55. This model consisted of a cylindrical component to represent the trachea, the TE voice prosthesis, and the approximate geometries to represent the esophagus, the PE segment and the pharynx. In order to simplify the complex geometries of Figures 54 and 55, the simplified geometry was built symmetric in relation to the sagittal plane. This simplified model is shown in Figure 56.

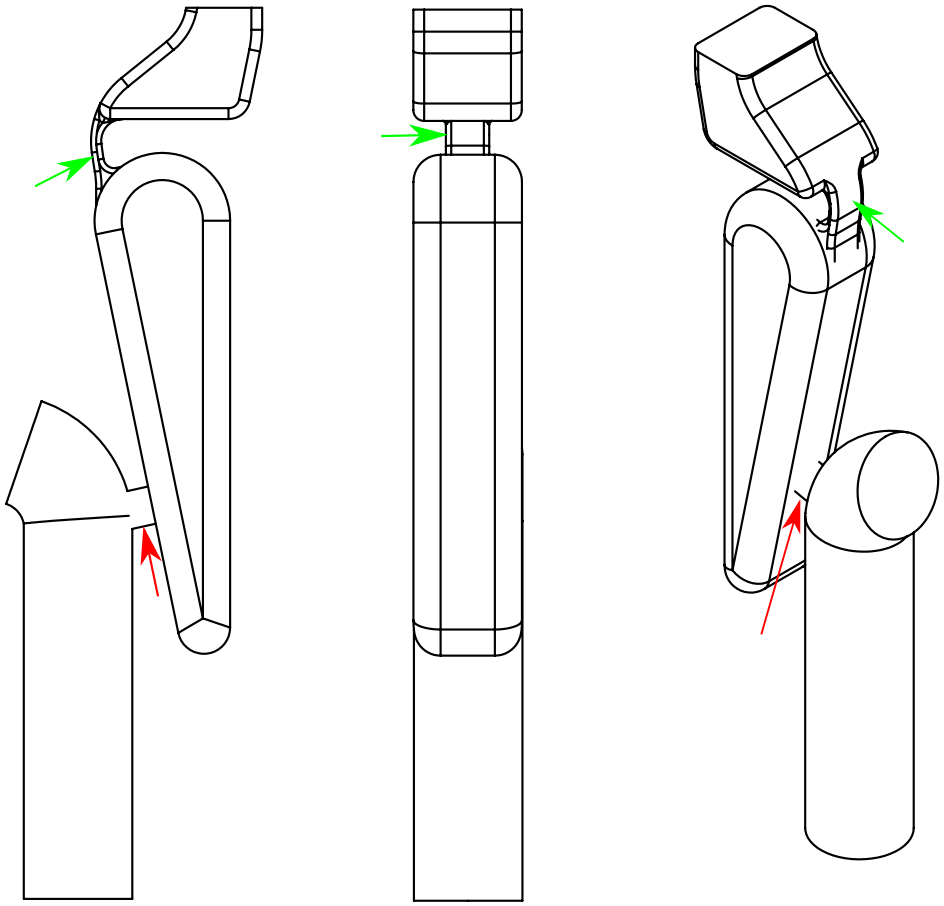

Figure 56 – The simplified geometry for the TE system. Green arrows indicate the PE segment, red arrows indicate TE voice prosthesis.

5.3 PROSTHESIS POSITIONING

To assess the influence of the prosthesis position on the aerodynamics of the TE system, three positions were defined for the prosthesis in the system. The idea is that if the axial direction of the prosthesis is oriented along the main axis of the flow, the trans-device pressure drop will decrease. With a lower pressure drop, the pressure in the esophagus should be higher, giving more energy to the flow through the PE segment. Figure 57 illustrates the three positions, here called "inferior", "middle", and "superior". In the inferior position (a) the prosthesis has an angulation of $0°$, in the middle position (b) the prosthesis has an angulation of $15°$, and in the superior position (c) the prosthesis has an angulation of $35°$, with respect to the horizontal line depicted in Figure 57.

To perform the simulation, the chosen boundary condition was an imposed volume flow, Q, at the system's inlet. The previous models used pressure boundary differences. However, in Chapter 4, the measured pressures of the experiment were for the trans-device pressure drop, from trachea to the esophagus. In that chapter, a computer model was developed and the relation

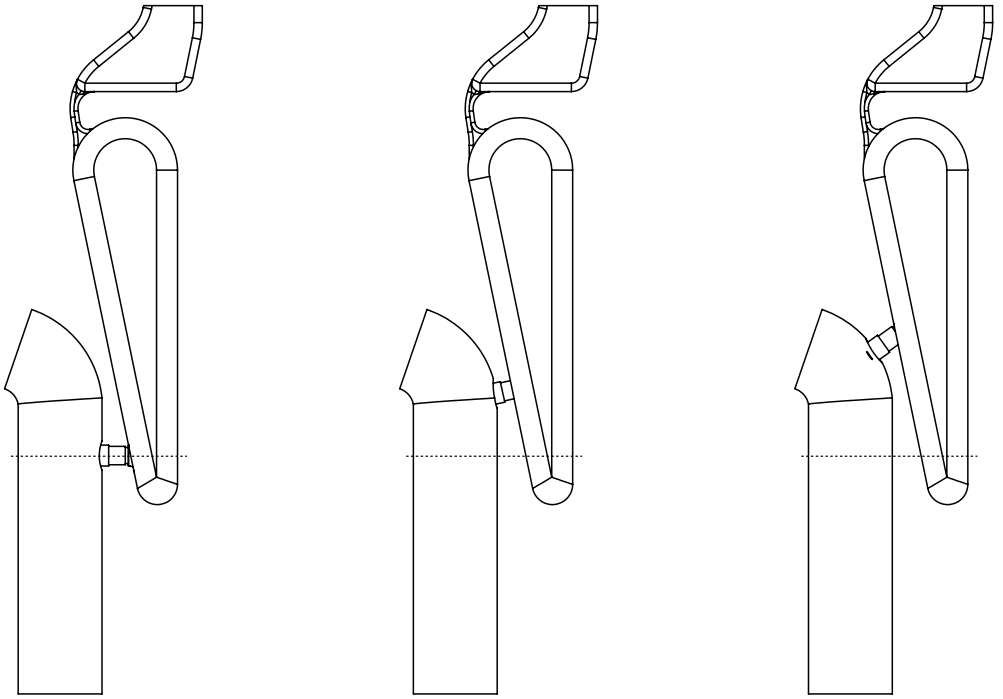

(a) Inferior position (b) Middle position (c) Superior position

Figure 57 – Three positions selected for simulations.

between pressure drop and volume flow was found. In this chapter, the volume flow boundary conditions will be set to those found in Figure 49. For each value of Q there is an existing prosthesis opening angle. This means a different geometry for each boundary condition set. In order to minimize the volume of simulations, three of the five volume flows in Figure 49 were selected. The selected volume flows were the lowest, $Q = 0.0372$ LPS; the median, $Q = 0.1650$ LPS; and the highest, $Q = 0.3640$ LPS. The associated prosthesis openings are, respectively, $9°$, $23°$, and $36°$. This amounts to nine simulations altogether.

The methods for these simulations are the ones described in Section 4.3, with the sole exception of the boundary conditions. For this model the inlet was set by imposing the aforementioned volume flows, Q, and the outlet was set to $P = 0$ kPa.

5.4 PRESSURE DROP

For each simulation, the pressure drop was obtained by subtracting the endoesophageal pressure, P_{E}, from the endotracheal pressure, P_{T}. Table 6 shows the the pressure drop, ΔP, associated with each prosthesis positioning and inlet volume flow, Q. The Re was calculated using an approximated effective flow area. If A is the cross sectional area of the prosthesis and Θ is the prosthesis' flap opening angle, the effective area of the flow can be approximated by

$$A_{\text{ef}} = A - A\cos\Theta, \tag{5.1}$$

which yields

$$D^2_{\text{ef}} = D^2 - D^2\cos\Theta, \tag{5.2}$$

being D the diameter of the prosthesis cross-section. The mean velocity across the effective area is given by

$$\bar{u} = \frac{Q}{A_{\text{ef}}}. \tag{5.3}$$

Inputing Equations (5.2) and (5.3) in (2.2) gives

$$\text{Re} = \frac{\rho Q\sqrt{D^2 - D^2\cos\Theta}}{A_{\text{ef}}\mu}.$$

Table 6 – Pressure drop in the TE system considering three different prosthesis positions.

Position	Θ [°]	Q [LPS]	ΔP [kPa]	Re
Inferior position	9	0.0372	409	2670
	23	0.1650	907	4660
	36	0.3640	1226	6633
Middle position	9	0.0372	409	2670
	23	0.1650	937	4660
	36	0.3640	1247	6633
Superior position	9	0.0372	422	2670
	23	0.1650	936	4660
	36	0.3640	1258	6633

Experimental results from Grolman et al. (2006) can be used for comparison with the data obtained. Grolman et al. (2006) performed tests with eight different patients, of which, four used the Provox 2 voice prosthesis and four used the VoiceMaster voice prosthesis. Figure 58 shows the comparison between the values obtained with the simulations with *in-vivo* results of Grolman et al. (2006). The best fit linear curve was also adjusted for the data.

The pressure drops displayed in Table 6 are close to those expected, found in Chapter 4. The pressure drops associated with the inlet flows are $\Delta P = 360$ Pa, $\Delta P = 850$ Pa, and $\Delta P = 1420$ Pa. All are within the same order of magnitude of the results of the simplified

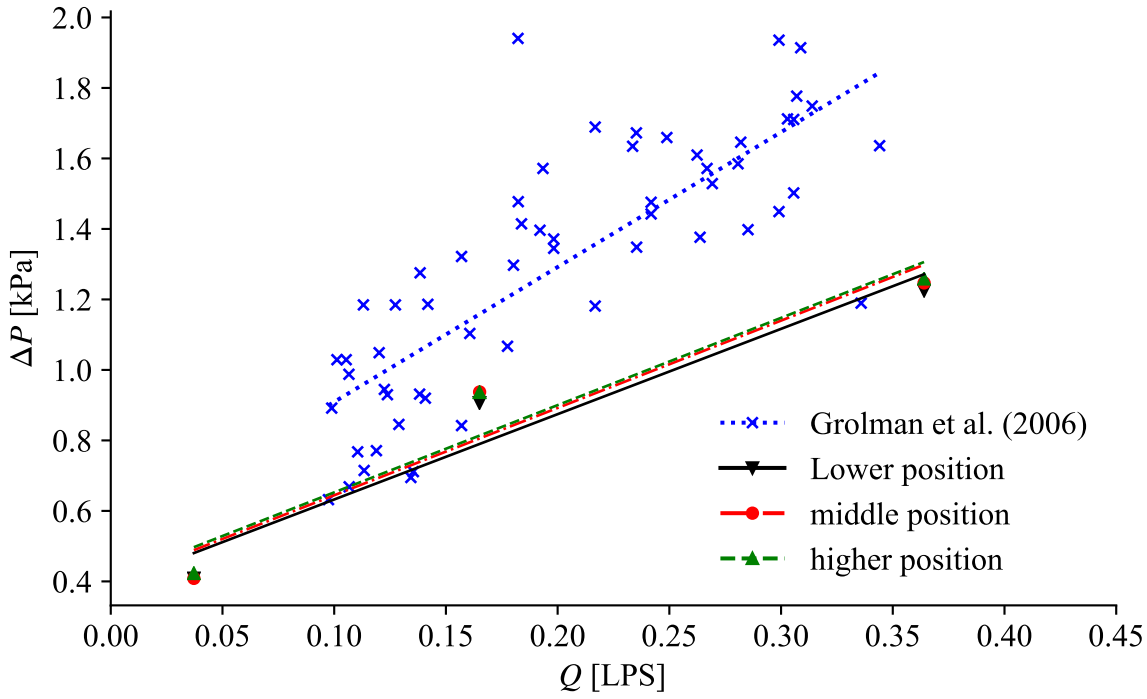

Figure 58 – Comparison of simulation results with Grolman et al. (2006) *in-vivo* results.

geometry. The influence of the prosthesis positioning was not significant, and contrary to what was expected, the pressure drop increased for the superior position. This can also be visualized in Figure 58, in which the adjusted curve for the superior position yields higher pressure drops than the inferior and middle positions.

The experimental curve of Grolman et al. (2006) shows a significant scatter and higher pressure drop when compared to the simulation cases. The experimental curve was obtained with data from eight patients, with half of those using the same prosthesis modeled in the simulation and the other half a prosthesis with a different valve mechanism. There is also the restitutive force of the valve mechanism causing further losses not present in the numerical model. This serves to illustrate that while the simulation captures the behavior of the prosthesis satisfactorily, there are still more factors to be considered. The physiological conditions also still dictate a significant portion of the flow behavior.

5.5 PRESSURE DISTRIBUTION IN THE PE SEGMENT

The pressure distribution in the PE segment should play an important role in voice production. To better understand how the prosthesis positioning affects this distribution, an analysis region was selected on the simplified model. Due to the symmetry of the geometry, the flow in the PE segment is also fairly symmetrical, and the analysis can be performed on the mid-sagittal

plane. Figure 59 shows the upper portions of the mid-sagittal cut of the TE system, including the upper part of the esophagus, the PE segment, and the pharynx. In this figure points A and B delimit the region in which the pressure distribution is assessed.

Figures 60 and 61 show the pressure distribution for the anterior and posterior esophageal wall, respectively; and for a volume flow $Q = 0.0372$ LPS. The left axis represents the normalized distance from A to B shown in Figure 59. The image on the right side of the figures shows, in red, which side of the PE segment is being analyzed. The same representations apply for Figures 62 and 63 for a volume flow of $Q = 0.1650$ LPS, and for Figures 64 and 65 for a volume flow of $Q = 0.3640$ LPS.

The pressure curves along the PE segment for the lowest volume flow (Figures 60 and 61) are very similar, with almost no variation for either the anterior or the posterior walls. The low volume flow entering the PE segment with low velocity could explain the low pressures found in these plots.

For the volume flow $Q = 0.1650$ LPS, differences start to appear between the tested positions. In Figure 62, the pressure acting on the anterior wall is unchanged from the inferior to the middle position, but it is grater with the prosthesis in the superior position, this difference decreases up until around $\frac{z}{B-A} = 0.7$. On the posterior wall (Figure 63) the pressure drops significantly at the initial portion of the segment, acting like a converging nozzle $\left(\frac{z}{B-A} < 0.15\right)$. For the superior position the pressure reaches lower values in the lower portions of the PE segment, but are not significantly affected in the upper portion.

In Figure 64, the pressure distribution behavior is very similar to those in Figure 60 and 62, with the superior position yielding the highest pressure and the middle position yielding the lowest. For the posterior wall, in Figure 65 the pressure distribution for the inferior position of the prosthesis has the largest variation of all cases.

These results show that the pressure distribution on the PE segment are only significantly affected by prosthesis positioning for higher volume flows, particularly on the posterior wall. To further understand the reasons for this, the velocity field in the PE segment is analyzed.

Figures 66, 67, and 68 show the streamlines of velocity in the PE segment for the three different boundary conditions, considering the three prosthesis positions. The y coordinate is normalized by points A and B of Figure 59.

In all cases, the flow entering the PE segment for the inferior position has the bulk of the velocity in the positive z direction. For the middle position, as the volume flow increases from $Q = 0.0372$ LPS to $Q = 0.3640$ LPS, the flow starts to gain negative x velocity. Finally, the phenomenon that occurs for the middle position in high volume flows is prevalent in all three cases for the superior position. Observing the prosthesis positions in Figure 57, and remembering the jet structures formed in the sagittal plane of the idealized model of Chapter 3 hit

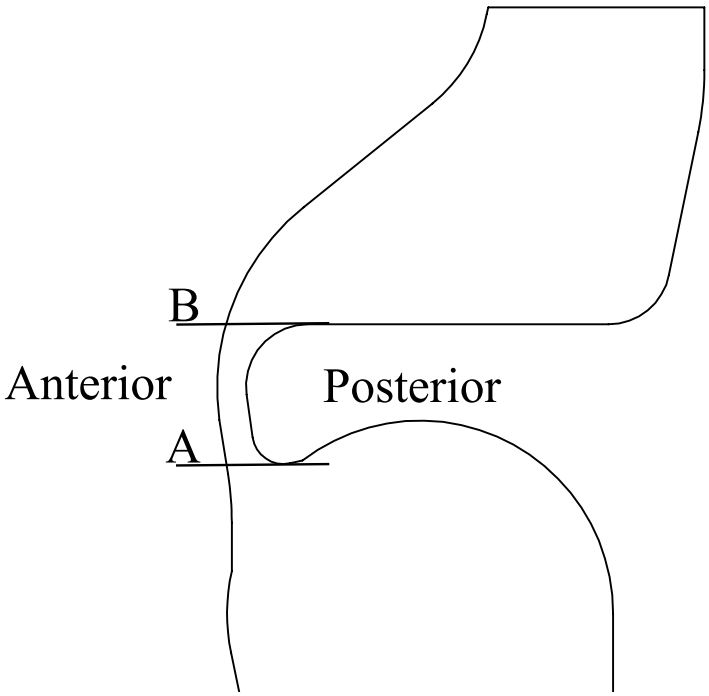

Figure 59 – Sagittal cut displaying the analysis region.

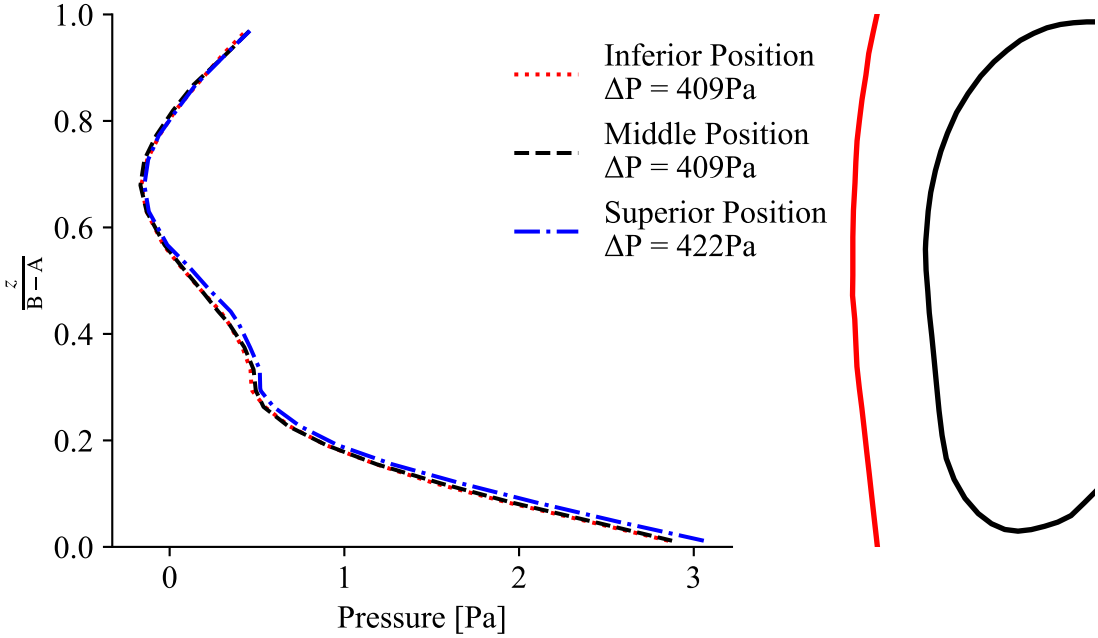

Figure 60 – Pressure on the anterior PE segment wall for a flap angle $\Theta = 9°$ and a volume flow of $Q = 0.0372$ LPS

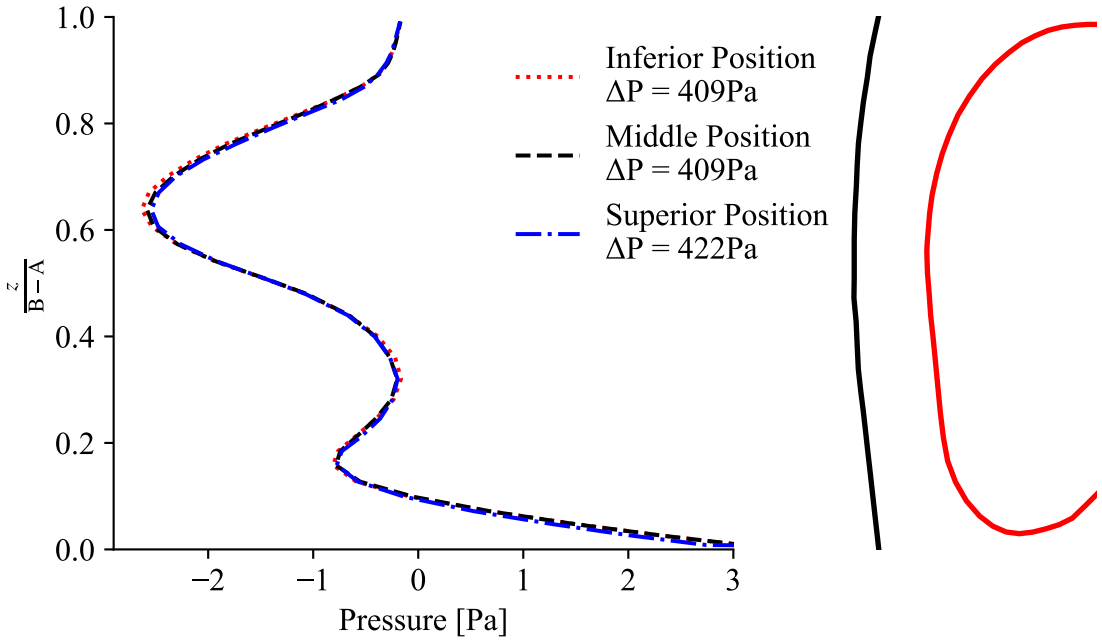

Figure 61 – Pressure on the posterior PE segment wall for a flap angle $\Theta = 9°$ and a volume flow of $Q = 0.0372$ LPS

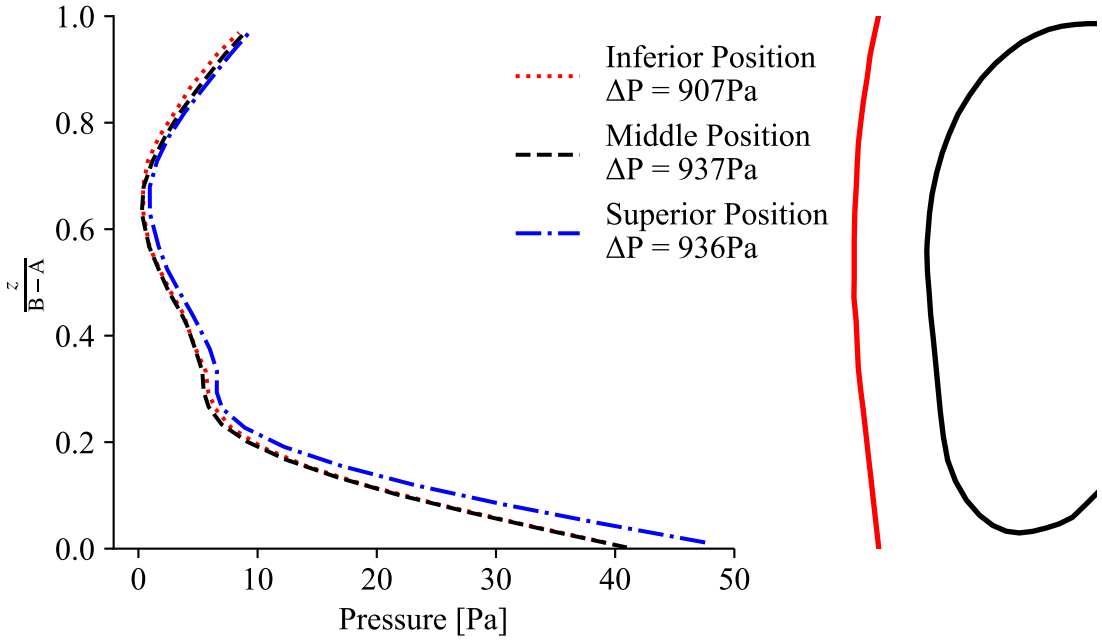

Figure 62 – Pressure on the anterior PE segment wall for a flap angle $\Theta = 23°$ and a volume flow of $Q = 0.1650$ LPS

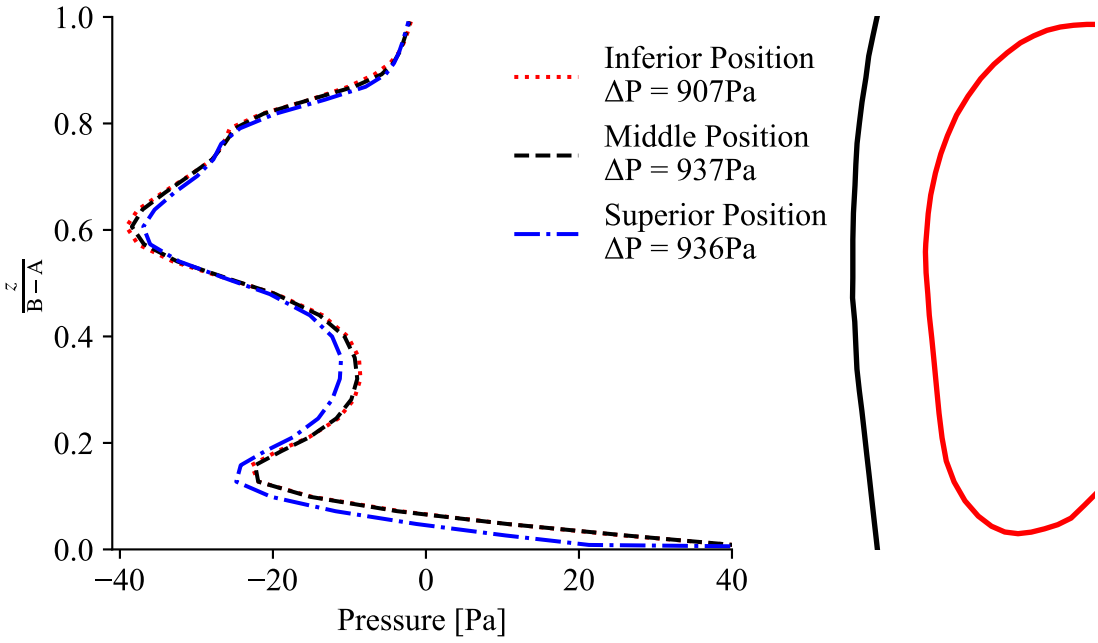

Figure 63 – Pressure on the posterior PE segment wall for a flap angle $\Theta = 23°$ and a volume flow of $Q = 0.1650$ LPS

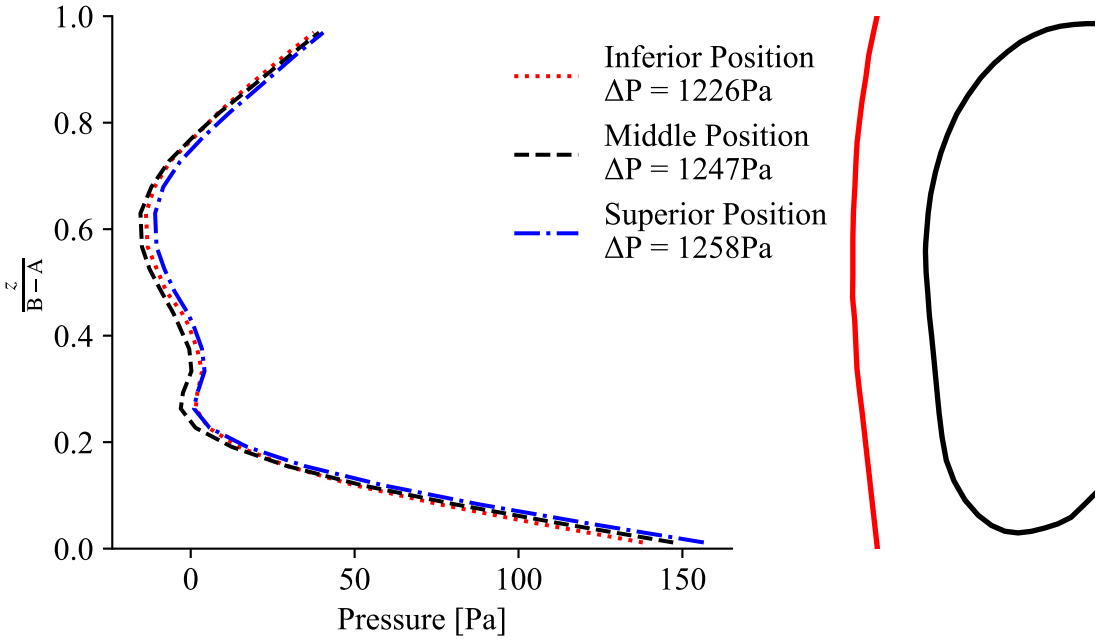

Figure 64 – Pressure on the anterior PE segment wall for a flap angle $\Theta = 369°$ and a volume flow of $Q = 0.3640$ LPS

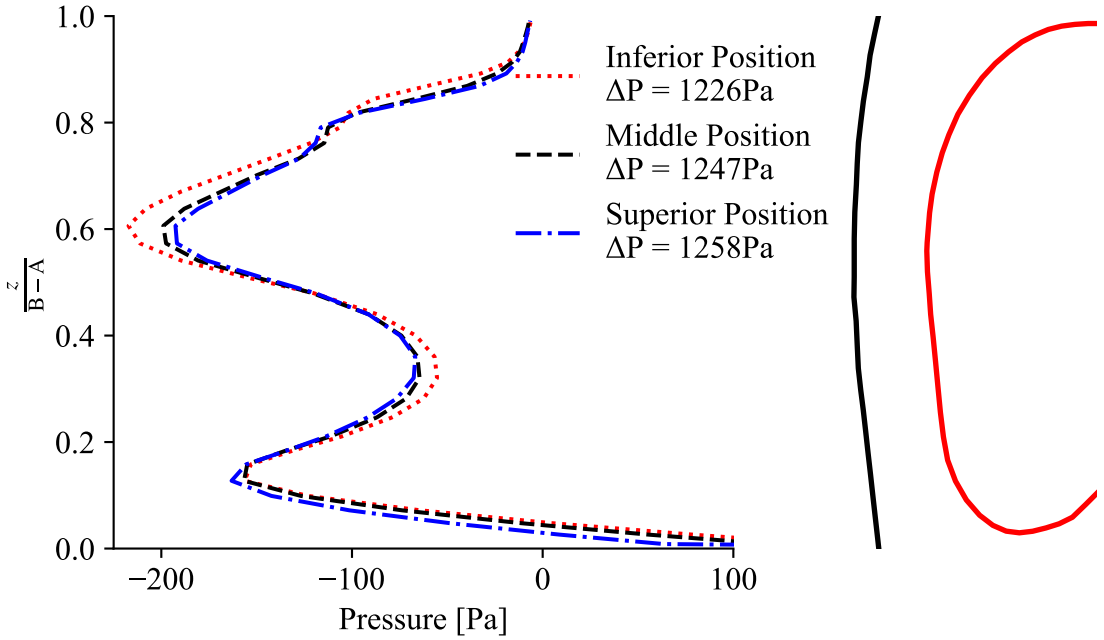

Figure 65 – Pressure on the posterior PE segment walls for a flap angle $\Theta = 36°$ and a volume flow of $Q = 0.3640$ LPS

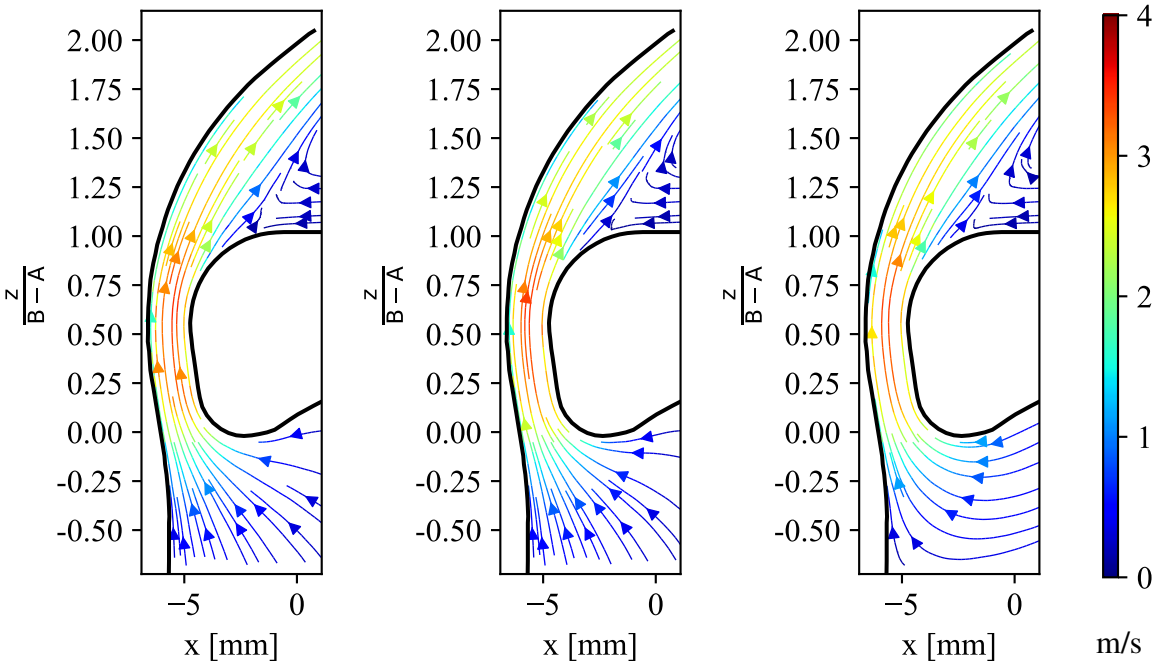

(a) Inferior position (b) Middle position (c) Superior position

Figure 66 – Velocity field streamlines of the mid-sagittal plane of the PE segment for a volume flow of $Q = 0.0372$ LPS (9 degrees valve flap opening).

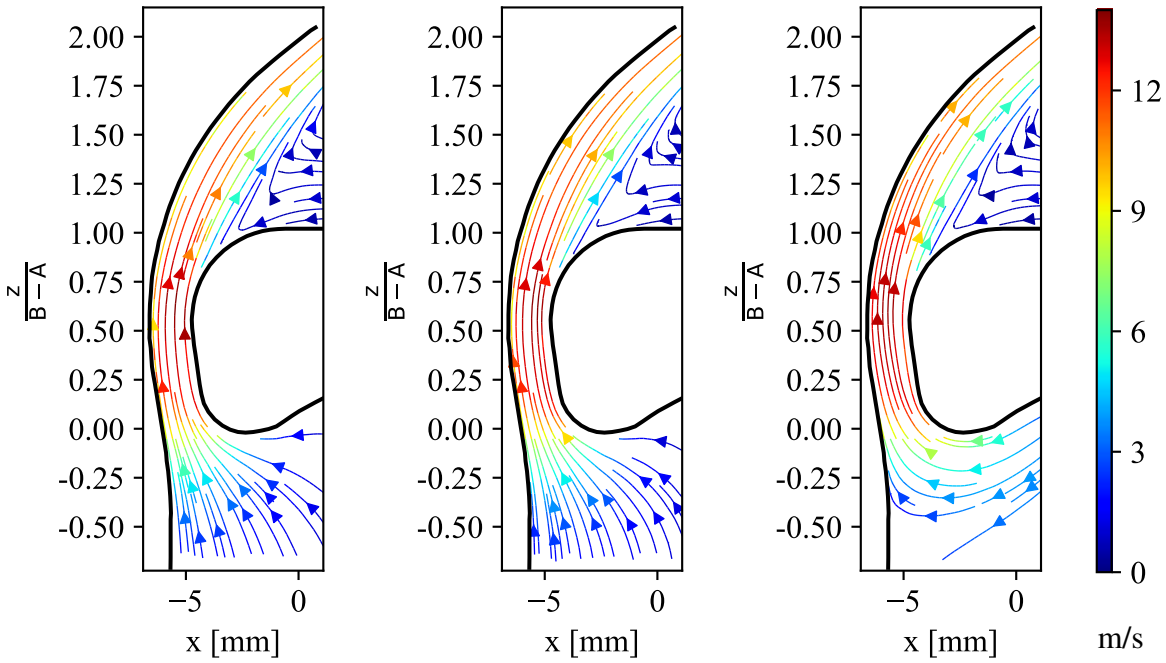

(a) Inferior position (b) Middle position (c) Superior position

Figure 67 – Velocity field streamlines of the mid-sagittal plane of the PE segment for a volume flow of $Q = 0.1650$ LPS (23 degrees valve flap opening).

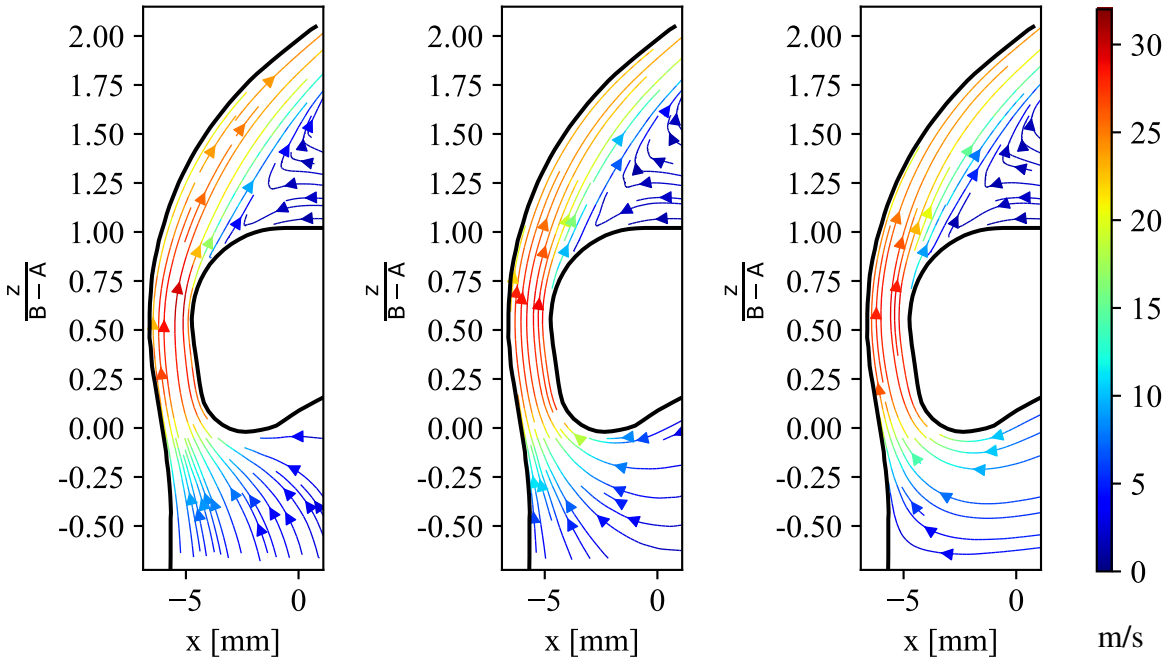

(a) Inferior position (b) Middle position (c) Superior position

Figure 68 – Velocity field streamlines of the mid-sagittal plane of the PE segment for a volume flow of $Q = 0.3640$ LPS (36 degrees valve flap opening).

the posterior esophageal wall, it is reasonable to assume that the behavior in this case will be identical. When the jet impinges the wall, the vortexes will travel downstream in the direction of the PE segment and towards the bottom end of the esophagus. The interaction of the vortex with the bottom end of the esophagus created a large recirculation zone in Figure 38 that caused the jet to tilt upwards towards the PE segment. In Figures 66c, 67c, and 68c there is a recirculation occurring below the PE segment that limits the effective area of the flow, causing the jet to tilt downwards and, ultimately, lose energy. This limits the velocity of the flow into the PE segment when the prosthesis is at the superior position. This seems counter intuitive, given the fact that the closer the prosthesis is to the PE segment, the lower the pressure losses should be. The Hermann voice prosthesis (KARSCHAY et al., 1986) tried to address this issue by designing the prosthesis esophageal end pointed up. However, this esophageal end was too big and proved to be unsuccessful due to the prosthesis opening being precluded by the esophageal walls, similarly to the Blom-Singer Duckbill prosthesis (BLOM, 1988). This study suggests that the tracheoesophageal geometry is of utmost importance in the determination of the volume flow through the TE system.

5.6 DISCUSSION

The results observed in this chapter suggest that the prosthesis position does not significantly change the pressure drop on the TE system for the given volume flows. These observations agree with Blom (1988), who claims that the main regulator of tracheoesophageal flow is the PE segment, as opposed to the prosthesis. The results go against the expectations by having the superior position—more aligned with the overall flow—increasing the pressure drop, especially in relation to the inferior position.

It is also shown that the most important aspect of the pressure distribution on the PE walls is related not to the pressure drop, but with the velocity profiles entering the PE segment that are highly influenced by tracheoesophageal geometry. However, the analyses were performed for a stedy-state model with rigid walls and an ideally symmetric geometry. From the observations made about the movement of the esophageal walls in Figures 50 and 51, we can infer that this assumption limits the scope of the analyses. The actual esophagus will have compliance; Betts et al. (2017) define compliance as "the ability of any compartment to expand to accommodate increased content." That means that the esophagus will change shapes according to the situation. While the PE segment has been observed from above during phonation, as can be seen in Schwarz et al. (2011) and Hüttner et al. (2015), the behavior of the esophagus is still unknown during actual phonation. Kinematic CT scan could be used to assert this. As for the choice of a steady state model, considering a frequency of 70 Hz (VERKERKE; THOMSON, 2014), a charac-

teristic length for the PE segment of $L = 0.003$ and the peak velocities found in Section 5.5, the Strouhal numbers yielded are between 0.0066 and 0.0525. These low Strouhal numbers show that the quasi-steady assumption is reasonable.

6 CONCLUSIONS

The TE voice recovery method developed by Singer and Blom (1980) is still the most effective method available. However, it has not changed significantly since its inception. There is still a non-negligible number of patients that are not capable of producing voice by using the TE voice prosthesis. Several studies have been conducted trying to assert the qualities of the prostheses, but the literature in TE prosthesis testing is still limited to experimental setups that do not represent the TE system in its entirety. Grolman et al. (2006) have shown that there is a significant difference between *in-vitro* tests and the actual use of the prosthesis. The Provox 2 used extensively throughout this work is no longer being distributed by the manufacturer. Newer prostheses like the Blom-Singer Advantage or the Provox Vega have yielded similar results in *in-vitro* tests but have improved characteristics concerning durability and patient comfort. Blom (1988) argues that better performance prostheses—in terms of aerodynamics—do not correlate with better speech capabilities, as the volume flow is regulated mainly by the PE segment.

The computer model of Chapter 3 was developed using an unsteady incompressible segregated FVM solver and a RANS realizable two-layer k-ϵ turbulence model. This model was based on the experiment by Erath and Hemsing (2016) and the experimental data was used as validation for the selected simulation techniques. The comparison of the results from the experimental model and the numerical model showed good agreement and the numerical method of this work was therefore validated.

Upon further analysis, the approximation used for the idealized prosthesis showed to be insufficient to assess the actual pressure drop in a TE system. Preliminary observations showed that the flow was highly influenced by the valve flap mechanism. The flap offered some resistance to the flow caused by a limited opening and reduced effective area for the flow outlet. To circumvent that issue, an experiment was devised to relate pressure drop and volume flow with the opening angle of the prosthesis flap. Using a simple setup consisting of a plenum chamber and measuring equipment, the data was extracted. This data was then used to further consolidate the developed computer model. Assuming that the flow was quasi-steady, a steady state simulation was performed using the same models from Chapter 3. The results were compared to the experimental results obtained previously and other experimental results found in the literature. However, the analysis was limited to only one prosthesis. The accuracy of the study could be increased by using a larger sample of the same prosthesis. Other prostheses models could also be tested to better understand the differences in mechanism. Nevertheless, the experimental setup could not work, for instance, with the Provox Vega or the Blom-Singer Advantage, because the experiment was based on photographs taken from the side of the prosthesis. In this sense, the

Provox 2 considered in this work was the only model that allowed for the visualization of the flap angle. The newer prostheses mentioned do not offer the same visibility. Another approach could be devised, using more sophisticated measuring techniques.

The results obtained in Chapter 5 suggest that the pressure drop in the TE system is not significantly affected by the change in positioning and angulation of the prosthesis. Despite the low variation, the results were the opposite of those expected, with the pressure drop increasing slightly for the upper positions. The jet formed at the exit of the valve hits the posterior esophageal wall and the vortexes formed travel up and down, similarly to the results seen in Chapter 3. While the superior position has the valve more closely aligned with the main orientation of the flow, the jet creates a recirculation zone right below the PE segment. This causes the jet to tilt downwards, away from the PE segment.

However, the pressure distribution on the wall is affected by the increase in volume flow, which could significantly impact the induced vibration of the PE segment. The velocity fields for the inferior and middle positions are very similar, entering the PE segment with most of the velocity vectors pointing "up" in the z direction. On the other hand, the velocity of the flow entering the PE segment when the prosthesis is at the superior position has a more significant velocity component in the x direction. This is the consequence of the formation of the recirculation zone inside the esophagus near the PE segment.

All the results suggest that the esophagus geometry plays an important part on the flow that leads into the PE segment. The developed model had a symmetric geometry without complex structures. The real geometries, obtained by CT scanning, are very asymmetrical. These asymmetries should influence the flow severely. It is also important to note that all the walls were assumed to be rigid in the present analysis. The actual esophagus will have compliance. That is, the esophagus will expand when air is injected and will deflate when the air escapes. This means that the esophageal walls could undergo displacement during the phonatory cycle. While the PE segment has been observed during phonation, it is not entirely clear how the esophagus behaves.

The analyses conducted on the fluid flow inside the TE system were for a steady state model, assuming that the flow behavior is quasi-steady.

6.1 SUGGESTIONS FOR FUTURE WORK

While the findings suggest that prosthesis position and angulation do not play a significant part in pressure drop, the analyses performed can still be useful in further investigations, such as:

- Use of a time-dependent model with fluid-structure interaction to model the oscillation of

the PE segment;

- Simulate the flow in the TE system with actual CT scan meshes;
- Create a new experimental methodology capable of obtaining the valve flap angle of different prosthesis by different manufactures in similar conditions;
- Create mathematical models of the valve opening behavior of the prosthesis;
- Optimization of prosthesis geometry to reduce losses;
- Quantify the contribution of secondary sound producing mechanism, as described by Stevens (2000).

REFERENCES

AMERICAN CANCER SOCIETY. Laryngeal and hypopharyngeal cancer. *The American Cancer Society*, n.d. Available at: <https://www.cancer.org/cancer/laryngeal-and-hypopharyngeal-cancer>. Retrieved June 4th 2019.

ATOS MEDICAL. Product page. n.d. Digital image. Available at: <https://www.atosmedical.com.br/product_category/laryngectomy-pt-br/>. Retrieved June 10th 2019.

BELFORTE, G. et al. Staffieri tracheo-oesophageal prosthesis for voice rehabilitation after laryngectomy: an evaluation of characteristics. *Medical & Biological Engineering & Computing*, v. 36, n. 6, p. 754–760, nov. 1998. ISSN 0140-0118, 1741-0444. <http://link.springer.com/10.1007/BF02518880>.

BELL, I. H. et al. Pure and Pseudo-pure Fluid Thermophysical Property Evaluation and the Open-Source Thermophysical Property Library CoolProp. *Industrial & Engineering Chemistry Research*, v. 53, n. 6, p. 2498–2508, feb. 2014. ISSN 0888-5885, 1520-5045. <http://pubs.acs.org/doi/10.1021/ie4033999>.

BETTS, J. G. et al. *Anatomy and physiology*. [n.a.: n.p.], 2017. ISBN 978-1-947172-04-3.

BLOM, E. D. Tracheoesophageal valves: Problems, solutions, and directions for the future. *Head & Neck Surgery*, v. 10, n. S2, p. S142–S145, 1988. ISSN 01486403, 19302398. <http://doi.wiley.com/10.1002/hed.2890100815>.

BLOM, E. D. Current status of voice restoration following total laryngectomy. *Oncology (Williston Park, N.Y.)*, v. 14, n. 6, p. 915–922; discussion 927–928, 931, jun. 2000. ISSN 0890-9091.

BLOM, E. D. Some Comments on the Escalation of Tracheoesophageal Voice Prosthesis Dimensions. *ARCH OTOLARYNGOL HEAD NECK SURG*, v. 129, p. 500–502, 2003.

BLOM, E. D.; SINGER, M. I.; HAMAKER, R. C. (Ed.). *Tracheoesophageal voice restoration following total laryngectomy*. San Diego: Singular Publ. Group, 1998. OCLC: 246210329. ISBN 978-1-56593-908-0.

BOHNENKAMP, T. A. Postlaryngectomy Respiratory System and Speech Breathing. In: DOYLE, P. C. (Ed.). *Clinical Care and Rehabilitation in Head and Neck Cancer*. Cham: Springer International Publishing, 2019. p. 103–117. ISBN 978-3-030-04701-6 978-3-030-04702-3. <http://link.springer.com/10.1007/978-3-030-04702-3_7>.

BROWN, D. H. et al. Postlaryngectomy Voice Rehabilitation: State of the Art at the Millennium. *World Journal of Surgery*, v. 27, n. 7, p. 824–831, jul. 2003. ISSN 0364-2313, 1432-2323. <http://link.springer.com/10.1007/s00268-003-7107-4>.

BROWNLEE, B. et al. Selective patient experience with the Blom-Singer Dual Valve voice prosthesis: Blom-Singer Dual Valve Voice Prosthesis. *The Laryngoscope*, v. 128, n. 2, p. 422–426, feb. 2018. ISSN 0023852X. <http://doi.wiley.com/10.1002/lary.26803>.

CANCER RESEARCH UK. Laryngeal cancer statistics. 2015. Available at: <http://www.cancerresearchuk.org/health-professional/cancer-statistics/statistics-by-cancer-type/laryngeal-cancer>. Retrieved in October 27th 2017.

CHEN, W.-C. et al. Clinical impact of human papillomavirus in laryngeal squamous cell carcinoma: a retrospective study. *PeerJ*, v. 5, p. e3395, may. 2017. ISSN 2167-8359. <https://peerj.com/articles/3395>.

DE VRIES, M. P. et al. Numerical simulation of self-sustained oscillation of a voice-producing element based on Navier–Stokes equations and the finite element method. *The Journal of the Acoustical Society of America*, v. 113, n. 4, p. 2077–2083, apr. 2003. ISSN 0001-4966. <http://asa.scitation.org/doi/10.1121/1.1560163>.

DEBRY, C. et al. Laryngeal replacement with an artificial larynx after total laryngectomy: The possibility of restoring larynx functionality in the future: Laryngeal replacement with an artificial larynx. v. 36, n. 11, p. 1669–1673, 2014. ISSN 10433074. <http://doi.wiley.com/10.1002/hed.23621>.

DEBRY, C.; VRANA, N. E.; DUPRET-BORIES, A. Implantation of an artificial larynx after total laryngectomy. v. 376, n. 1, p. 97–98, 2017. ISSN 0028-4793, 1533-4406. <http://www.nejm.org/doi/10.1056/NEJMc1611966>.

D'ASCANIO, L.; PIAZZA, F. More on implantation of an artificial larynx after total laryngectomy. v. 376, n. 14, p. e29, 2017. ISSN 0028-4793, 1533-4406. <http://www.nejm.org/doi/10.1056/NEJMc1701193>.

ERATH, B. D.; HEMSING, F. S. Esophageal aerodynamics in an idealized experimental model of tracheoesophageal speech. *Experiments in Fluids*, v. 57, n. 3, mar. 2016. ISSN 0723-4864, 1432-1114. <http://link.springer.com/10.1007/s00348-015-2111-7>.

FOX, R. W. et al. *Fox and McDonald's introduction to fluid mechanics*. [n.a.: n.p.], 2016. OCLC: 1011038743. ISBN 978-1-118-91265-2 978-1-118-92187-6.

GATES, G. A. et al. Current status of laryngectomee rehabilitation: I. Results of therapy. *American Journal of Otolaryngology*, v. 3, n. 1, p. 1–7, jan. 1982. ISSN 01960709. <https://linkinghub.elsevier.com/retrieve/pii/S0196070982800252>.

GROLMAN, W. et al. Aerodynamic and Sound Intensity Measurements in Tracheoesophageal Voice. *ORL*, v. 69, n. 2, p. 68–76, nov. 2006. ISSN 0301-1569, 1423-0275. <https://www.karger.com/Article/FullText/97401>.

HILGERS, F.; CORNELISSEN, M.; BALM, A. Aerodynamic characteristics of the Provox low-resistance indwelling voice prosthesis. *European Archives of Oto-Rhino-Laryngology*, v. 250, n. 7, nov. 1993. ISSN 0937-4477, 1434-4726. <http://link.springer.com/10.1007/BF00180379>.

HILGERS, F. J.; SCHOUWENBURG, P. F. A New Low-Resistance, Self-Retaining Prosthesis (Provox) for Voice Rehabilitation After Total Laryngectomy:. *The Laryngoscope*, v. 100, n. 11, p. 1202–1207, nov. 1990. ISSN 0023-852X. <http://doi.wiley.com/10.1288/00005537-199011000-00014>.

HILGERS, F. J. M. et al. Physical and psychosocial consequences of total laryngectomy. *Clinical Otolaryngology*, v. 15, n. 5, p. 421–425, oct. 1990. ISSN 1749-4478, 1749-4486. <http://doi.wiley.com/10.1111/j.1365-2273.1990.tb00494.x>.

HILGERS, F. J. M. et al. Development and Clinical Evaluation of a Second-generation Voice Prosthesis (Provox®2), Designed for Anterograde and Retrograde Insertion. *Acta Oto-Laryngologica*, v. 117, n. 6, p. 889–896, jan. 1997. ISSN 0001-6489, 1651-2251. <http://www.tandfonline.com/doi/full/10.3109/00016489709114220>.

HILGERS, F. J. M. et al. A New Problem-solving Indwelling Voice Prosthesis, Eliminating the Need for Frequent Candida- and "Underpressure"-related Replacements: Provox ActiValve. *Acta Oto-Laryngologica*, v. 123, n. 8, p. 972–979, aug. 2003. ISSN 0001-6489, 1651-2251. <https://www.tandfonline.com/doi/full/10.1080/00016480310015371>.

HILGERS, F. J. M. et al. Prospective clinical phase II study of two new indwelling voice prostheses (Provox Vega 22.5 and 20 Fr) and a novel anterograde insertion device (Provox Smart Inserter). *The Laryngoscope*, 2010. ISSN 0023852X, 15314995. <http://doi.wiley.com/10.1002/lary.20925>.

HILGERS, F. J. M. et al. Clinical phase I/feasibility study of the next generation indwelling Provox voice prosthesis (Provox Vega). *Acta Oto-Laryngologica*, v. 130, n. 4, p. 511–519, apr. 2010. ISSN 0001-6489, 1651-2251. <http://www.tandfonline.com/doi/full/10.3109/00016480903283766>.

HüTTNER, B. et al. Development of a time-dependent numerical model for the assessment of non-stationary pharyngoesophageal tissue vibrations after total laryngectomy. *Biomechanics and Modeling in Mechanobiology*, v. 14, n. 1, p. 169–184, jan. 2015. ISSN 1617-7959, 1617-7940. <http://link.springer.com/10.1007/s10237-014-0597-1>.

INHEALTH TECHNOLOGIES. *InHealth Product Catalog*. 2010.

INHEALTH TECHNOLOGIES. Product page. n.d. Digital image. Available at: <https://www.inhealth.com>. Retrieved July 10th 2019.

INNAUMATION. *Aum Voice Prosthesis*. n.d. Available at: <http://www.innaumation.com>. Retrieved in July 8th 2019.

INSTITUTO NACIONAL DE CâNCER. Câncer de laringe. 2018. Available at: <http://www2.inca.gov.br/wps/wcm/connect/tiposdecancer/site/home/laringe>. Retrieved in May 24th 2019.

JONES, E. et al. *SciPy: Open source scientific tools for Python*. 2001. Available at: <http://www.scipy.org/>. Retrieved in August 1st 2019.

KARSCHAY, P. et al. Experiments in Surgical Voice Restoration Using Valve Prostheses. *Acta Oto-Laryngologica*, v. 101, n. 3-4, p. 341–347, jan. 1986. ISSN 0001-6489, 1651-2251. <http://www.tandfonline.com/doi/full/10.3109/00016488609132848>.

KIKINIS, R.; PIEPER, S. D.; VOSBURGH, K. G. 3d Slicer: A Platform for Subject-Specific Image Analysis, Visualization, and Clinical Support. In: JOLESZ, F. A. (Ed.). *Intraoperative Imaging and Image-Guided Therapy*. New York, NY: Springer New York, 2014. p. 277–289. ISBN 978-1-4614-7656-6 978-1-4614-7657-3. <http://link.springer.com/10.1007/978-1-4614-7657-3_19>.

KNAPP, B. A.; PANJE, W. R. A voice button for laryngectomees. *AORN Journal*, v. 36, n. 2, p. 183–192, aug. 1982. ISSN 00012092. <http://doi.wiley.com/10.1016/S0001-2092(07)63014-2>.

KRAMP, B.; DOMMERICH, S. Tracheostomy cannulas and voice prosthesis. *GMS Current Topics in Otorhinolaryngology - Head and Neck Surgery; 8:Doc05; ISSN 1865-1011*, 2009. <http://www.egms.de/en/journals/cto/2011-8/cto000057.shtml>.

KRESS, P.; SCHäFER, P. *Characteristic curves - low resistance voice prostheses*. 2010. Available at: <https://stimmprothese.com/1/forschung/>. Retrieved in July 1st 2019.

LEDER, S. B. et al. Voice Restoration With the Advantage Tracheoesophageal Voice Prosthesis. *Otolaryngology–Head and Neck Surgery*, v. 133, n. 5, p. 681–684, nov. 2005. ISSN 0194-5998, 1097-6817. <http://journals.sagepub.com/doi/10.1016/j.otohns.2005.08.009>.

LEWIN, J. S. et al. Device Life of the Tracheoesophageal Voice Prosthesis Revisited. *JAMA Otolaryngology–Head & Neck Surgery*, v. 143, n. 1, p. 65, jan. 2017. ISSN 2168-6181. <http://archotol.jamanetwork.com/article.aspx?doi=10.1001/jamaoto.2016.2771>.

LORENZ, K. J. Rehabilitation after Total Laryngectomy—A Tribute to the Pioneers of Voice Restoration in the Last Two Centuries. *Frontiers in Medicine*, v. 4, jun. 2017. ISSN 2296-858X. <http://journal.frontiersin.org/article/10.3389/fmed.2017.00081/full>.

MARKóW, M. et al. Computational fluid dynamics in the assessment of patients' postoperative status after glottis-widening surgery. *Advances in Clinical and Experimental Medicine*, v. 26, n. 6, p. 947–952, sep. 2017. ISSN 1899-5276. <http://www.advances.umed.wroc.pl/en/article/2017/26/6/947/>.

MOON, J. B.; WEINBERG, B. Aerodynamic and Myoelastic Contributions to Tracheoesophageal Voice Production. *Journal of Speech, Language, and Hearing Research*, v. 30, n. 3, p. 387–395, sep. 1987. ISSN 1092-4388, 1558-9102. <http://pubs.asha.org/doi/10.1044/jshr.3003.387>.

MOTTA, S.; GALLI, I.; DI RIENZO, L. Aerodynamic Findings in Esophageal Voice. *Archives of Otolaryngology–Head & Neck Surgery*, v. 127, n. 6, p. 700, jun. 2001. ISSN 0886-4470. <http://archotol.jamanetwork.com/article.aspx?doi=10.1001/archotol.127.6.700>.

NALBADIAN, M. et al. Factors influencing quality of life in laryngectomized patients. *European Archives of Oto-Rhino-Laryngology*, v. 258, n. 7, p. 336–340, sep. 2001. ISSN 0937-4477, 1434-4726. <http://link.springer.com/10.1007/s004050100376>.

NATIONAL CANCER INSTITUTE. Cancer of the larynx - cancer stat facts. n.d. Available at: <https://seer.cancer.gov/statfacts/html/laryn.html>. Retrieved in October 27th 2017.

NIJDAM, H. F. et al. A new prosthesis for voice rehabilitation after laryngectomy. *Archives of Oto-Rhino-Laryngology*, v. 237, n. 1, p. 27–33, dec. 1982. ISSN 0302-9530, 1434-4726. <http://link.springer.com/10.1007/BF00453713>.

PHILIP, R. Ingestion of a Voice-Master Prosthesis Followed by a Potentially Fatal Aspiration. v. 61, n. 2, p. 3, 2006.

RODI, W. Experience with two-layer models combining the k-epsilon model with a one-equation model near the wall. In: *29th Aerospace Sciences Meeting*. Reno, NV, U.S.A.: American Institute of Aeronautics and Astronautics, 1991. <http://arc.aiaa.org/doi/10.2514/6.1991-216>.

RUTY, N. et al. An in vitro setup to test the relevance and the accuracy of low-order vocal folds models. *The Journal of the Acoustical Society of America*, v. 121, n. 1, p. 479–490, jan. 2007. ISSN 0001-4966. <http://asa.scitation.org/doi/10.1121/1.2384846>.

SAKALLIOGLU, O. Laryngeal Transplantation: A Review. *Turk Otolarengoloji Arsivi/Turkish Archives of Otolaryngology*, v. 53, n. 3, p. 128–132, dec. 2015. ISSN 03044793, 2149553X. <http://www.turkarchotolaryngol.net/sayilar/64/buyuk/128-1323.pdf>.

SANKARANARAYANAN, R. et al. (Ed.). *Cancer survival in Africa, Asia, the Caribbean and Central America*. Lyon, France: International Agency for Research on Cancer, World Health Organization, 2011. (IARC scientific publications, no. 162). OCLC: ocn730012256. ISBN 978-92-832-2162-3.

SCHLICHTING, H. *Boundary-layer theory*. 7th ed. ed. New York: McGraw-Hill, 1979. (McGraw-Hill series in mechanical engineering). ISBN 978-0-07-055334-7.

SCHNEIDER, C. A.; RASBAND, W. S.; ELICEIRI, K. W. NIH Image to ImageJ: 25 years of image analysis. *Nature Methods*, v. 9, n. 7, p. 671–675, jul. 2012. ISSN 1548-7105.

SCHOUWENBURG, P.; EERENSTEIN, S.; GROLMAN, W. The VoiceMaster voice prosthesis for the laryngectomized patient. *Clinical Otolaryngology and Allied Sciences*, v. 23, n. 6, p. 555–559, dec. 1998. ISSN 0307-7772, 1365-2273. <http://doi.wiley.com/10.1046/j.1365-2273.1998.2360555.x>.

SCHUTTE, H. K. *The efficiency of voice production*. PhD Thesis (Doctoral Thesis) — University of Groningen, Groningen, 1980. <http://www.rug.nl/research/portal/en/publications/the-efficiency-of-voice-production(859a910f-f03b-4084-9cec-aeea3c66caf0).html>.

SCHWARTZ, A. W.; HOLLINSHEAD, W. H.; DEVINE, K. D. Laryngectomy: Anatomy and Technique. *Surgical Clinics of North America*, v. 43, n. 4, p. 1063–1079, aug. 1963. ISSN 00396109. <https://linkinghub.elsevier.com/retrieve/pii/S0039610916370426>.

SCHWARZ, R. et al. Substitute Voice Production: Quantification of PE Segment Vibrations Using a Biomechanical Model. *IEEE Transactions on Biomedical Engineering*, v. 58, n. 10, p. 2767–2776, oct. 2011. ISSN 0018-9294, 1558-2531. <http://ieeexplore.ieee.org/document/5764823/>.

SEARL, J. Alaryngeal Speech Aerodynamics: Lower and Upper Airway Considerations. In: DOYLE, P. C. (Ed.). *Clinical Care and Rehabilitation in Head and Neck Cancer*. Cham: Springer International Publishing, 2019. p. 209–230. ISBN 978-3-030-04701-6 978-3-030-04702-3. <http://link.springer.com/10.1007/978-3-030-04702-3_13>.

SIEMENS. *STAR-CCM+® Documentation*. 2016. Version 11.02.

SINGER, M. I.; BLOM, E. D. An Endoscopic Technique for Restoration of Voice after Laryngectomy. *Annals of Otology, Rhinology & Laryngology*, v. 89, n. 6, p. 529–533,

nov. 1980. ISSN 0003-4894, 1943-572X. <http://journals.sagepub.com/doi/10.1177/000348948008900608>.

SINGH, s.; HAMDY, s. The upper oesophageal sphincter. *Neurogastroenterology and Motility*, v. 17, n. s1, p. 3–12, jun. 2005. ISSN 1350-1925, 1365-2982. <http://doi.wiley.com/10.1111/j.1365-2982.2005.00662.x>.

STEVENS, K. N. *Acoustic phonetics*. 1. paperback ed. ed. Cambridge, Mass.: MIT Press, 2000. (Current studies in linguistics, 30). OCLC: 248883560. ISBN 978-0-262-69250-2 978-0-262-19404-4.

STEWART, B. W.; WILD, C. P. *World Cancer Report 2014*. Lyon: International Agency for Research on Cancer/World Health Organization, 2014. ISBN 978-92-832-0443-5.

STROME, M. et al. Laryngeal transplantation and 40-month follow-up. v. 344, n. 22, p. 1676–1679, 2001. ISSN 0028-4793, 1533-4406. <http://www.nejm.org/doi/abs/10.1056/NEJM200105313442204>.

TACK, J. W. et al. Clinical evaluation of a membrane-based voice-producing element for laryngectomized women. *Head & Neck*, v. 30, n. 9, p. 1156–1166, sep. 2008. ISSN 10433074, 10970347. <http://doi.wiley.com/10.1002/hed.20853>.

TACK, J. W. et al. In vitro evaluation of a double-membrane–based voice-producing element for laryngectomized patients. *Head & Neck*, v. 29, n. 7, p. 665–674, jul. 2007. ISSN 10433074, 10970347. <http://doi.wiley.com/10.1002/hed.20560>.

TACK, J. W. et al. Development of a Double-Membrane Sound Generator for Application in a Voice-Producing Element for Laryngectomized Patients. *Annals of Biomedical Engineering*, v. 34, n. 12, p. 1896–1907, dec. 2006. ISSN 0090-6964, 1573-9686. <http://link.springer.com/10.1007/s10439-006-9196-3>.

TANG, C. G.; SINCLAIR, C. F. Voice Restoration After Total Laryngectomy. *Otolaryngologic Clinics of North America*, v. 48, n. 4, p. 687–702, aug. 2015. ISSN 00306665. <https://linkinghub.elsevier.com/retrieve/pii/S0030666515000596>.

TAUB, S.; SPIRO, R. H. Vocal rehabilitation of laryngectomees. *The American Journal of Surgery*, v. 124, n. 1, p. 87–90, jul. 1972. ISSN 00029610. <https://linkinghub.elsevier.com/retrieve/pii/0002961072901742>.

THOMSON, S. L.; TACK, J. W.; VERKERKE, G. J. A numerical study of the flow-induced vibration characteristics of a voice-producing element for laryngectomized patients. *Journal of Biomechanics*, v. 40, n. 16, p. 3598–3606, jan. 2007. ISSN 0021-9290, 1873-2380. <http://www.jbiomech.com/article/S0021-9290(07)00266-7/fulltext>.

TUCKER, H. M. Total laryngectomy: Technique. *Operative Techniques in Otolaryngology-Head and Neck Surgery*, v. 1, n. 1, p. 42–44, mar. 1990. ISSN 10431810. <https://linkinghub.elsevier.com/retrieve/pii/S1043181010802726>.

VAN AS, C. J. *Tracheoesophageal Speech. A Multidimensional Assessment of Voice Quality*. PhD Thesis (PhD) — University of Amsterdam, 2001.

VAN DEN HOOGEN, F. J. A. et al. The Groningen, Nijdam and Provox Voice Prostheses: A Prospective Clinical Comparison Based on 845 Replacements. *Acta Oto-Laryngologica*, v. 116, n. 1, p. 119–124, jan. 1996. ISSN 0001-6489, 1651-2251. <http://www.tandfonline.com/doi/full/10.3109/00016489609137724>.

VAN DEN HOOGEN, F. J. A. et al. In vivo aerodynamic characteristics of the nijdam voice prosthesis. *Acta Oto-Laryngologica*, v. 117, n. 6, p. 897–902, jan. 1997. ISSN 0001-6489, 1651-2251. <http://www.tandfonline.com/doi/full/10.3109/00016489709114221>.

VAN DER PLAATS, A. et al. An In-vitro Test Set-Up for Evaluation of a Voice-Producing Element Under Physiologic Acoustic Conditions. *Annals of Biomedical Engineering*, v. 34, n. 5, p. 893–900, may. 2006. ISSN 0090-6964, 1573-9686. <http://link.springer.com/10.1007/s10439-006-9083-y>.

VAN DER TORN, M. et al. Alternative Voice After Laryngectomy Using a Sound-Producing Voice Prosthesis. *The Laryngoscope*, v. 111, n. 2, p. 336–346, 2001. <http://onlinelibrary.wiley.com/doi/10.1097/00005537-200102000-00027/full>.

VAN DER TORN, M. et al. Assessment of alaryngeal speech using a sound-producing voice prosthesis in relation to sex and pharyngoesophageal segment tonicity. *Head & Neck*, v. 28, n. 5, p. 400–412, may. 2006. ISSN 1043-3074, 1097-0347. <http://doi.wiley.com/10.1002/hed.20355>.

VERKERKE, G.; THOMSON, S. Sound-Producing Voice Prostheses: 150 Years of Research. *Annual Review of Biomedical Engineering*, v. 16, n. 1, p. 215–245, jul. 2014. ISSN 1523-9829, 1545-4274. <http://www.annualreviews.org/doi/10.1146/annurev-bioeng-071811-150014>.

VERKERKE, G. J. et al. Analysis of the Mechanical Behavior of the Nijdam Voice Prosthesis. *The Laryngoscope*, v. 107, n. 12, p. 1656–1660, 1997. ISSN 0023852X, 15314995. <http://doi.wiley.com/10.1097/00005537-199712000-00015>.

VERSTEEG, H. K.; MALALASEKERA, W. *An introduction to computational fluid dynamics: the finite volume method*. 2nd ed. ed. Harlow, England ; New York: Pearson Education Ltd, 2007. OCLC: ocm76821177. ISBN 978-0-13-127498-3.

WEIR, N. F. Theodore Billroth: The first laryngectomy for cancer. *The Journal of Laryngology & Otology*, v. 87, n. 12, p. 1162–1170, dec. 1973. ISSN 0022-2151, 1748-5460. <http://www.journals.cambridge.org/abstract_S0022215100078130>.

WORLD HEALTH ORGANIZATION. Cancer of the larynx - cancer stat facts. *World Health Organization - International Agency for Cancer Research*, 2018. Available at: <http://gco.iarc.fr/today/home>. Retrieved in November 13th 2019.

ZENGA, J. et al. State of the art: Rehabilitation of speech and swallowing after total laryngectomy. v. 86, p. 38–47, 2018. ISSN 13688375. <https://linkinghub.elsevier.com/retrieve/pii/S1368837518303142>.

ANNEX A – Post-processing of tomography images

Universidade Federal de Santa Catarina
Centro Tecnológico
Laboratório de Vibrações e Acústica

Processamento de imagens de tomografia para construção de modelos 3D

I.C.: Camila Zandavalli
Orientador: Andrey R. da Silva, Dr. Eng.

Florianópolis - SC

Março de 2019

10 páginas

Índice

1 Introdução

O presente relatório insere-se em um projeto de pesquisa do Laboratório de Vibrações e Acústica da Universidade Federal de Santa Catarina que visa o desenvolvimento de próteses de voz (ou traqueoesofágicas) para pacientes que tiveram as pregas vocais removidas em decorrência de câncer na laringe. Tem-se como objetivo registrar os métodos utilizados para a geração de modelos 3D do segmento faringoesofágico e da traqueia a partir de imagens de tomografia de pacientes laringectomizados. Tais modelos contribuirão para o estudo da vibração induzida pelo escoamento de ar no segmento faringoesofágico, cujo entendimento é essencial para a elaboração das próteses traqueoesofágicas.

As imagens de tomografia foram obtidas em parceria com o Centro de Pesquisas Oncológicas (CEPON) de Florianópolis.

2 Características de medição

2.1 Máquina utilizada

O tomógrafo utilizado foi o Aquilion Prime (160 slices), capaz de gerar 160 fatias de 0.5mm por rotação. A parte do corpo medida foi a partir do meio dos olhos até um pouco abaixo da traqueia, como mostrado no esquema abaixo.

Figura 1 – Seção de medição

As imagens foram realizadas no Centro de Pesquisas Oncológicas de Florianópolis, localizado na Rod. Admar Gonzaga, 655, bairro Itacorubi.

2.2 Dados dos pacientes

Foram feitas imagens de dois pacientes, ambos do sexo masculino. O paciente 1 possuía 68 anos e o paciente 2 possuía 60 anos na data de realização das tomografias.

3 Aquisição das imagens

As imagens em formato DICOM foram abertas no *software 3D Slicer* e alguns cortes sagitais podem ser vistos abaixo:

3.1 Paciente 1

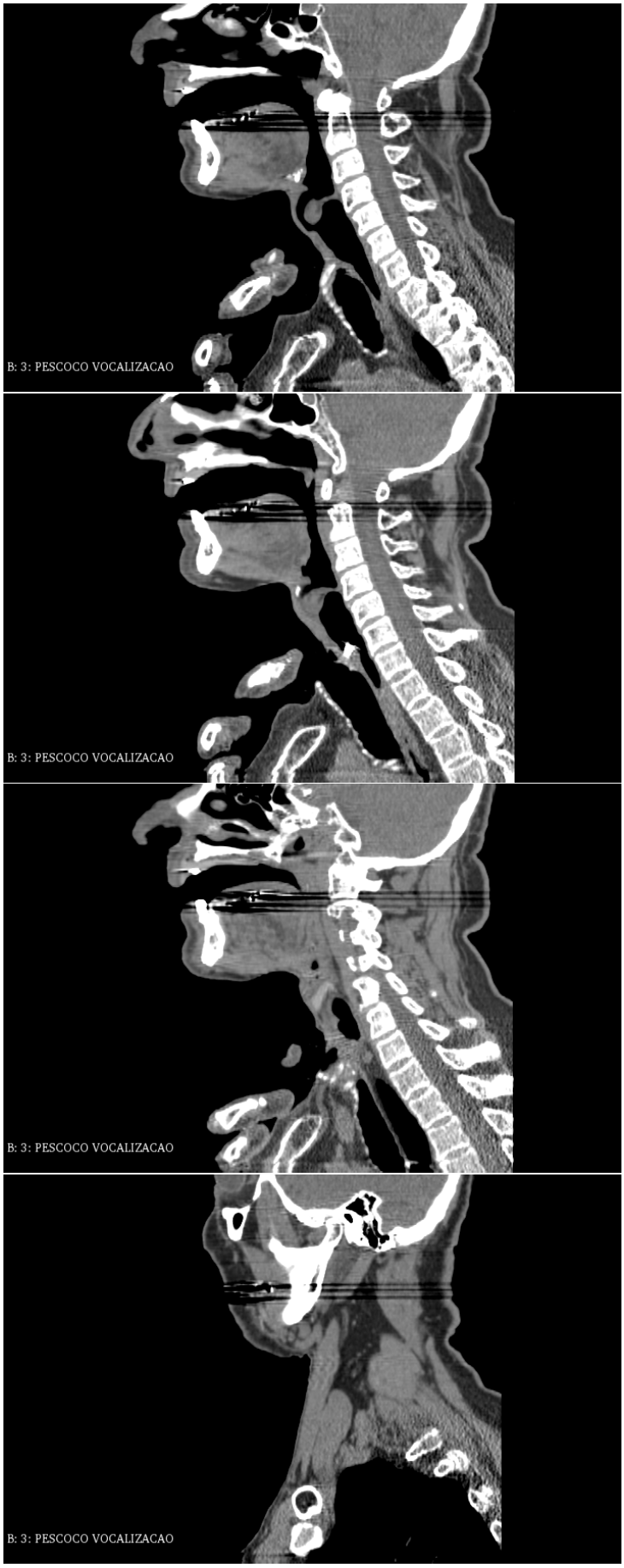

Figura 2 – Cortes sagitais do paciente 1

3.2 Paciente 2

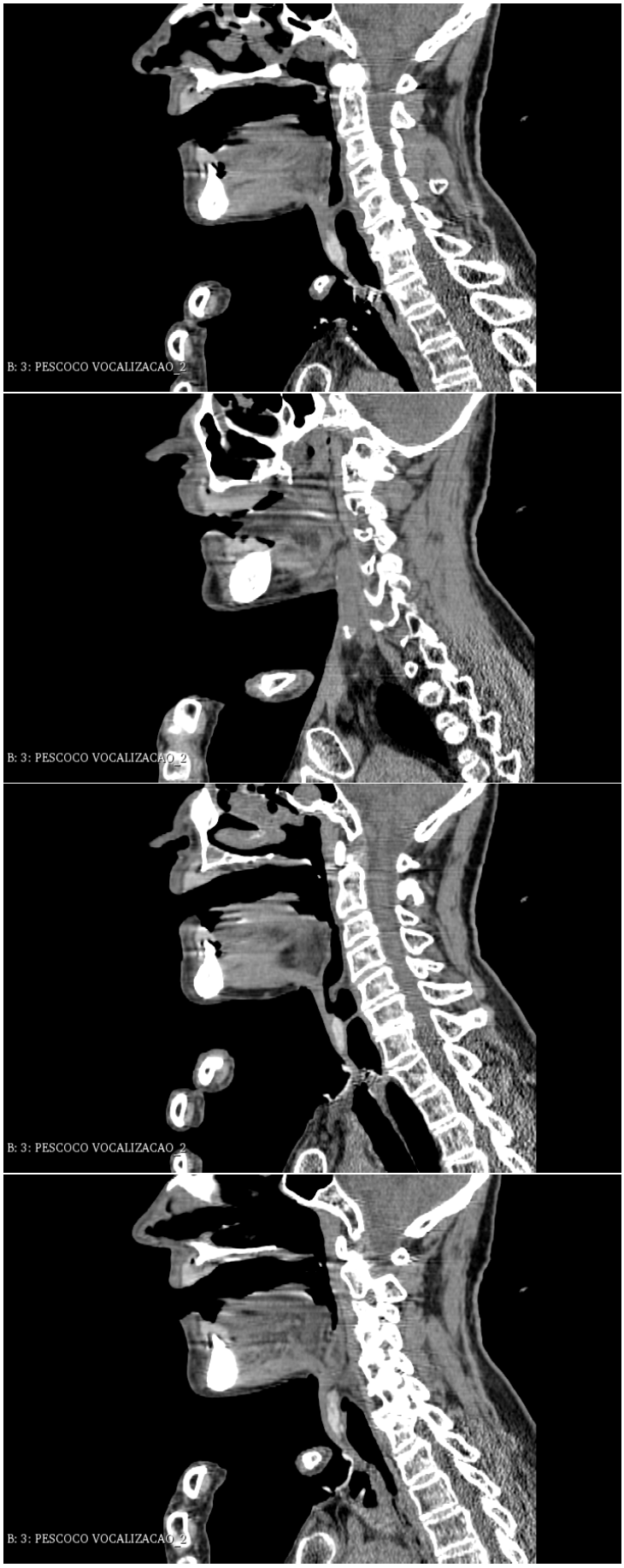

Figura 3 – Cortes sagitais do paciente 2

4 Transformação da imagem de tomografia para modelo 3D

4.1 *Softwares* e métodos

A transformação das imagens de tomografia para modelos 3D foi feita através dos *softwares 3D Slicer* e *MeshLab*. Ambos são *softwares open source* e foram escolhidos devido à sua disponibilidade e ferramentas inclusas.

Para o desenvolvimento do modelo 3D, utilizou-se o programa *3D Slicer*. Nele, selecionou-se nas imagens de tomografia as partes desejadas através do módulo *Editor* do programa. No módulo, utilizou-se as ferramentas *Paint Effect* para selecionar a área desejada com o pincel, *Fast Marching Effect*, que permite selecionar zonas de cores e intensidades similares às definidas com o pincel, e *Dilate Effect* para expandir a seleção. Uma vez que a área desejada foi selecionada, criou-se o modelo 3D dessa área, através da ferramenta *Make Model Effect*.

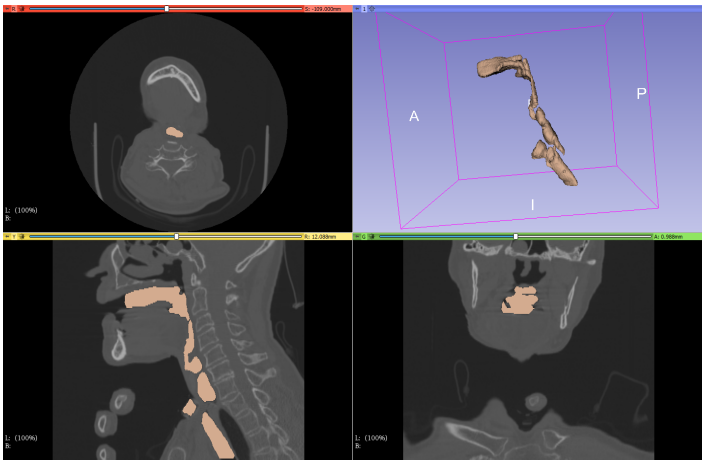

Figura 4 – Interface do *3D Slicer* após as etapas descritas

O modelo 3D criado no *3D Slicer* apresenta alta rugosidade e partículas isoladas. Isso porque a seleção da área desejada é feita com os pixels da imagem de mesma cor daqueles selecionados pelo pincel, criando "pontas"ao invés de uma superfície lisa e regular. Assim, o *software MeshLab* foi utilizado para o tratamento dos modelos 3D, exportados para .STL.

No *MeshLab*, utiliza-se a ferramenta *Remove Isolated Pieces (wrt diameter)* para remover as partículas isoladas e as ferramentas *Depth Smooth* e *Laplacian Smooth* para suavizar a superfície do modelo. Após essas etapas, chegamos ao modelo 3D final.

4.2 Dificuldades encontradas

As principais dificuldades encontradas foram devido ao método que o *3D Slicer* utiliza para selecionar as zonas de mesma cor pela ferramenta *Fast Marching Effect*. Essa seleção costuma deixar de lado zonas muito finas das imagens e não abrange toda a área do esôfago e da traqueia.

Para contornar esses erros, foi feita a seleção manual das zonas finas com o pincel, pela ferramenta *Paint Effect*, e utilizou-se a ferramenta *Dilate Effect* para expandir a zona selecionada, incluindo todo o esôfago e traqueia.

4.3 Imagens resultantes

4.3.1 Paciente 1 - apneia

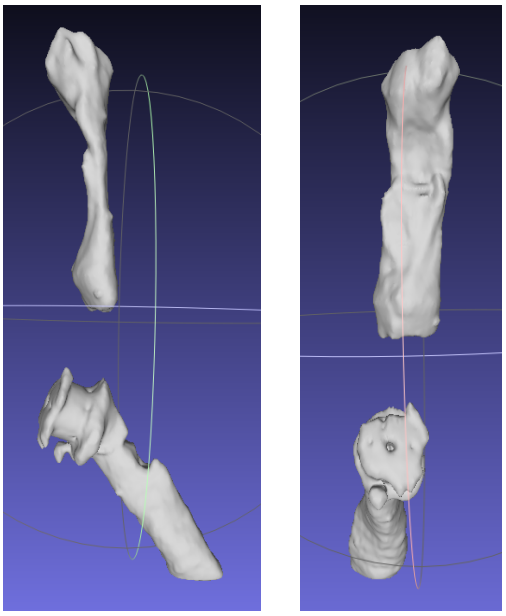

Figura 5 – Modelo 3D do paciente 1 em apneia

4.3.2 Paciente 1 - fonação

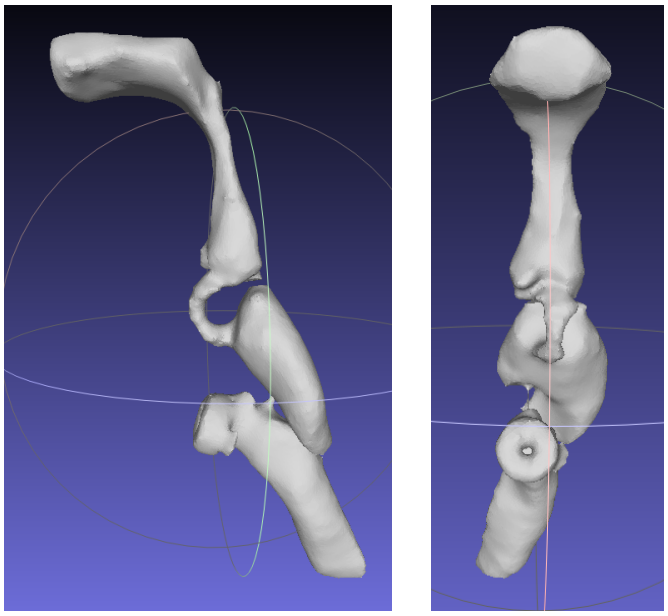

Figura 6 – Modelo 3D do paciente 1 em fonação

4.3.3 Paciente 2 - apneia

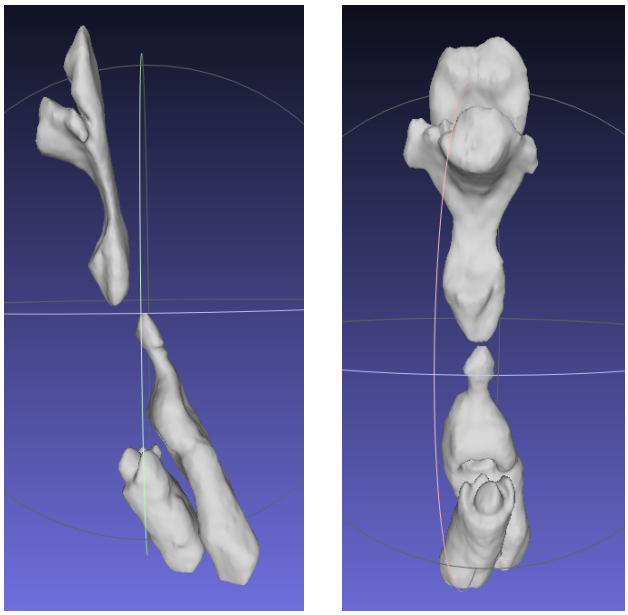

Figura 7 – Modelo 3D do paciente 2 em apneia

4.3.4 Paciente 2 - fonação

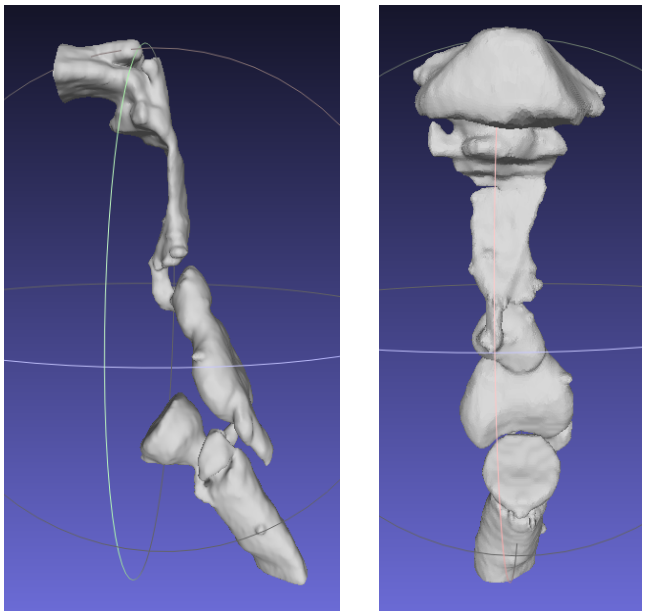

Figura 8 – Modelo 3D do paciente 2 em fonação

5 Conclusão

Os modelos 3D obtidos representam bem a geometria do segmento faringoesofágico e da traqueia e auxiliarão no entendimento da vibração induzida pelo escoamento nos mesmos, cumprindo com o propósito deste trabalho. Geometrias mais fiéis podem ser alcançadas a partir do processamento de imagens de tomógrafos com melhor resolução (menor espessura das fatias de corte), e também com o uso de *softwares* mais especializados.

ANNEX B – Parecer cosubstanciado do CEP

PARECER CONSUBSTANCIADO DO CEP

DADOS DA EMENDA

Título da Pesquisa: Desenvolvimento de Prótese de Voz Traqueo Esofágica para Pacientes Laringectomizados

Pesquisador: Andrey Ricardo da Silva

Área Temática:

Versão: 3

CAAE: 61242016.2.0000.0121

Instituição Proponente: Departamento de Engenharia Mecânica - Centro Tecnológico

Patrocinador Principal: Financiadora de Estudos e Projetos - FINEP

DADOS DO PARECER

Número do Parecer: 3.054.135

Apresentação do Projeto:

"Desenvolvimento de Prótese de Voz Traqueo-Esofágica para Pacientes Laringectomizados". Este projeto pretende desenvolver uma nova prótese que possibilite o re-estabelecimento da voz em pacientes que foram submetidos a uma laringectomia total (com a retirada das pregas vocais) a partir de uma válvula de conexão entre a traqueia e o esôfago.

Objetivo da Pesquisa:

Apresentar a Segunda Emenda do projeto a fim de propor a realização de um breve exame de tomografia computadorizada de pacientes laringectomizados totais, para a uma caracterização mais precisa das características do segmento faringoesofágico desses pacientes.

Avaliação dos Riscos e Benefícios:

Não se aplica.

Comentários e Considerações sobre a Pesquisa:

Trata o presente da segunda Emenda do projeto de pesquisa "Desenvolvimento de Prótese de Voz Traqueo -Esofágica para Pacientes Laringectomizados" cuja justificativa dos pesquisadores é que considerando-se que os resultados dos procedimentos anteriores, embora bem sucedidos, indicam que a geometria da região estudada é amplamente variável e, portanto, são necessárias mais informações para caracterizar as propriedades mecânicas desses tecidos. Assim, propõe-se,

neste momento, que seja realizado um breve exame de tomografia computadorizada de pacientes laringectomizados totais, para a uma caracterização mais precisa das características do segmento faringoesofágico desses pacientes. Ressalta-se que o exame não irá utilizar a ingestão ou injeção de qualquer tipo de contraste em sua realização - minimizando os riscos e desconfortos para os participantes. Um novo Termo de Consentimento Livre e Esclarecido TCLE foi apresentado e o mesmo cumpre todas as exigências da Resolução CNS nº 466/12 e suas complementares. Assim, recomendamos a aprovação da segunda Emenda do projeto em questão.

Considerações sobre os Termos de apresentação obrigatória:

Foram apresentados os seguintes documentos obrigatórios:

1) PB - INFORMAÇÕES BÁSICAS (justificativa da Emenda);

2) TCLE.

O TCLE apresentado atende na íntegra a Resolução CNS nº 466/12.

Recomendações:

Sem recomendações.

Conclusões ou Pendências e Lista de Inadequações:

Não se aplica.

Considerações Finais a critério do CEP:

Este parecer foi elaborado baseado nos documentos abaixo relacionados:

Tipo Documento	Arquivo	Postagem	Autor	Situação
Informações Básicas do Projeto	PB_INFORMAÇÕES_BÁSICAS_1260166_E2.pdf	19/11/2018 09:44:52		Aceito
TCLE / Termos de Assentimento / Justificativa de Ausência	TCLE_tomografia.pdf	19/11/2018 09:41:45	Andrey Ricardo da Silva	Aceito
TCLE / Termos de Assentimento / Justificativa de Ausência	TCLE_versao2.pdf	20/03/2018 14:30:17	Andrey Ricardo da Silva	Aceito
Projeto Detalhado / Brochura Investigador	vivavox_menor.pdf	21/10/2016 11:23:15	Andrey Ricardo da Silva	Aceito

Folha de Rosto	folha_rosto.pdf	21/10/2016 11:17:23	Andrey Ricardo da Silva	Aceito

Situação do Parecer:
Aprovado

Necessita Apreciação da CONEP:
Não

FLORIANOPOLIS, 03 de Dezembro de 2018

Assinado por:
Nelson Canzian da Silva
(Coordenador(a))

Endereço: Universidade Federal de Santa Catarina, Prédio Reitoria II, R: Desembargador Vitor Lima, nº 222, sala 401
Bairro: Trindade **CEP:** 88.040-400
UF: SC **Município:** FLORIANOPOLIS
Telefone: (48)3721-6094 **E-mail:** cep.propesq@contato.ufsc.br

ANNEX C – Termo de consentimento livre e esclarecido

TERMO DE CONSENTIMENTO LIVRE E ESCLARECIDO

Convidamos o (a) Sr (a) para participar da pesquisa **Desenvolvimento de Prótese de Voz Tráqueo-Esofágica para Pacientes Laringectomizados**, sob a responsabilidade do pesquisador Andrey Ricardo da Silva, o qual pretende desenvolver uma nova prótese fonatória que possibilite o reestabelecimento da voz, a partir de uma válvula posicionada entre traquéia e esôfago de pacientes adultos, acima de 18 anos, provenientes do Centro de Pesquisas Oncológicas (CEPON) em Florianópolis, que foram submetidos ao procedimento cirúrgico de retirada da laringe incluindo pregas vocais, denominado laringectomia total.

Sua participação é voluntária e se dará por meio de um exame de tomografia computadorizada dividido em duas partes. Na primeira parte, serão obtidas imagens da sua região do pescoço em repouso. Na segunda etapa, as imagens da região do pescoço serão obtidas enquanto você pronuncia a vogal “i” durante alguns segundos. Em nenhum dos exames será utilizado meio de contraste (você não precisará ingerir ou injetar nenhuma substância para o exame).

O tempo de duração máximo do exame no aparelho de tomografia computadorizada será de vinte segundos. O objetivo deste exame é é determinar as características geométricas médias do esôfago e da laringe de pacientes que foram submetidos à laringectomia total. As imagens obtidas pelo exame serão utilizadas em uma simulação computacional.

Os riscos decorrentes de sua participação na pesquisa são mínimos e seguem as recomendações de segurança definidas pelo Colégio Brasileiro de Radiologia e Diagnóstico por Imagem. Dentre os riscos envolvidos, citam-se como por exemplo o deslocamento até o local da pesquisa, incidentes durante o trajeto e/ou incidentes no CEPON como: cansaço ou desconforto durante o teste. Entretanto durante os procedimentos de coleta de dados você estará sempre acompanhado por pesquisadores envolvidos e por uma Fonoaudióloga vinculada ao projeto, que lhe prestará toda a assistência necessária ou que acionará pessoal competente, caso você tenha alguma intercorrência.

Se você aceitar participar, estará contribuindo para o maior conhecimento sobre os mecanismos de geração de voz e no desenvolvimento de próteses de voz mais efetivas que se adequem as características fisiológicas de cada paciente. Além disso autoriza o uso de informações adicionais coletadas em prontuários e/ou dados demográficos.

Se depois de consentir em sua participação o Sr (a) desistir de continuar participando, tem o direito e a liberdade de retirar seu consentimento em qualquer fase da pesquisa, seja antes ou depois da coleta dos dados, independente do motivo e sem nenhum prejuízo a sua pessoa.

O (a) Sr (a) não terá nenhuma despesa e também não receberá nenhuma remuneração advinda da sua participação na pesquisa, uma vez que a legislação brasileira não permite qualquer compensação financeira, mas você será ressarcido nas despesas de transporte e alimentação pelos pesquisadores nos termos descritos no projeto. Caso alguma despesa extraordinária associada à pesquisa venha a ocorrer, você será ressarcido nos termos da lei. Caso você tenha algum prejuízo material ou imaterial em decorrência da pesquisa poderá solicitar indenização, de acordo com a legislação vigente.
Os resultados da pesquisa serão analisados e publicados, porém sua identidade não será divulgada, sendo guardada em sigilo.

Para qualquer outra informação, o (a) Sr (a) poderá entrar em contato com o pesquisador no Laboratório de Vibrações e Acústica, Depto. de Engenharia Mecânica, Universidade Federal de Santa Catarina, Bairro Trindade - Florianópolis – Brasil Fone: (48) 37217224, ou pelo email andrey.rs@ufsc.br, ou ainda, com o Comitê de Ética em Pesquisa com Seres Humanos da UFSC, localizado no Prédio Reitoria II, 4° andar, sala 401, localizado na Rua Desembargador Vitor Lima, 222, Trindade, Florianópolis- SC CEP 88040-900. Telefone para contato: 37216094.

O pesquisador responsável, que também assina esse documento, se compromete a conduzir a pesquisa de acordo com o que preconiza a Resolução 466/12 de 12/12/2012, que trata dos preceitos éticos e da proteção aos participantes da presente pesquisa.

TERMO DE CONSENTIMENTO LIVRE E ESCLARECIDO

Eu, _____, RG _____fui informado sobre o que o pesquisador quer fazer e porque precisa da minha colaboração, e entendi a explicação. Por isso, eu concordo em participar do projeto, sabendo que não vou ganhar nada e que posso sair quando quiser. Este documento é emitido em duas vias que serão ambas assinadas por mim e pelo pesquisador, ficando uma via com cada um de nós.

_____ Data: ___/ ____/ _____
Assinatura do participante

_____
Assinatura do Pesquisador Responsável